NOTE TO USERS

This reproduction is the best copy available.

UMI®

uOttawa

L'Université canadienne
Canada's university

FACULTÉ DES ÉTUDES SUPÉRIEURES ET POSTOCTORALES

uOttawa

L'Université canadienne
Canada's university

FACULTY OF GRADUATE AND POSDOCTORAL STUDIES

Emily Roadhouse
AUTEUR DE LA THÈSE / AUTHOR OF THESIS

M.Sc. (Geography)
GRADE / DEGREE

Department of Geography
FACULTÉ, ÉCOLE, DÉPARTEMENT / FACULTY, SCHOOL, DEPARTMENT

Air and Ground Surface Temperature Relations in a Mountainous Basin, Wolf Creek, Yukon Territory
TITRE DE LA THÈSE / TITLE OF THESIS

Antoni Lewkowicz
DIRECTEUR (DIRECTRICE) DE LA THÈSE / THESIS SUPERVISOR

CO-DIRECTEUR (CO-DIRECTRICE) DE LA THÈSE / THESIS CO-SUPERVISOR

Sharon Smith

Peter Johnson

Konrad Gajewski

Gary W. Slater
Le Doyen de la Faculté des études supérieures et postdoctorales / Dean of the Faculty of Graduate and Postdoctoral Studies

Air and Ground Surface Temperature Relations in a Mountainous Basin, Wolf Creek, Yukon Territory.

Emily A. Roadhouse, B.A. (Hons)

Thesis submitted to the
Faculty of Graduate and Postdoctoral Studies
In partial fulfillment of the requirements
For the degree of

Master of Science in Physical Geography

Department of Geography
Faculty of Arts
University of Ottawa

Emily A. Roadhouse, Ottawa, Canada, 2010

Library and Archives Canada

Published Heritage Branch

395 Wellington Street
Ottawa ON K1A 0N4
Canada

Bibliothèque et
Archives Canada

Direction du
Patrimoine de l'édition

395, rue Wellington
Ottawa ON K1A 0N4
Canada

Your file Votre référence
ISBN: 978-0-494-69038-3
Our file Notre référence
ISBN: 978-0-494-69038-3

NOTICE:

The author has granted a non-exclusive license allowing Library and Archives Canada to reproduce, publish, archive, preserve, conserve, communicate to the public by telecommunication or on the Internet, loan, distribute and sell theses worldwide, for commercial or non-commercial purposes, in microform, paper, electronic and/or any other formats.

The author retains copyright ownership and moral rights in this thesis. Neither the thesis nor substantial extracts from it may be printed or otherwise reproduced without the author's permission.

AVIS:

L'auteur a accordé une licence non exclusive permettant à la Bibliothèque et Archives Canada de reproduire, publier, archiver, sauvegarder, conserver, transmettre au public par télécommunication ou par l'Internet, prêter, distribuer et vendre des thèses partout dans le monde, à des fins commerciales ou autres, sur support microforme, papier, électronique et/ou autres formats.

L'auteur conserve la propriété du droit d'auteur et des droits moraux qui protège cette thèse. Ni la thèse ni des extraits substantiels de celle-ci ne doivent être imprimés ou autrement reproduits sans son autorisation.

In compliance with the Canadian Privacy Act some supporting forms may have been removed from this thesis.

While these forms may be included in the document page count, their removal does not represent any loss of content from the thesis.

Conformément à la loi canadienne sur la protection de la vie privée, quelques formulaires secondaires ont été enlevés de cette thèse.

Bien que ces formulaires aient inclus dans la pagination, il n'y aura aucun contenu manquant.

Canada

ABSTRACT

The links between climate and permafrost are well known, but the precise nature of the relationship between air and ground temperatures remains poorly understood, particularly in complex mountain environments. Although previous studies indicate that elevation and potential incoming solar radiation (PISR) are the two leading factors contributing to the existence of permafrost at a given location, additional factors may also contribute significantly to the existence of mountain permafrost, including vegetation cover, snow accumulation and the degree to which individual mountain landscapes are prone to air temperature inversions. Current mountain permafrost models consider only elevation and aspect, and have not been able to deal with inversion effects in a systematic fashion. This thesis explores the relationship between air and ground surface temperatures and the presence of surface-based inversions at 27 sites within the Wolf Creek basin and surrounding area between 2001 and 2006, as a first step in developing an improved permafrost distribution TTOP model.

The TTOP model describes the relationship between the mean annual air temperature and the temperature at the top of permafrost in terms of the surface and thermal offsets (Smith and Riseborough, 2002). Key components of this model are n-factors which relate air and ground climate by establishing the ratio between air and surface freezing (winter) and thawing (summer) degree-days, thus summarizing the surface energy balance on a seasonal basis. Here we examine (1) surface offsets and (2) freezing and thawing n-factor variability at a number of sites through altitudinal treeline in the southern Yukon. Thawing n-factors (*n*t) measured at individual sites remained relatively constant from one year to the next and may be related to land cover. During the winter, the insulating effect

of a thick snow cover results in higher surface temperatures, while thin snow cover results in low surface temperatures more closely related to the winter air temperatures. The application of n-factor modeling techniques within the permafrost region, and the verification of these techniques for a range of natural surfaces, is essential to the determination of the thermal and physical response to potential climate warming in permafrost regions.

The presence of temperature inversions presents a unique challenge to permafrost probability mapping in mountainous terrain. While elsewhere the existence of permafrost can be linearly related to elevation, the presence of frequent inversions challenges this assumption, affecting permafrost distribution in ways that the current modeling techniques cannot accurately predict. At sites across the Yukon, inversion-prone sites were predominantly situated in U-shaped valleys, although open slopes, mid-slope ridges and plains were also identified. Within the Wolf Creek basin and surrounding area, inversion episodes have a measurable effect on local air temperatures, occurring during the fall and winter seasons along the Mount Sima trail, and year-round in the palsa valley. Within the discontinuous permafrost zone, where average surface temperatures are often close to zero, even a relatively small change in temperature in the context of future climate change could have a widespread impact on permafrost distribution.

ACKNOWLEDGEMENTS

This thesis would not have been possible without the knowledgeable supervision of Antoni Lewkowicz, whose guidance, dedication and incredible patience were paramount to the successful completion of this research. Countless hours spent discussing, planning and reviewing together have finally come to fruition – many, many thanks.

This research was supported financially by the Canadian Foundation for Climate and Atmospheric Sciences, Natural Sciences and Engineering Research Council (NSERC), the Northern Scientific Training Program (INAC), the Geological Survey of Canada, and the Yukon Geological Survey.

Many people assisted in the field component of this project. Thanks to Antoni Lewkowicz and Bernd Etzelmüller for help setting up numerous monitoring stations in unexplored and often inaccessible portions of the valley. A special thanks to Professor Etzelmüller for his many (unsuccessful) attempts to teach me German – Danke. I wish to thank Jim Coates and Martina Knopp for help with field data retrieval, for remaining calm during our grizzly encounter and for teaching me the fine art of off-road driving. Thanks are also extended to Philip Bonnaventure for assisting in the field and in the lab. His friendship, support and expert knowledge related to GIS modeling proved invaluable on many occasions.

Special thanks to my family and friends, whose unwavering support and encouragement kept me headed in the right direction. Last but not least, many thanks to my loving husband Ken for accepting my nerdy "love of frozen rocks", for agreeing to a honeymoon in Alaska and for sticking by my side through thick and thin.

TABLE OF CONTENTS

1.0 INTRODUCTION & BACKGROUND 1

1.1 Research Objectives 4

1.2 The Climate-Permafrost Relationship 5
1.2.1 The Surface Energy Balance 7
1.2.2 The N-Factor 9

1.3 Topography 11

1.4 Mountain Permafrost Modeling 14

2.0 STUDY AREA & METHODOLOGY 15

2.1 Study Area 15
2.1.1 Climate 18
2.1.2 Vegetation 18
2.1.3 Permafrost 20
2.1.4 Temperature Inversions 20

2.2 Study Sites 22
2.2.1 Site Selection 22
2.2.2 Site Descriptions 26
2.2.3 Additional Study Sites 31
2.2.4 Site Instrumentation 32

2.3 Data Collection and Analysis 32
2.3.1 Regional Lapse Rates and Calculation of Inversion Effect 34
2.3.2 Calculation of N-Factors 35
2.3.3 Potential Incoming Solar Radiation Mapping 36

2.4 Air Temperature Modeling 38
2.4.1 Regression Analysis 38
2.4.2 Modeling Mean July Air Temperatures 39
2.4.3 Treeline Analysis 39
2.4.4 Evaluation of the Model 40

3.0 AIR & GROUND SURFACE TEMPERATURE RELATIONS 40

3.1 Air Temperatures 40
3.1.1 Palsa valley site and Whitehorse Airport 41
3.1.2 Coal Ridge Transect 48
3.1.3 Mount Sima Trail 54
3.1.4 Newly Installed Wolf Creek Sites 65
3.1.5 Climatic Regions of the Yukon 69
3.1.6 Lapse Rates 73

3.2 Ground Surface Temperatures 74
3.2.1 Coal Ridge Transect 75
3.2.2 Mount Sima Trail 82
3.2.3 Newly Installed Wolf Creek Sites 87

3.3 **Air and Ground Surface Temperature Relations** 87
3.3.1 Potential Incoming Solar Radiation 91
3.3.2 Snow Accumulation 91
3.3.3 The Relationship between Air and Ground Surface Temperatures 99
3.3.4 The Surface Offset 101
3.3.5 The N-Factor 103

4.1 **Regression Analysis** 111

4.2 **Modeled Mean July Air Temperatures** 114

4.3 **Evaluation of the Model** 114

5.0 **DISCUSSION AND CONCLUSIONS** 124

5.1 **Discussion** 124
5.1.1 Air Temperature Inversions 124
5.1.2 N-Factors 125
5.1.3 Modeling Mountain Permafrost 127

5.2 **Conclusions** 129

5.3 **Future Research** 132

6.0 **REFERENCES** 135

LIST OF TABLES

		Page
Table 1	Site Descriptions	**21**
Table 2	Inversion episodes between YXY and P9 based on daily averages (2001-2006)	**43**
Table 3	Mean and standard deviation of air temperatures measured at YXY and P9 over five freezing and five thawing seasons (2001-2006)	**46**
Table 4	Inversion episodes along the Coal Ridge transect based on daily averages (2004-2006)	**52**
Table 5	Mean and standard deviation of air temperatures measured along the Coal Ridge transect over three freezing and two thawing seasons (2003-2006)	**53**
Table 6	Inversion episodes along the Mount Sima trail based on daily averages (2004-2006)	**61**
Table 7	Mean and standard deviation of air temperatures measured along the Mount Sima trail over two freezing and two thawing seasons (2004-2006)	**62**
Table 8	Mean annual air temperatures along the Mount Sima trail (August 2004 to July 2006)	**66**
Table 9	Average Air Temperatures at the Newly Installed Wolf Creek Valley Sites (June and July 2006)	**68**
Table 10	Lapse Rates	**72**
Table 11	Mean and standard deviation of ground surface temperatures measured along the Coal Ridge transect over three freezing and two thawing seasons (2003-2006)	**76**
Table 12	Mean and standard deviation of ground surface temperatures measured along the Mount Sima trail over two freezing and two thawing seasons (2004-2006)	**83**
Table 13	Average Ground Surface Temperatures at the Newly Installed Wolf Creek Valley Sites (June and July 2006)	**89**
Table 14	Maximum snow depth at the study sites over the 2005-2006 freezing season	**94**
Table 15	Annual surface offsets (Aug 2001 – Jul 2006)	**102**
Table 16	Seasonal dates used to determine n-factors at each of the study sites	**104**
Table 17	Freezing season n-factors (2001-2006	**105**
Table 18	Thawing season-n-factors (2002-2005)	**108**

Table 19	Summary of coefficients in the linear regression equation that includes elevation (Equation 6)	**113**
Table 20	Summary of coefficients in the linear regression equation that includes elevation, topography and PISR (Equation 7)	**113**
Table 21	Summary of coefficients in the linear regression equation that includes elevation and topography (Equation 8)	**113**

LIST OF FIGURES

		Page
Figure 1	Distribution of permafrost in the Yukon Territory	**2**
Figure 2	Mean annual temperature profile through the surface boundary layer, showing the relationship between air temperature and permafrost temperature (from Smith and Riseborough, 2002).	**6**
Figure 3	Study Area	**17**
Figure 4	Climate at Whitehorse	**19**
Figure 5	Topographic Position Index for Wolf Creek and Surrounding Areas	**25**
Figure 6	Site Photographs – Mount Sima Trail	**27**
Figure 7	Site Photographs - Coal Ridge Transect	**28**
Figure 8	Site Photographs – Newly installed Wolf Creek valley sites	**30**
Figure 9	Typical site instrumentation	**33**
Figure 10	Relations between average daily air temperatures at YXY and P9 (August 2001 to August 2006)	**42**
Figure 11	Average daily air temperatures at P9 and YXY in 2004	**44**
Figure 12	Relations between seasonal air temperatures at YXY and P9 (April 2001 to May 2006).	**47**
Figure 13	Mean annual air temperatures at P9 and YXY (August 2001 to July 2006)	**49**
Figure 14	Mean daily air temperatures at P9 and CR4 in 2004.	**51**
Figure 15	Average seasonal air temperatures along the Coal Ridge transect during five thawing and five freezing seasons (2001 to 2006).	**55**
Figure 16	Mean annual air temperatures along the Coal Ridge transect (August 2001 to July 2006)	**56**
Figure 17	Relations between daily air temperatures at Talmark and the Mount Sima trail sites	**58**
Figure 18	Mean daily air temperatures at T2 and T4 (November 2004 to February 2005)	**59**
Figure 19	Mean monthly air temperature along the Mount Sima trail (June 2004 to August 2006)	**60**
Figure 20	Average seasonal air temperatures along the Mount Sima trail during two thawing and two freezing seasons (2004 to 2006)	**64**

Figure 21	Mean Daily Air Temperatures at the Newly Installed Wolf Creek Valley Sites (May to August 2006)	**67**
Figure 22	Relationship between elevation and air temperature within five climatic regions of the Yukon for June and July 2006	**70**
Figure 23	Mean daily ground surface temperatures at P9 and CR4 (2004)	**77**
Figure 24	Average seasonal ground surface temperatures along the Coal Ridge transect during five thawing and five freezing seasons (2001 to 2006)	**79**
Figure 25	Mean annual ground surface temperatures along the Coal Ridge transect (August 2001 to July 2006)	**80**
Figure 26	Mean monthly ground surface temperatures along the Coal Ridge transect (August 2005 to July 2006)	**81**
Figure 27	Mean daily ground surface temperatures at T2 and T4 (2005)	**84**
Figure 28	Average seasonal ground surface temperatures along the Mount Sima trail during one thawing and two freezing seasons (2004 to 2006)	**85**
Figure 29	Mean annual ground surface temperatures along the Mount Sima trail (August 2004 to July 2006)	**86**
Figure 30	Mean monthly ground surface temperatures along the Mount Sima trail (August 2005 to July 2006)	**88**
Figure 31	Mean Daily Ground Surface Temperatures at the Newly Installed Wolf Creek Valley Sites (May to August 2006)	**89**
Figure 32	Potential incoming solar radiation density at the study sites for both the freezing and thawing seasons	**92**
Figure 33	Daily snow on the ground at the Whitehorse airport (October 2005 to April 2006).	**95**
Figure 34	Snow on the ground along the Mount Sima trail (October 2005 to May 2006)	**96**
Figure 35	Snow on the ground along the Coal Ridge transect (October 2005 to May 2006)	**98**
Figure 36	Mean monthly air and ground surface temperatures at T2 (boreal forest), CR3 (sub-alpine taiga), and CR4 (alpine tundra) over three years (August 2003 – July 2006)	**100**

Figure 37	The relationship between elevation, vegetation and seasonal n-factors at the study sites (2001-2006).	**106**
Figure 38	Calculated 9-day freezing and thawing n-factors for sites located within the boreal forest (T2), sub-alpine taiga (CR2), and alpine tundra (CR4) ecological zones (August 2003 – July 2006).	**110**
Figure 39	Modeled mean July air temperature – Elevation Model (Equation 6)	**115**
Figure 40	Modeled mean July air temperature – Final Temperature Model (Equation 8)	**116**
Figure 41	Location of treed areas according to NTS map sheets	**117**
Figure 42	Treed area as interpreted from Google Earth images	**119**
Figure 43	Location of treed area as interpreted from Google Earth images	**120**
Figure 44	Evaluation of the Model based on (a) NTS treeline and (b) interpreted treeline compared to the preliminary elevation model; and (c) NTS treeline and (d) interpreted treeline compared to the final temperature model.	**121**

1.0 INTRODUCTION & BACKGROUND

Permafrost is a thermal condition in which the temperature of earth materials remains at or below 0°C for at least two consecutive years (Brown and Péwé, 1973). It is a fundamental characteristic of the Canadian north, with nearly half of the total land surface of Canada located within regions where permafrost exists (Smith and Burgess, 2004). The distribution of permafrost in Canada is generally represented in terms of two broad zones, in which occurrence is described as continuous or discontinuous based on the proportion of the ground that is perennially cryotic (Heginbottom et al., 1995). The discontinuous zone is further subdivided into regions of widespread, sporadic and isolated patches of permafrost. Permafrost conditions within each of these zones are not uniform, with local factors playing an important role in the determination of distribution and thermal regime (Brown, 1973; Smith, 1975; Smith and Riseborough, 1983). The distribution of permafrost within the Yukon Territory in shown on **Figure 1**.

The general links between climate and permafrost are well known, although the precise nature of the relationship between air and ground temperatures remains poorly understood, particularly in complex mountain environments. At a continental scale, climate is the main factor controlling the formation and existence of permafrost (Brown and Péwé, 1973), with distribution defined primarily as a function of mean annual air temperatures. Within the discontinuous permafrost zone, site-specific conditions controlling ground heat flow and surface temperature regimes play an important role in determining permafrost presence or absence (Smith, 1975; Smith and Riseborough, 1983). Local environmental factors such as the depth of snow cover (Gold and

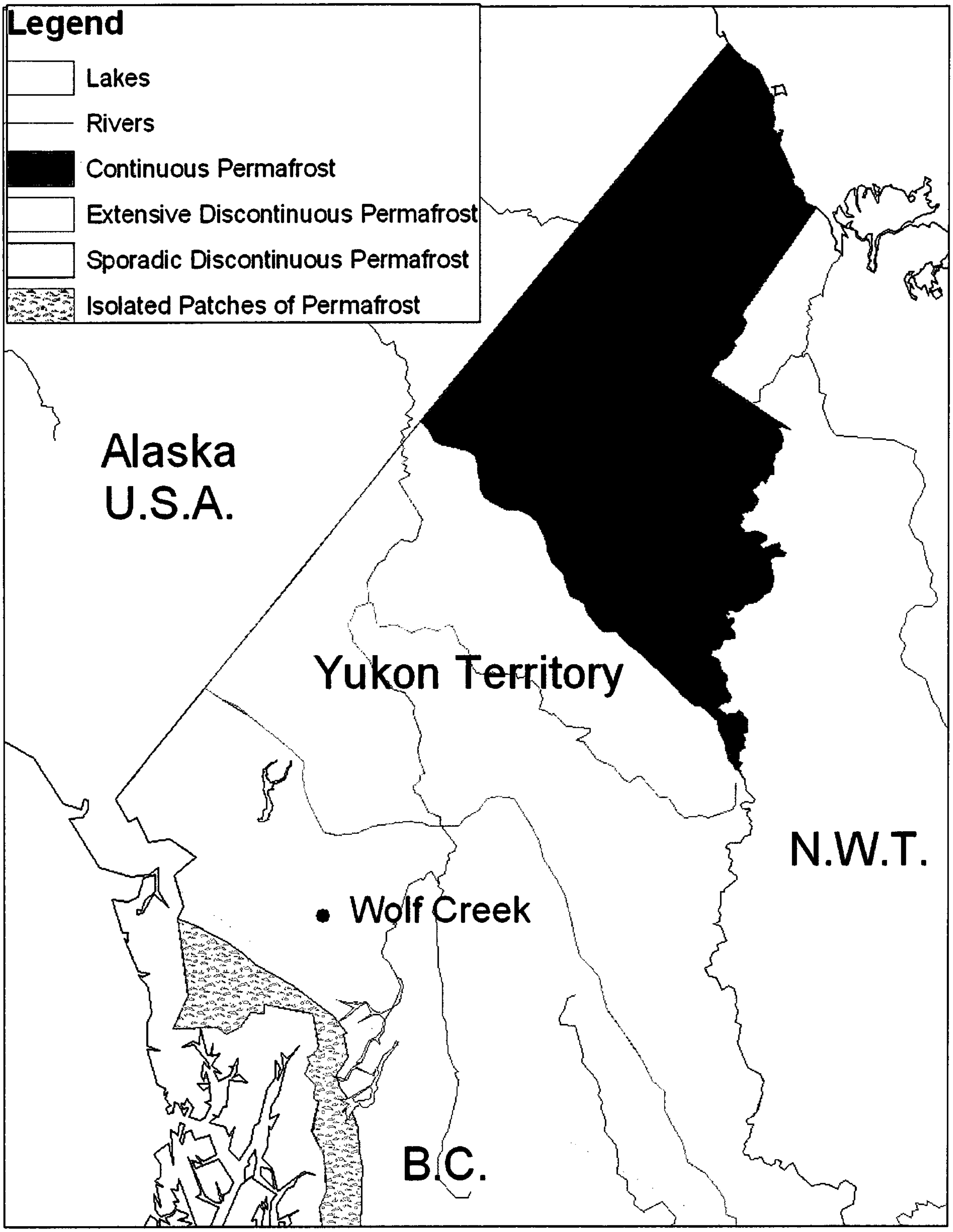

Figure 1: Distribution of permafrost in the Yukon Territory (Source: P. Bonnaventure)

Lachenbruch, 1973; Smith, 1975; Goodrich, 1978, 1982; Smith and Riseborough, 1983), soil properties (Goodrich, 1982; Smith and Riseborough, 1983), and the nature of the vegetation canopy (Smith, 1975; Jorgenson and Krieg, 1988; Beltrami and Kellman, 2003) are critical influences on the distribution of permafrost in these regions.

Within mountain environments, topography has been identified as one of the most important factors governing the distribution and occurrence of permafrost (Brown, 1973). Local relief influences the amount of potential incoming solar radiation (PISR) received at the ground surface, as well as snow accumulation patterns and vegetation growth (Brown, 1973; Etzelmüller et al., 2001). Within the discontinuous permafrost zone, the strong topographic and micro-climatic variability associated with mountainous terrain may lead to sporadic or patchy permafrost occurrence. Here, the effects of orientation and degree of slope are particularly evident and may result in the existence of permafrost on north-facing slopes, while absent on adjacent south-facing slopes (Brown, 1973). The phenomenon of mountain permafrost becomes increasingly complex when the influence of altitudinal changes of air temperature and the effects of atmospheric air temperature inversions on the surface energy balance are considered.

The ground surface temperature regime may be determined through detailed analysis of the energy balance, but this is impractical for prediction of permafrost distribution over large areas (Romanovsky and Osterkamp, 1995; Smith and Riseborough 1996; Klene et al., 2001). Accordingly, climate-permafrost relations must be simplified in order to produce regional permafrost maps, to assess the influence of various factors on localized ground temperatures, and to predict the potential effects of climate change on the ground thermal regime (Romanovsky and Osterkamp, 1995; Smith and Riseborough 1996, 2002;

Klene et al., 2001). Increased mean annual global air temperatures, in response to rising levels of atmospheric greenhouse gas levels, will affect the distribution and existence of permafrost, particularly within the discontinuous (warm) permafrost zone, where the magnitude, as well as the rate of climate warming, and projected future changes are expected to be more pronounced (Smith and Burgess, 2004).

1.1 Research Objectives

This thesis aims to advance the understanding of the climate-permafrost relationship as a first step in developing an improved permafrost distribution TTOP model (Juliussen and Humlum, 2007). Current mountain permafrost models consider only elevation and aspect (Lewkowicz and Ednie, 2004), and have not been able to deal with inversion effects in a systematic fashion. This study explores the effects of topography on the development of temperature variations in complex terrain, as it is believed that the occurrence of air temperature inversions may significantly affect permafrost distribution in these areas (Harris, 1982; Lewkowicz and Ednie, 2004; Lovatt and Lewkowicz, 2009). The research objectives are:

- To describe the relationship between air and ground surface temperatures within the Wolf Creek basin over the freezing and thawing seasons based on surface offsets, n-factors, elevation, snow accumulation and vegetation (2001-2006).
- To investigate mountain climate in various regions of the Yukon, including the frequency of air temperature inversions and the ability of the Topographic Position Index (TPI) to indentify inversion-prone sites.

- To produce an empirical-statistical model to predict mean monthly air temperatures for July, using treeline as an indicator of temperature, to test the output of a model that includes topography.

1.2 The Climate-Permafrost Relationship

The relationship between climate and permafrost can be represented by the mean annual air temperature and the permafrost surface temperature regimes (Lachenbruch et al., 1988), as defined by the surface and thermal offsets (**Figure 2**).

The surface offset is equal to the difference between the mean annual ground temperature (MAGT) and the mean annual air temperature (MAAT), as a function of the surface energy balance. The ground surface temperature (T_s) is influenced not only by air temperature (T_a) variations, but also by vegetation, snow cover and soil moisture availability, through a complex and complicated series of processes (Beltrami and Kellman, 2003). The thermal offset, as a function of the frozen ground thermal conductivities (Romanovsky and Osterkamp, 1995; Smith and Riseborough, 2002), is equal to the difference between the mean annual ground surface temperature (MAGST) and the mean annual temperature at the top of permafrost (TTOP). This offset arises because the thermal conductivity increases significantly from thawed to frozen soils. Accordingly, it has been demonstrated that the MAGT profile is offset within the active layer to progressively lower values at depth – with the coldest temperatures recorded at the top of permafrost (Goodrich, 1978; Smith and Riseborough, 1996). These findings are significant, as they provide an explanation for the presence of equilibrium permafrost

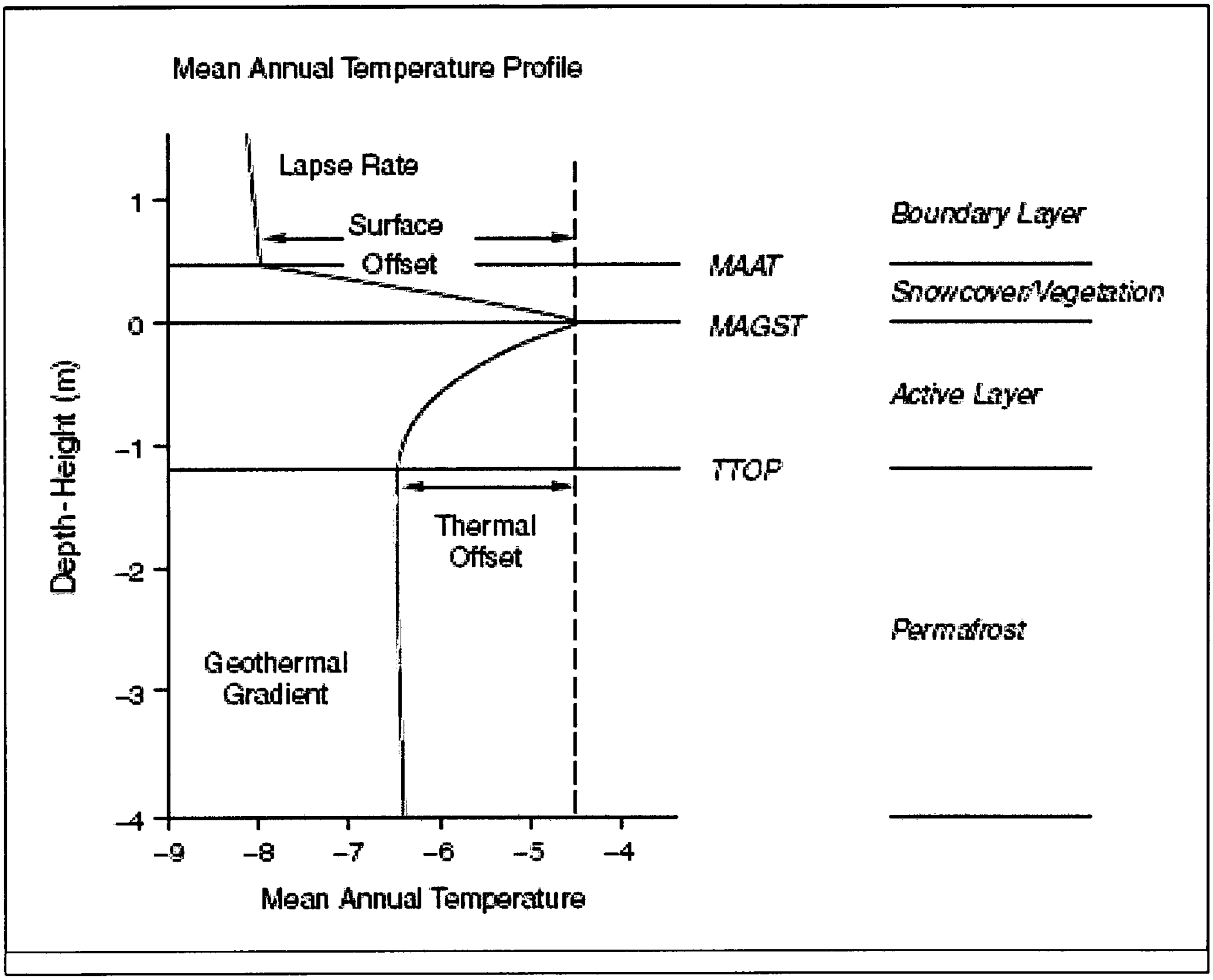

Figure 2: Mean annual temperature profile through the surface boundary layer, showing the relationship between air temperature and permafrost temperature (from Smith and Riseborough, 2002).

within the localized permafrost zone, where mean annual surface temperatures may be greater than 0°C. Furthermore, while permafrost is primarily controlled by climate, the thermal and surface offsets regulate the distribution of permafrost in both the continuous and discontinuous permafrost zones. The thermal offset, through the ground thermal conductivity, controls permafrost occurrence at the southern limit of the discontinuous permafrost zone; snow cover, via the nival offset, is the critical determining factor at the northern limit of the discontinuous zone (Smith and Riseborough, 2002). The focus of this thesis is on the air to ground surface temperature relationship, as there is currently limited data on heat transfer within the active layer and underlying permafrost available from the study sites.

1.2.1 The Surface Energy Balance

The Earth's radiation balance involves short-wave radiation (K) emitted by the sun and long-wave radiation (L) emitted by the earth-atmosphere system (Oke, 1978). The net radiation (Q*) at the ground surface is expressed as:

[1] $$Q^* = (K\downarrow - K\uparrow) + (L\downarrow - L\uparrow)$$

where $K\downarrow$ is the short wave radiation emitted from the sun, $K\uparrow$ is the short wave radiation reflected off the surface, $L\downarrow$ is the long wave emitted by the atmosphere or by local surface objects, and $L\uparrow$ is the long wave radiation emitted by the surface.

The amount of short wave radiation received by the surface, after any losses in the atmosphere, depends primarily on the angle at which the sun's rays strike the earth and the length of time of exposure to the rays. Thus, insolation varies on both a daily and seasonal basis. On a given day, values of $K\downarrow$ are greatest at noon, when the sun is highest, and lowest at sunrise and sunset. During the summer, when the sun's path is highest in the sky, the amount of $K\downarrow$ is high. Conversely, during the winter, when the duration of daylight is short, $K\downarrow$ is low. Other factors, such as increased cloud cover also affect values of $K\downarrow$, as varying amounts of radiation are absorbed, scattered and reflected back (Oke, 1978).

Locally, the surface energy balance further describes these fluxes of energy towards or away from the ground surface:

[2] $$Q^* = Q_H + Q_E + Q_G$$

where Q^* is the net radiation, which corresponds to a combination of the sensible (Q_H), latent (Q_E), and ground heat fluxes (Q_G). Conditions at and below the ground surface influence these heat fluxes, and account for spatial and temporal differences in the surface temperature (Smith, 1975; Karunaratne and Burn, 2004). In addition to the seasonal changes described above, variations in Q^* are also the result of changes to the surface albedo, caused by seasonal changes in snow accumulation and vegetation cover (Smith, 1975; Smith et al., 1998), or as the result of forest fires (Burn, 1998a). Similarly, changes in moisture availability are among the influences that regulate Q_H and Q_E, while changes in Q_G often reflect variations in the ground thermal conductivity (Karunaratne and Burn, 2004). The influence of variations in these fluxes on surface temperatures may in fact be stronger than increases in air temperatures (Smith and Riseborough, 1983). The low thermal conductivity of snow cover restricts sensible heat transfer, resulting in a warming at the ground surface, despite cold winter air temperatures (Gold and Lachenbruch, 1973; Smith, 1975; Goodrich, 1982). Likewise, lower rates of latent heat transfer through evapotranspiration, as the result of reduced vegetation cover following forest fires, lead to increases in surface temperatures in the absence of corresponding air temperature increases (Burn, 1998a).

While ground surface temperatures may be determined through a detailed analysis of the surface energy balance, these studies become increasingly complex when spatial variability is considered. An in-depth examination of the energy balance requires numerous field measurements to determine heat flux values for a given site (Klene et al., 2001). As a result, large-scale predictions of permafrost distribution present a unique challenge (Romanovsky and Osterkamp, 1995; Smith and Riseborough 1996; Stocker-Mittaz et al., 2002; Karunaratne and Burn, 2004).

1.2.2 The N-Factor

Regional modeling of permafrost distribution necessitates the simplification of energy balance calculations, so that the number of site-specific variables required is reduced to manageable levels (Klene et al., 2001; Smith and Riseborough, 2002; Smith and Burgess, 2004). Index methods relate T_s to T_a through the application of empirical n-factors (Lunardini, 1978). Using this method, the ratio between air and surface freezing (winter) and thawing (summer) degree-days is established (Burn, 2004). In order to obtain local surface temperatures, n-factors are applied as multipliers to seasonal air temperature indices, taking into account the influence of vegetation and snow cover (Smith and Riseborough, 1996; Burn, 2004). The thawing n-factor (*nt*) incorporates the effects of seasonal vegetation cover, while the freezing n-factor (*nf*) is dominated by the influence of winter snow conditions. These seasonal n-factors can be expressed as:

[3a] $$nt = \frac{TDD_s}{TDD_a}$$

and

[3b] $$nf = \frac{FDD_s}{FDD_a}$$

where FDD_a, TDD_a, and FDD_s, TDD_s, are the freezing (FDD) and thawing (TDD) degree-days for the air and surface, respectively (Taylor, 1995; Klene et al., 2001; Karunaratne and Burn, 2004). These indices are typically listed as part of climate normals recorded at Canadian climate stations across the north (Karunaratne and Burn, 2004).

When first developed, n-factors were generally used for artificial surfaces for the purposes of engineering, with relatively few considerations made for natural ground cover (Lunardini, 1978). Fuelled by intensified concerns about future climate warming, n-factors have been derived for a number of natural surfaces to assist in modeling regional permafrost conditions, and to predict the response of the permafrost environment to future climatic changes (Jorgenson and Kreig, 1988; Taylor, 1995; Smith et al., 1998; Burn, 1998b; Klene et al., 2001).

Published n-factor values suggest a number of generalities pertaining to the relationship between freezing and thawing indices (Jorgenson and Kreig, 1988; Taylor, 1995; Smith et al., 1998; Burn, 1998b; Klene et al., 2001; Kurunaratne and Burn, 2004).

Values of *nt* are generally higher than *nf*, indicating the separate influences of both the summer and winter seasons. As shown by Karunaratne and Burn (2004), values for *nt* tend to demonstrate more variability between sites, ranging from 0.10 in a closed spruce forest near Dawson City, Yukon (Smith et al., 1998) to 1.25 at a barren site in the Kuparuk River basin, Alaska (Klene et al., 2001). An n-factor of 1.0 corresponds to equivalent air and surface indices, while elevated values for either *nf* or *nt* indicate relatively cold winter surface temperatures and warm summer surface temperatures, respectively (Karunaratne and Burn, 2004). The values of *nf* and *nt* are subject to a number of seasonal influences, primarily snow and vegetation cover. Local snow cover distribution patterns are extremely variable from season to season, and over different terrain types for a given location (Smith and Riseborough, 1996), while summer surface conditions are generally more consistent (Karunaratne and Burn, 2004). Based on this inter-annual variability, values for *nf* are generally more inconsistent than for *nt* through time. The influence of additional factors, including the effect of latent heat transfers during annual freezeback, soil moisture contents, and site shading, must also be considered (Karunaratne and Burn, 2004).

1.3 Topography

Topography exerts a major influence on local climate, and is of particular interest to the development of temperature variations in alpine regions (Harris, 1986; Wahl *et al.*, 1987, Whiteman, 2000). In mountainous areas, the amount of incoming solar radiation can vary significantly within short distances, due to changes in elevation, surface orientation, and topographic shading (Thompson, 1986; Tabony, 1985; Gustavsson *et al.*, 1998; Colette *et al.*, 2003). This irregularity leads to high spatial and temporal variability in local environmental factors such as air and soil temperature regimes, evapotranspiration, snow melt patterns, and soil moisture availability (Manley, 1944). Within the discontinuous zone, the distribution and thickness of permafrost is primarily controlled by these terrain factors, which modify the effects of climate on the ground thermal regime (Brown and Péwé, 1973; Harris, 1986).

While the relationship between topographic factors and air temperature variations has been widely reported, much of this research has focused on the evolution and structure of the atmospheric boundary layer (e.g. Kuwagata and Kimura, 1990; Antequetin *et al.*, 1998; Clements *et al.*, 2003). This research base has its roots in the field of applied meteorology, involving systematic numerical investigations through which complex conceptual models of mountain boundary layer formation and destruction are formulated (e.g. Stull, 1973; Fast *et al.*, 1996). Other studies have been conducted to explore the ways in which changes in valley topographic parameters affect the structure and development of air temperature inversions (e.g. Tabony, 1985; Laughlin and Kalma, 1990; Lindkvist and Lindqvist, 1997). Rather than taking a fundamentally meteorological approach, these papers focus on the investigation of the spatial variability of air temperature patterns associated with cold air drainage and the pooling of cold air in mountainous areas (Gustavsson *et al.*, 1998). This literature on the effects of topography on the development of temperature variations in complex terrain is the most relevent.

The influence of geographic parameters on the air temperature variations in mountainous terrain has been attributed to two main factors: basin shape and shading (e.g. Kondo and Okusa, 1989; Gustavsson *et al.*, 1998; Colette *et al.*, 2003). The influence of valley geometry on inversion characteristics has been explored for a number of actual (Sakiyama, 1990) and idealized (Colette *et al.*, 2003) valleys, with variations in valley depth and shape parameters commonly identified as the governing topographic parameters (e.g. Borgen and Gustavsson, 1989; McKee and O'Neal, 1989; Kondo and Okusa, 1990). Sakiyama (1990) used the drainage area to volume ratio developed by Müller and Whiteman (1988) to analyse temperature differences in valleys with differing geometries. According to this model, relevant valley geometry is characterized by defining a topographic amplification factor (TAF), the basis of which lies in the thermal energy budget approach (Müller and Whiteman, 1988). The influence of topography is strongest when the width of the valley bottom is small (Colette *et al.*, 2003). As the valley floor widens, the slope effects become increasingly less important until the valley atmosphere behaves similarly to the boundary layer over flat terrain (Bader and McKee, 1985). Based on this understanding, the expected temperature changes during the day and night on the floor of a U-shaped valley would be less compared to the floor of a valley with a V-shaped profile. Other studies indicate that the depth and persistence of inversion layers is linked to the degree of incision of the valley (Gustavsson *et al.*, 1998; Colette *et al.*, 2003).

Thompson (1986) demonstrated that cold air pools may develop in the absence of cold air drainage, and instead attributed the development of strong temperature variations to the sheltering effect of topography in complex terrain. Following this premise, Colette *et al.* (2003) showed that local shelter plays an important role in the early morning development of valley slope winds, especially in steep, narrow valleys, where local topographic shading is greatest. In these areas, turbulent mixing of the cold surface air with the warmer air aloft is prevented, and as a result, surface cooling rates are intensified

(Tabony, 1985; Gustavsson *et al.*, 1998). Local shelter for the cold surface air may also be affected by differing valley orientations (Colette *et al.*, 1998) and dense vegetation cover (Gustavsson, 1995). As this suggests, differences in surface roughness and albedo influence the cooling profile, with increased roughness allowing sensible heat to be transported more efficiently, thus resulting in stronger air cooling (Kondo and Okusa, 1990). Similarly, Gustavsson *et al.* (1998) showed that the intensity of cold air pools is larger during the winter snow-covered state, when surface albedo is higher.

1.4 Mountain Permafrost Modeling

In recent years, a number of studies aimed at developing improved spatial models of mountain permafrost have been undertaken (Hoelzle et al., 2001). Current permafrost distribution models can generally be divided into two main categories: regionally calibrated empirical-statistical models and more physically based process-oriented models. Empirical-statistical models directly relate documented occurrences of permafrost to topo-climatic factors such as elevation, slope, aspect, MAAT and PISR (Hoelzle et al., 2001; Etzelmüller et al., 2001). Unlike the detailed energy balance measurements required by process-oriented models, these factors can be easily determined without treating the complex energy exchange processes at the ground surface explicitly (Hoelzle et al., 2001; Etzelmüller et al., 2001). As noted previously, the application of such detailed energy balance models is difficult in complex mountainous terrain, and is typically limited to small-scale areas where an extensive set of input parameters are readily available (Hoelzle et al., 2001). Therefore, permafrost modeling research has been primarily focused on the use of more easily applied empirical-statistical models (Stocker-Mittaz et al., 2002).

Recognizing the need for a spatial permafrost model, Juliussen and Humlum (2007) tested the regional Canadian TTOP model (Smith and Riseborough, 1996) against an existing model based on the basal temperature of snow (BTS) method and geophysical soundings in central-eastern Norway. The TTOP model involves a simple formulation of the climate-permafrost relationship and provides a framework for analyzing the influences of snow depth, ground surface characteristics and topographic effects on the ground thermal regime (Smith and Riseborough, 1996). The model uses seasonal n-factors and air temperature to model mean annual ground surface temperatures and a ratio of thawed to frozen thermal conductivity to model the average TTOP. While originally developed for use in continental-scale permafrost modeling, results from this study indicate that the TTOP model has potential in ground temperature modeling in mountainous terrain (Juliussen and Humlum, 2007).

2.0 STUDY AREA & METHODOLOGY

The purpose of this chapter is to describe the study area and methodology used for this thesis. Specifically, this chapter will provided a detailed description of the location and physical characteristics of both the study area and the study sites. In addition, a summary of the methods used in the field, as well as those used during data analysis and the modeling of temperature data is provided.

2.1 Study Area

Most of this study was carried out in and around the Wolf Creek basin (60°29'N, 135°12'W), an area of 195 km^2 in the headwaters region of the Yukon River, with elevations ranging from 800 m to 2250 m (Janowicz, 1999). The basin provides an ideal setting to examine air and ground surface temperature relations for a number of reasons. Glacial action in the area has resulted in complex terrain, characterized by gentle to rugged topography with deeply incised streams, creating localized extreme slope and aspect conditions over small lateral distances (Francis *et al.*, 1997). As a result, the basin exhibits strong topographic and micro-climatic variability in terms of elevation, potential incoming solar radiation, vegetation cover, and winter snow accumulation, often within short distances.

These variable conditions are represented within a relatively small, and easily accessible area, with logistic support available from Whitehorse, located approximately 15 km north of the basin (**Figure 3**). Research in the basin has been ongoing since the early 1990s, when the *Wolf Creek Research Basin Project* was initiated to provide a dedicated site to carry out applied research in the Yukon Sub-Arctic. Using an ecosystem approach, the project continues to integrate information from a variety of environmental studies, with a focus on hydrological, meteorological and ecological research. These studies, along with meteorological measurements collected at the Whitehorse Airport since April 1942, provided both context and additional data for this research.

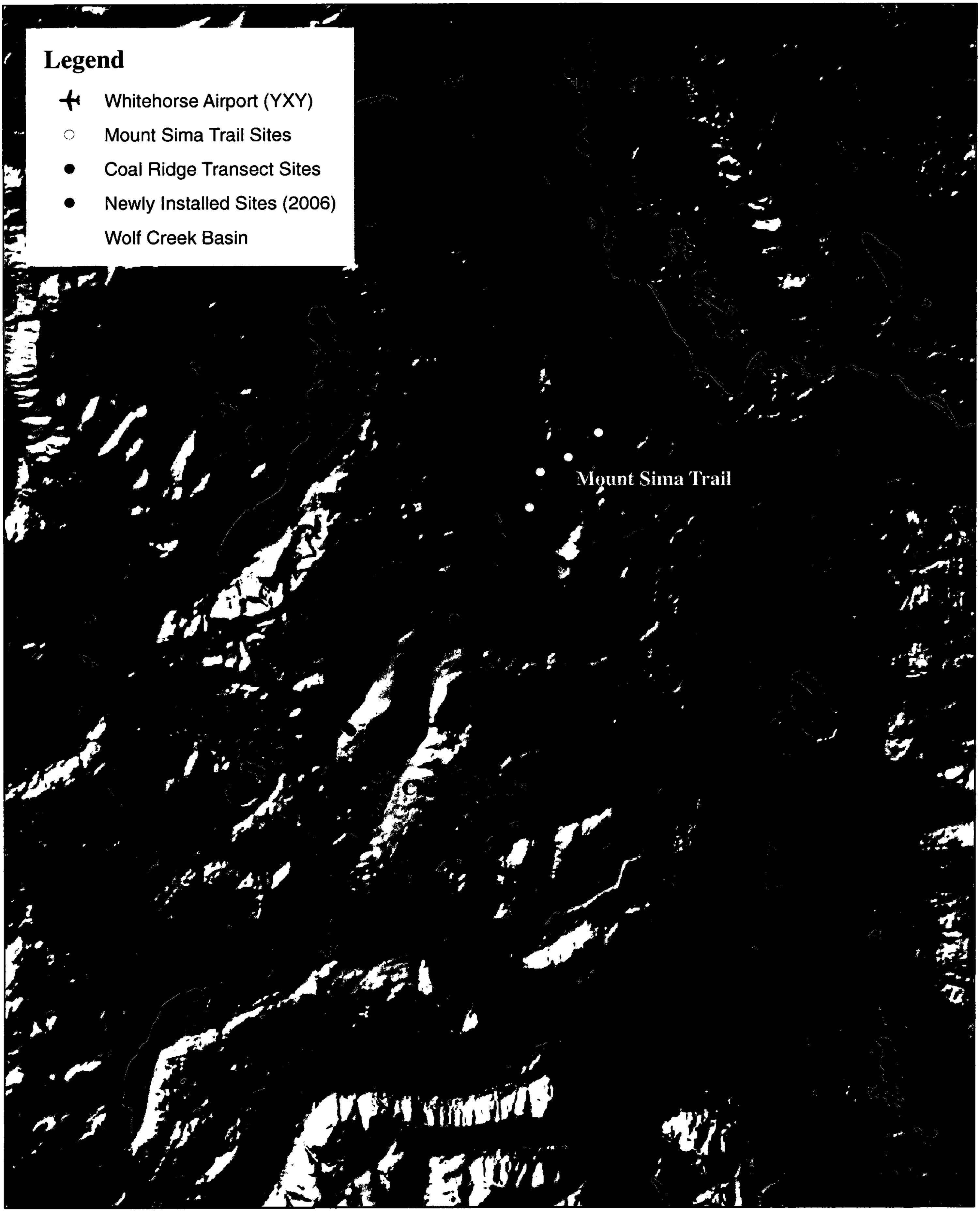

Figure 3: Study Area

2.1.1 Climate

The Wolf Creek basin is characterized by a large temperature range during the year, low relative humidity and relatively low precipitation rates, typical of a sub-arctic continental climate (Wahl *et al.*, 1987). Between 1971 and 2000, the temperature at the Whitehorse Airport (706 m) averaged -0.7°C, with approximately 267 mm of precipitation annually (Canadian Climate Normals 1971-2000, 2002) (**Figure 4**). The mean annual air temperature (MAAT) in Wolf Creek (at an unspecified elevation) is approximately -3°C, with summer and winter extremes reaching 25°C and -40°C, respectively (Janowicz, 1999). Precipitation averages 300 to 400 mm annually, an estimated 40% percent of which falls as snow (Janowicz, 1999). Snow cover is generally greatest on north-facing slopes, while high sublimation rates modify accumulation on south-facing slopes (Woo and Carey, 1999).

2.1.2 Vegetation

Francis *et al.* (1997) describe the Wolf Creek basin in terms of three major ecological zones that are mainly related to elevation: boreal forest, sub-alpine taiga and alpine tundra (Francis *et al.*, 1997). At elevations below 1100 m, where the terrain is characterized by a gentle rolling topography, vegetation is dominated by boreal spruce and pine forests (Francis *et al.*, 1997). Forming a broad zone between the forested lowlands and the alpine tundra, the sub-alpine taiga comprises open spruce forest and shrub communities which extend over the majority of the basin, with treeline situated at approximately 1300 m (Francis *et al.*, 1997; Janowicz, 1999). Localized areas of relief above 1500 m result in an abrupt transition to the alpine tundra zone, where slopes are dominated by low-lying shrub communities or are unvegetated (Francis *et al.*, 1997).

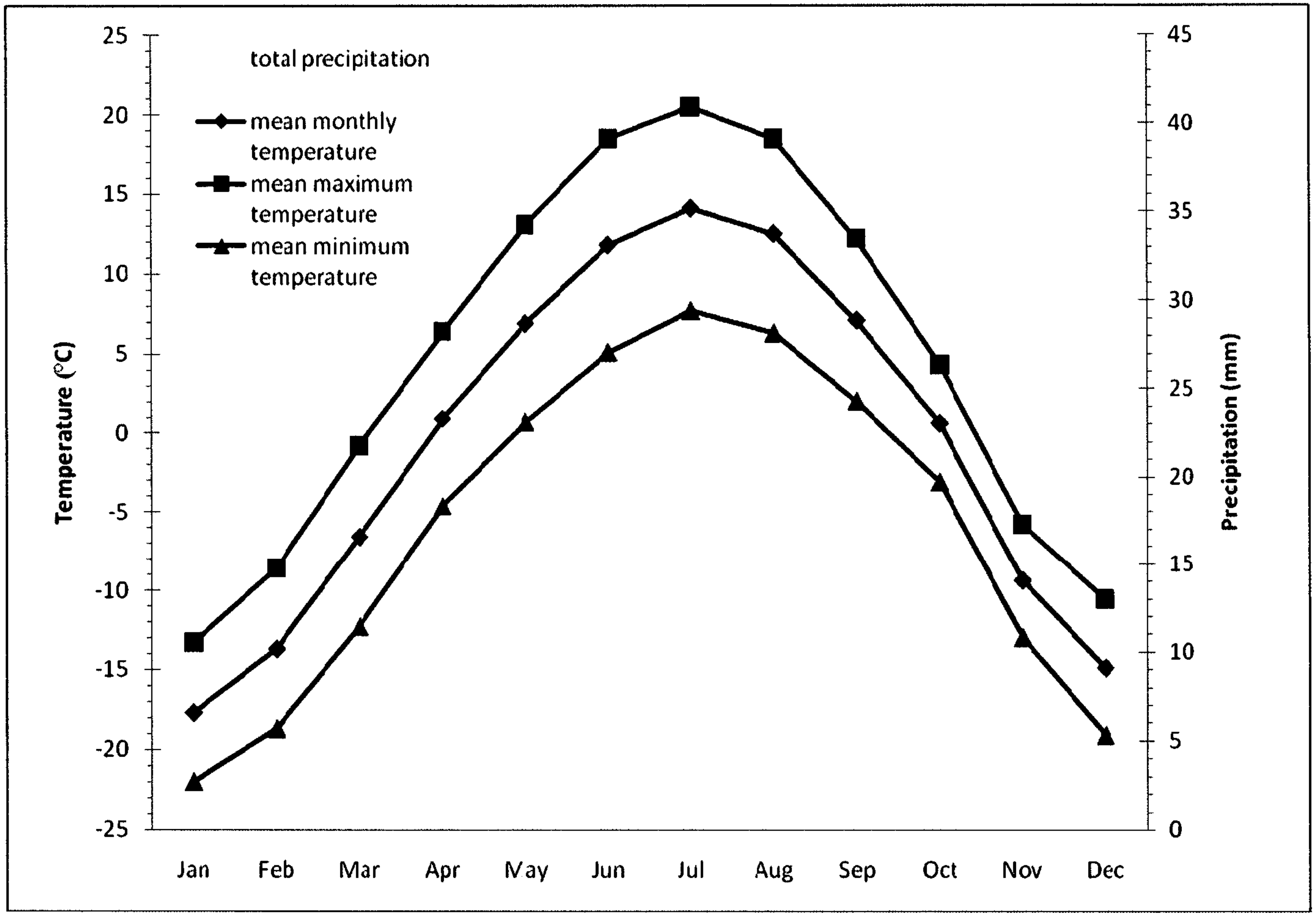

Figure 4: Climate at Whitehorse (Canadian Climate Normals 1971-2000, 2002)

The study sites located along the Coal Ridge transect and Mount Sima trail are distributed across these zones (**Table 1**). The three lowest sites along the Mount Sima trail (T1, T2 and T3) are located within the boreal forest, the uppermost Mount Sima trail site (T4) and lower Coal Ridge transect sites (P9, CR1, CR2 and CR3) are located within the sub-alpine tundra (which includes shrubs and scattered trees), and the remaining Coal Ridge sites (C4, CR5 and CR6) along with the bowl site (WC-Bowl) are located in the alpine tundra zone.

2.1.3 Permafrost

The basin is located within the sporadic discontinuous permafrost zone, with continuous permafrost found on mountain peaks at high elevation (Brown, 1973; Lewkowicz and Ednie, 2004). A previous study indicates that approximately 43 percent of the basin is underlain by permafrost (Lewkowicz and Ednie, 2004). According to Lewkowicz and Ednie (2004), permafrost probability varies from <0.1 in the lower areas to >0.9 on the peaks. However, field observations indicate that for a U-shaped valley adjacent to Coal Ridge (1250 m), actual permafrost probability is nearly twice that predicted by the model.

2.1.4 Temperature Inversions

Temperature inversions are known to occur in the main valleys of the Yukon (Wahl *et al.*, 1987), and air temperature records, starting in 2003 in upper Wolf Creek and extending into the main valley of the Yukon River in 2004, have shown that inversions are also frequent in the mountains. Inversion episodes are common year-round, occurring on average about 42% of the time, but are especially large and persistent in the winter

Table 1:Site Descriptions

Site	Elevation (m)	Slope (°)	Aspect	TPI	Ecological Zone	Description of Vegetation
WC-P9	1254	Flat		u-shaped valley	sub-alpine taiga	dwarf birch and willow (upto 80cm), some grasses
WC-CR1	1260		NW	u-shaped valley	sub-alpine taiga	10-15m below base of treeline
WC-CR2	1271		NW	u-shaped valley	sub-alpine taiga	lower treeline
WC-CR3	1363		NW	u-shaped valley	sub-alpine taiga	mid treeline
WC-CR4	1457		NW	mid-slope ridge	alpine tundra	upper treeline
WC-CR5	1495		NW	mesa	alpine tundra	above upper treeline: short alpine tundra and a few short shrubs (80%), clast-rich surface
WC-CR6	1555	Flat		mesa	alpine tundra	above upper treeline: willow/birch (60cm) slight S exposure
WC-Talmark	630	n/a		u-shaped valley	n/a	n/a
WC-T1	868	Flat		plains	boreal forest	open spruce (upto 9m), thick sphagnum
WC-T2	1011		NE	open slope	boreal forest	open spruce (upto 10m), willow-aspen understorey, thick decaying organics
WC-T3	1145		NE	open slope	boreal forest	moderately dense spruce (4-6m), moss/lichen
WC-T4	1290		NE	open slope	sub-alpine taiga	scattered trees, dwarf birch (upto 50-75cm), feather moss, adjacent to small stand of spruce (5-7m); just downslope of snow bank site
WC-Bowl	1640			mid-slope drainage	alpine tundra	scattered dwarf willow (upto 30cm), peat and grasses
WC2006-DR	1225	Flat		u-shaped valley	sub-alpine taiga	vegetation regrowth: grasses, young willow (30cm), flowering plants; bare ground
WC2006-1	1266	2	W	plains	sub-alpine taiga	at treeline: scattered pine/spruce (upto 7m), birch, grass and lichen
WC2006-2	1349	4	S	u-shaped valley	sub-alpine taiga	dense vegetation: birch (70-100cm), thick organic ground cover, some moss
WC2006-3	1387	10	SW	mid-slope ridge	sub-alpine taiga	70% birch (30-40cm), isolated spruce/pine, organic mat with lichen, small amounts of moss, and grass (some open grassy areas surrounding)
WC2006-4	1386	13	S	mid-slope ridge	sub-alpine taiga	85% birch (50-100cm), some willow (nearby), isolated spruce (above/below), 100% ground cover: grass, lichen, berry
WC2006-5	1390	8	SW	mid-slope drainage	sub-alpine taiga	65% willow (1.5-2m), grassy patches
WC2006-6	1426	16	SW	open slope	sub-alpine taiga	dense vegetation (100%): birch (30-50cm), some willow (70cm), no obvious ground cover: patch of lichen/herb to the N
WC2006-7	1288	4	S	u-shaped valley	sub-alpine taiga	50% birch (60-75cm), ground cover: moss, grass
WC2006-8	2066	Flat		mt. top	alpine tundra	felsenmeer - groundcover of lichen with some moss/grasses (40%)
WC2006-9	1378	10	N	mid-slope ridge	sub-alpine taiga	95% birch (50-70cm), 100% ground cover: moss, lichen and herb
WC2006-10	1373	23	N	mid-slope ridge	sub-alpine taiga	birch (to 2m), thick organic mat/ground cover: sphagnum, lichen, herbs, and grass
WC2006-11	1376	20	NW	mid-slope drainage	sub-alpine taiga	dwarf birch, 45% lichen, moss, and herb
WC2006-12	1373	15	N	open slope	sub-alpine taiga	50% birch (30-100cm), lichen, herbs and some moss (open patches)

(Lewkowicz and Smith, 2004). Previous studies indicate that cold air drainage likely has a considerable influence on the distribution of permafrost in the discontinuous zone, with inversions serving to maintain permafrost in valleys at low and mid-elevations (Harris, 1982; Taylor *et al.*, 1998). The frequency of air temperature inversions in the Wolf Creek basin is thought to affect permafrost distribution and may be responsible for permafrost at elevations where it would otherwise not be present (Lewkowicz and Ednie, 2004).

2.2 Study Sites

Air and ground surface temperature data were collected using temperature at thirteen sites, located along two previously established transects. The first transect is located in the main Yukon River valley, starting in the city of Whitehorse (607 m) and extending along the Mount Sima trail to nearly 1300 m. The second transect, running from 1230 m to 1600 m, is located in a mid-elevation valley in the Wolf Creek basin, approximately 20 km to the south. Thirteen additional air and ground monitoring sites were established in previously unexplored parts of the basin in late-May and early-June 2006. Also included in this record are air and ground surface temperatures collected from WC2006-DR, installed in a recently drained lake site located south of Coal Lake in May 2006.

2.2.1 Site Selection

Initial site selection was completed prior to spring fieldwork (2006), and involved the identification of local variations in topography to ensure that temperature monitoring stations were not exclusively installed on the same type of terrain. The required (30 m) digital elevation model (DEM) was obtained from *GeoBase*, and was projected in a GIS environment using ArcView software. Since the study area is covered by four 1:50,000 scale NTS sheets (105D6, 105D7, 105D10 and 105D11), initial preparations required editing to mosaic the tiles together and to correct minor projection errors. Subsequent steps included the use of the 'Spatial Analyst' extension to calculate neighbourhood statistics and the 'Topographic Position Index' (TPI) extension to classify the landscape. The latter uses ArcView software to calculate TPI grids from elevation grids, and provides a simple method for classifying the landscape into terrain units relating to slope position (e.g. ridge top, valley bottom, mid-slope) and landform category (e.g. open slope, U-shaped valley, plains) (Jenness, 2005). More specifically, the TPI is generated by comparing the elevation at each point on the DEM with the mean elevation of those cells that fall within a specified neighbourhood around that point, in this case a circle. Units are measured in metres above/below the mean elevation within the neighbourhood with positive values indicating a location higher than the surrounding area, and negative values representing lower elevations; values approaching zero may indicate a plain if slope is shallow, or a mid-slope area if the slope is more significant (Weiss, 2001; Jenness, 2005). The TPI is highly scale dependent, and classifications produced depend on the neighbourhood size selected for analysis. At a fine scale of 100 m, the topographic position of a point at the bottom of a large valley may be classified as a flat plain, while the same point is classified as a canyon or valley bottom at a scale of several kilometers. This larger scale is appropriate for research involving basin hydrology, mesoclimate, wind exposure, and cold air drainage (Weiss, 2001). By combining the TPI at both the small and large scale, a variety of nested landforms may be distinguished (Weiss, 2001). Landform classifications are, therefore, determined based on a combination of TPI values from different scales and slope position. Using standard deviation to distinguish between classes, grid cells can be identified as canyon, mid-slope drainage, upland drainage, U-shaped valley, plains, open slope, upper slope and mesa, local ridge, mid-slope ridge or mountain top. For the purpose of this research, the number of landform classifications was reduced from ten to seven; mid-slope and upland drainages were combined, mid-slope ridges were expanded to include local ridges, and canyons were grouped with U-shaped valleys.

Individual monitoring stations were sited to examine the effects of topographic position on air and ground surface temperatures, and to evaluate the importance of air temperature inversions. The sampling scheme aimed to reduce the effects of elevation, while maximizing variations in insolation values. Therefore, sites were located on both north and south facing slopes, at approximately the same elevation within the selected valley. The valley was chosen based on accessibility (by trail) and the presence of a range of landform classifications at approximately the same elevation and desired orientation. Eleven monitoring stations were installed between May 19 and June 8, 2007, within an elevation band of between 1288 m to 1426 m. Topographic positions were determined by combining TPI grids at the 300 m and 1500 m neighbourhood scales. Sites were classified as mid-slope ridges, open slopes or mid-slope drainages, with two valley bottom locations (**Figure 5**). Two additional measurement sites were established in exposed areas at different elevations; the first is located at the top of Mount Granger (2066 m) and the second on an exposed plain near treeline (1266 m). These sites were used to calculate air temperature control values, assuming that their temperatures are

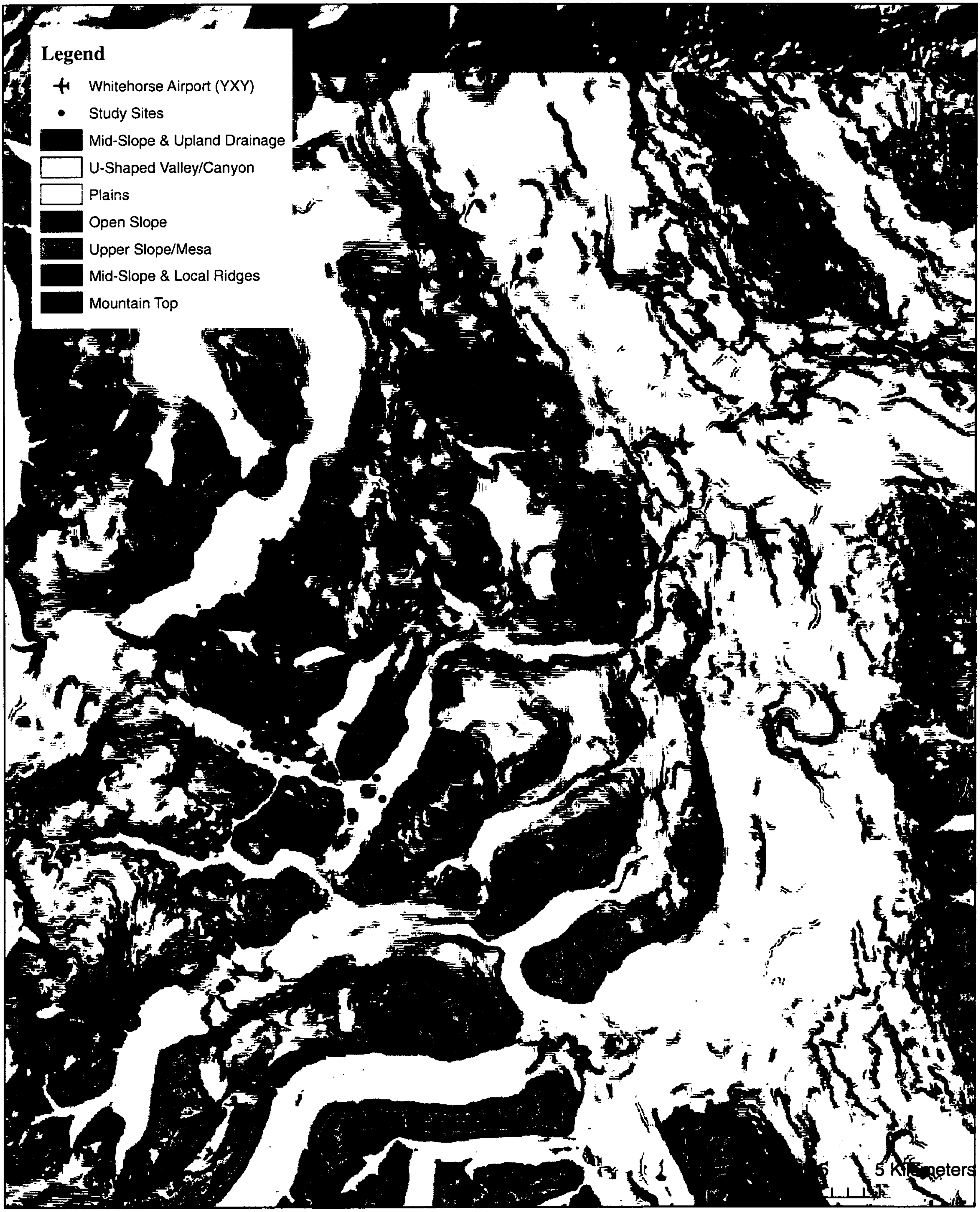

Figure 5: Topographic Position Index (TPI) for Wolf Creek and Surrounding Areas

representative of the boundary layer at the same elevations. The difference between the two also provides an estimate of the regional atmospheric lapse rate.

2.2.2 Site Descriptions

The twenty-five measurement sites used in this study are located within three distinct regions of the Wolf Creek basin and the surrounding area, as described above. This section provides detailed site descriptions for each of the sites, including elevation, aspect, vegetation cover and topographic position, as shown in **Table 1**. **Appendix A** provides the site coordinates.

There are four measurement sites located along the Mount Sima trail, representing a zone of transition between the boreal forest and sub-alpine taiga zones (**Figure 6**). The lowest site (T1) is located approximately 150 m from the base of the Mount Sima Road trail, in an open spruce forest with a thick sphagnum ground cover; the second boreal forest site (T2) is located within an area of similar vegetation cover, with spruce trees up to 10 m in height. Farther along the trail, the third site (T3) is located amid moderately dense spruce and a moss-lichen ground cover. The uppermost site (T4) is located immediately above treeline in the sub-alpine taiga zone. This site is located amid scattered trees and dwarf birch (50-75cm), and is adjacent to a small stand of spruce. A fifth site, located on the side of the Talmark building in downtown Whitehorse, provides air temperature data from the main Yukon River valley.

The Coal Ridge transect is located in a mid-elevation valley in the Wolf Creek basin, extending from the valley floor to the Coal Ridge summit plateau (**Figure 7**). The palsa valley site (P9) is located amid dwarf birch and willow measuring up to 80 cm and surrounded by various grasses and herbs. The remaining transect sites are located to the

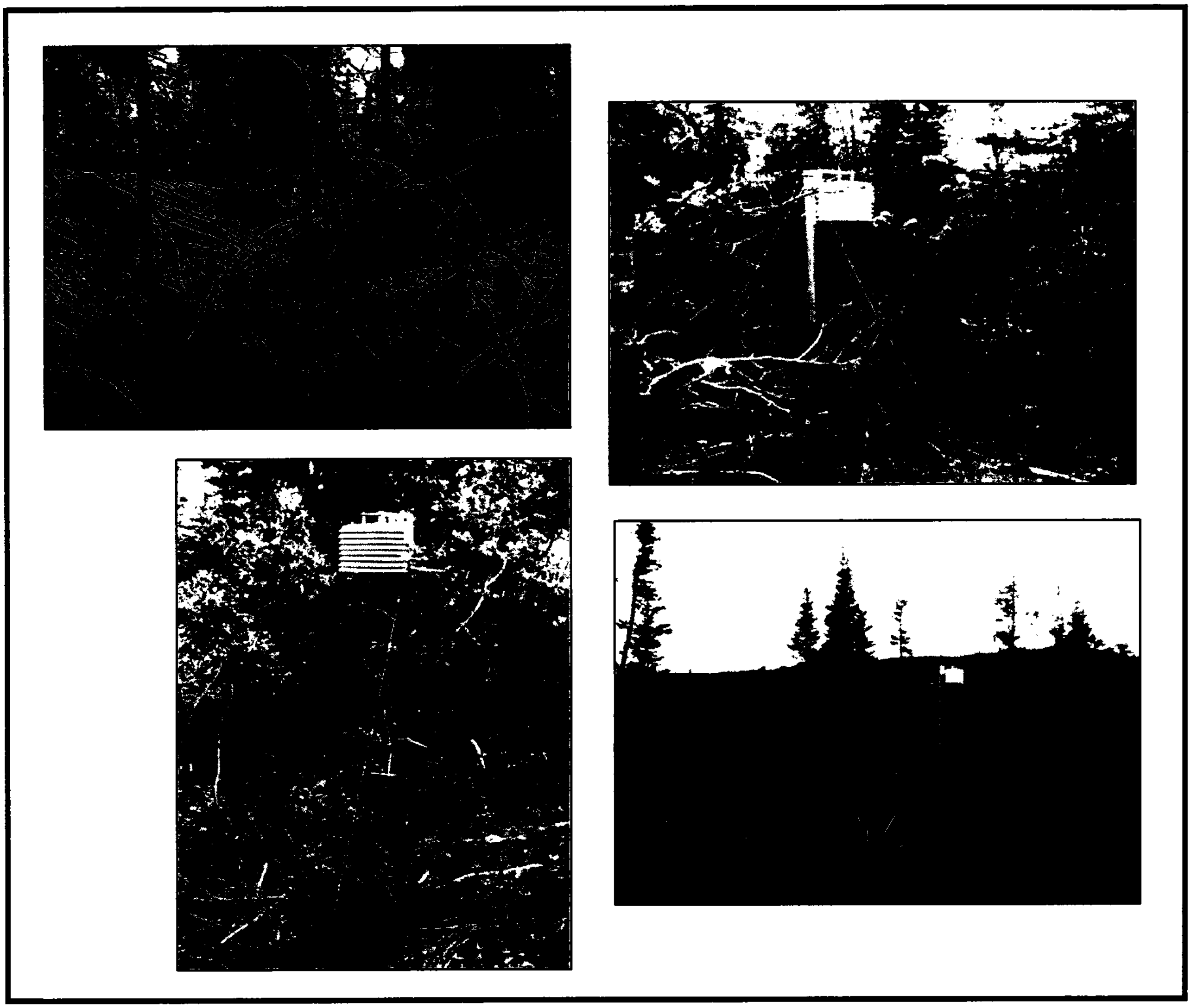

Figure 6: Site Photographs – Mount Sima Trail

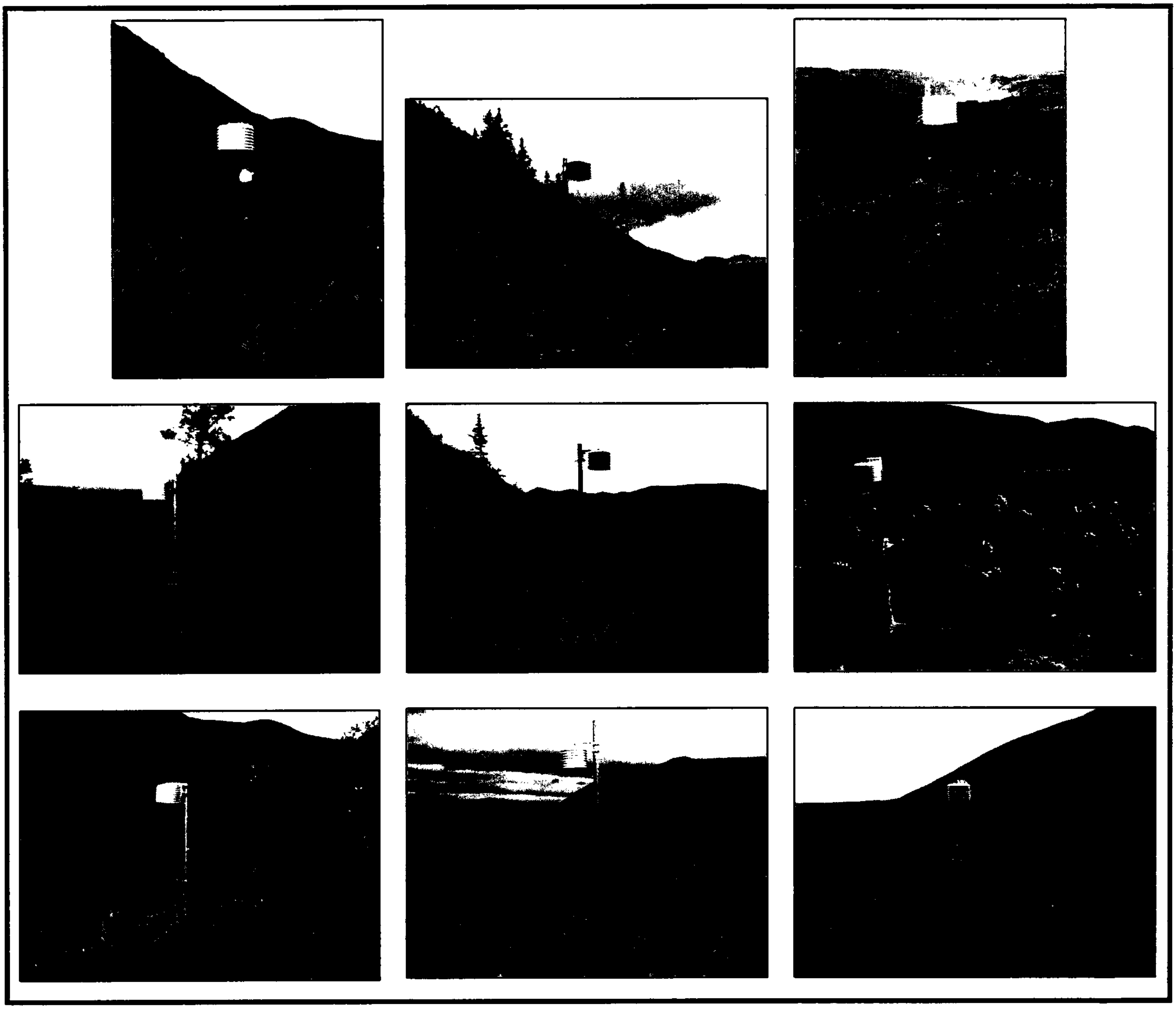

Figure 7: Site Photographs - Coal Ridge Transect.

Note: WC2006-DR and BOWL sites are not along the transect, but have been included because of proximity to Coal Ridge north of a sizeable debris flow fan, with the lowest site (CR1) located approximately 10 m below the base of treeline. Three stations are located within the transition zone between sub-alpine taiga and alpine tundra, with sites situated within lower (CR2), mid (CR3) and upper (CR4) treeline. Two additional monitoring stations (CR5 and CR6) were installed on the Coal Ridge plateau, above upper treeline, in summer 2005. Both sites are located within the alpine tundra zone, and are characterized by lower (CR5) or higher (CR6) dwarf birch and willow shrubs and a clast-rich surface. Also included with these sites is a station located within the alpine tundra zone to the south of Mount Granger, in the centre of a bowl feature (WC-Bowl) amid scattered dwarf birch and a thick sphagnum ground cover. An additional site was installed to the south of Coal Lake, within the sub-alpine taiga zone in Spring. This station is located in a recently drained lake site (WC2006-DR), where new vegetation growth had recently been established. The site is surrounded by grasses and various flowering plants.

During spring 2006, ten additional monitoring stations were established in a mid-elevation valley located in the south-western portion of the Wolf Creek basin, at the terminus of the Mount Sima Road trail (**Figure 8**). These sites are located within the sub-alpine taiga zone, and comprise a variety of vegetation covers along both north- and south-facing slopes. The sites are located at approximately the same elevation, with two sites located in the valley bottom – one in the eastern section of the valley (WC2006-7) and the other in the west (WC2006-2). These sites are located amid dwarf birch and willow measuring up to 100 cm and surrounded by moss and various grasses. Vegetation cover on the north-facing slope (WC2006-9, WC2006-10, WC-2006-11 and WC2006-12)

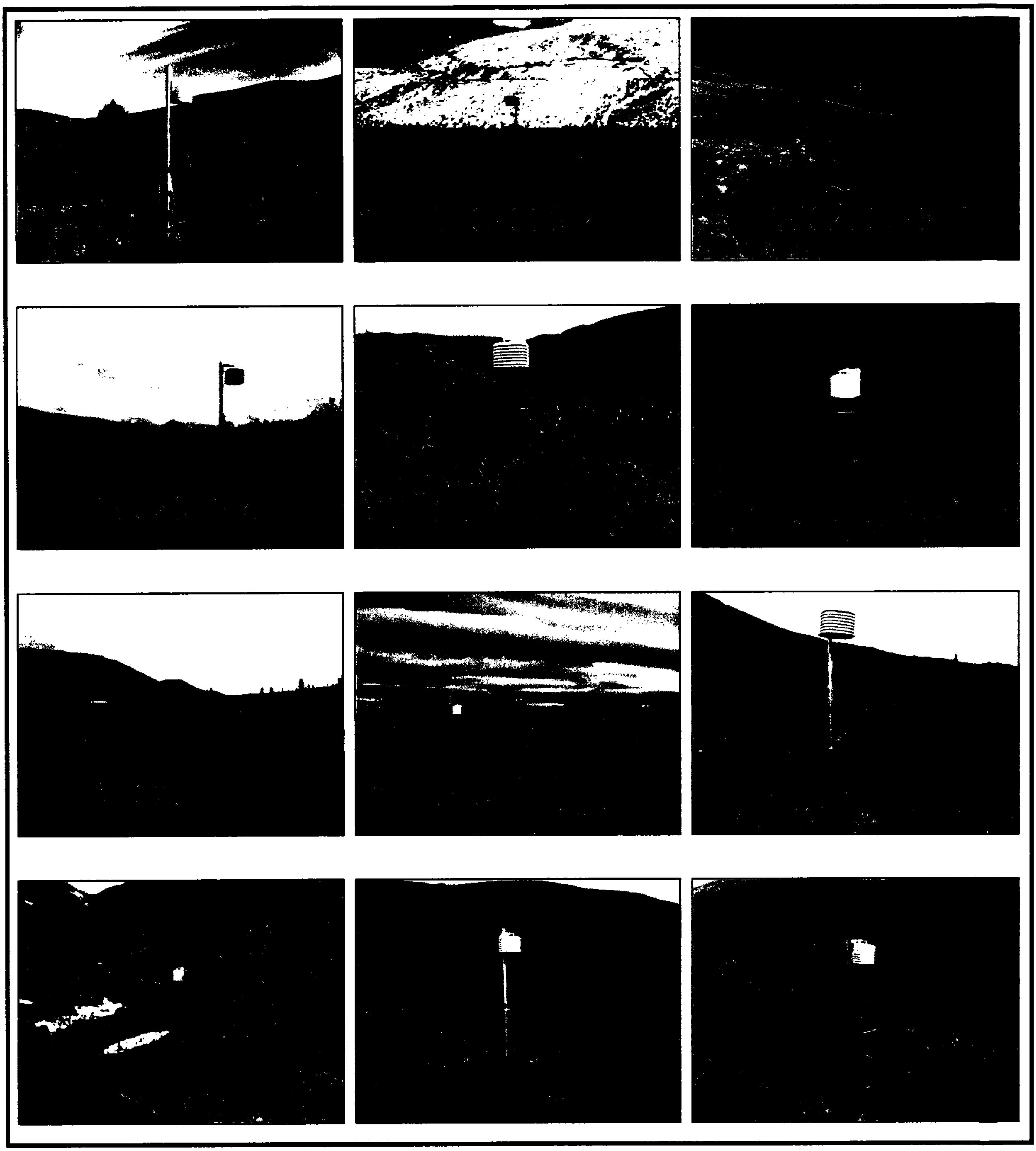

Figure 8: Site Photographs – Newly installed Wolf Creek valley sites

consists primarily of dwarf birch, with a varied ground cover of moss, grass, lichen and herbs.

Along the south-facing slope (WC2006-3, WC2006-4, WC2006-5 and WC2006-6), vegetation is both denser and more varied. The slope comprises dwarf birch and willow surrounded by isolated spruce and pine; ground cover at these sites is often quite thick, consisting mainly of grasses, herbs and berries. Two additional measurement sites were established in exposed sites outside the valley – the first on the almost unvegetated surface on the top of Mount Granger (WC2006-8), in an area covered largely by felsenmeer, and the second near treeline, amid tall willow and birch shrubs and scattered spruce and pine (WC2006-1).

2.2.3 Additional Study Sites

Ongoing permafrost research within the Yukon Territory provided an opportunity to collect additional data from a network of more than 50 air and ground temperature monitoring stations installed during the 2006 spring field season. These sites are situated within four of the climatic regions of the Yukon, as identified by Wahl et al. (1987), including the *Ogilvie-Mackenzie Mountains Climatic Region* (Keno), the *Central Yukon Basin Climatic Region* (Faro), the *Pelly-Cassiar Mountains Climatic Region* (Johnson's Crossing), and the *Liard Basin Climatic Region* (Sa Dena Hes mine site, north of Watson Lake). Data collected from these sites were used for comparison with air and ground surface temperatures recorded in the Wolf Creek basin, and to further assess the role played by topography on temperature variations in complex terrain. Individual stations were sited using the TPI (see Section 2.2.1) and instrumented according to the methods described in Section 2.2.4.

2.2.4 Site Instrumentation

Instrumentation at each site consists of two Onset Hobo Pro 8 data loggers; each logger measures temperature values hourly and is equipped with an internal and external thermistor (accuracy of ± 0.2°C across most of the measurement range) (**Figure 9**). The body of each logger, containing an internal thermistor, was installed just below the ground surface within the organic layer (< 5 cm). The external sensor was mounted within a solar radiation shield to measure hourly air temperature at a height of 1.5-1.6 m. Snowpack development over the winter was tracked using iButtons mounted in a vertical array onto a wooden stake (Lewkowicz, 2008). To reduce the potential for melt-pitting around the sensors, the stake is oriented northwards. Based on the relatively thin snowpacks in the study area, the loggers are installed at 10, 20, 30, 40, 60 and 80 cm. Temperature measurements are recorded by the I-Buttons sensors six times daily at four hour intervals. The iButton data was interpreted by comparing the measured values to air temperatures, by looking for trends and differences among the iButtons at a given site (Lewkowicz, 2008).

2.3 Data Collection and Analysis

Air and ground surface temperatures were measured at the previously established sites between August 2003 and August 2006, with supplementary data collected at the palsa valley site since April 2001. Snowpack development at the existing sites was tracked over the 2005-2006 winter season using the I-Button stakes installed during the previous summer's fieldwork.

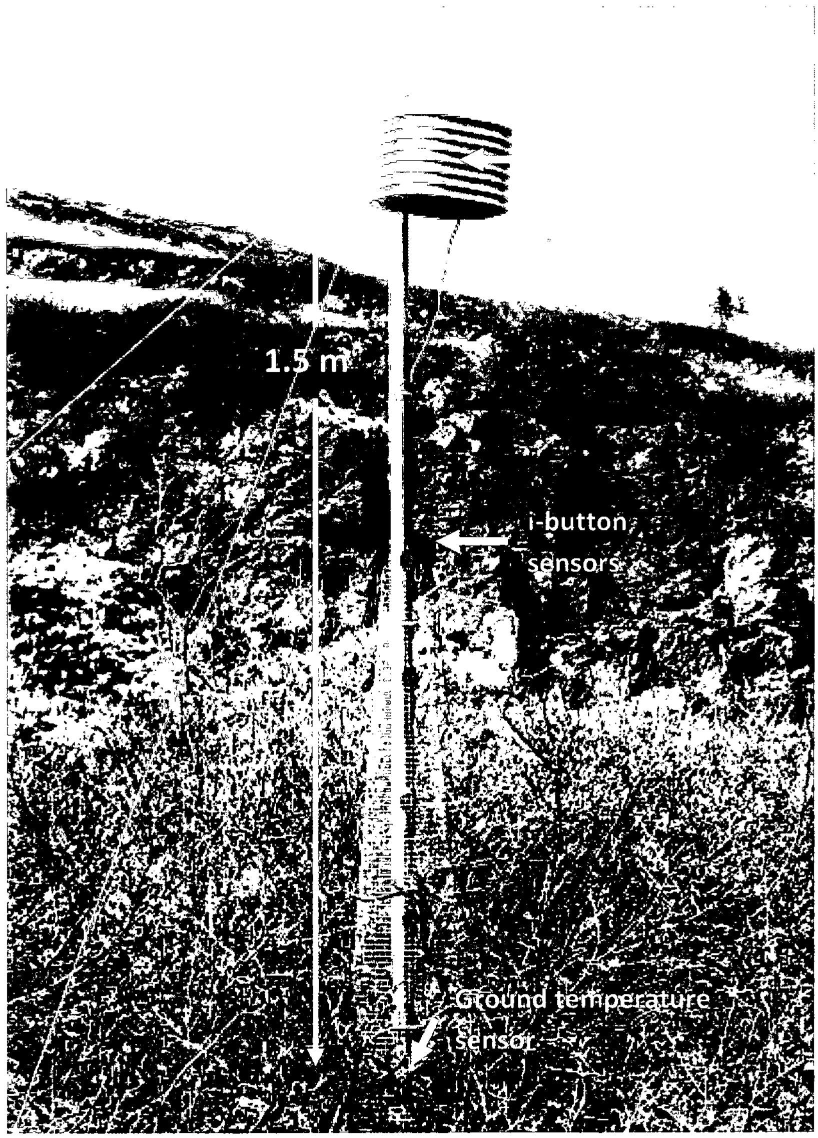

Figure 9: Typical site instrumentation

Summer air and ground surface temperatures measured between mid-May and late-August 2006 at the twelve newly installed sites provide two additional complete months of data for analysis (June and July 2006). Problems with logger failure hindered data collection at WC2006-4, and as a result there is no air temperature data available from this site. Lingering snow cover delayed installation of sites on the north-facing slope (WC2006-9, WC2006-10, WC2006-11 and WC2006-12), and as a result the period of record from these sites is shorter by one week; average June temperatures are, therefore, based on this shortened timeframe.

2.3.1 Regional Lapse Rates and Calculation of Inversion Effect

Lapse rates were calculated for each region based on two exposed control sites, one typically situated on a mountain top or high ridge, and the second at a lower elevation, typically located on a plains. These lapse rates were used to estimate the monthly air temperature for all remaining sites within a given region. Regional lapse rates were calculated as the ratio between the difference in average monthly air temperatures and the difference in elevation between the control sites. The following equation was used:

[4] $(T_{a1} - T_{a2}) / (z_2 - z_1)$

where T_{a1} is the average monthly temperature at the lower exposed site, T_{a2} is the average monthly temperature at the upper exposed site, z_1 is the elevation of the lower exposed site, and z_2 is the elevation of the upper exposed site.

Average monthly air temperatures at each of the sites within a given region were then estimated based on the average temperature at the upper exposed site, the regional lapse rate and elevation using the following equation:

[5] $T_{a2} + (z_2 - z_n) \times \text{lapse rate}$

Inversion-prone sites were identified as having lower air temperatures than predicted using equation [5]. The inversion effect was calculated as the difference between the measured average monthly air temperature and the estimated temperature at a given site. In order to take potential measurement errors into account, only those sites with temperatures 0.4°C cooler (or more) than predicted were considered inversion-prone.

2.3.2 Calculation of N-Factors

The n-factor is used to relate air and ground surface temperatures, thus summarizing the surface energy balance on a seasonal basis. In order to facilitate comparison of seasonal and inter-annual variability both at and among the study sites, initial analysis of air and ground surface temperature data used standard dates to define the freezing and thawing seasons. Over the study period, mean daily air temperatures measured at the study sites were generally above 0°C from May to September, and the thawing season is therefore defined as the period between May 1 and September 30. Conversely, mean daily air temperatures measured at the study sites were generally below 0°C from October to April over the study period, and the freezing season is therefore defined as the period between October 1 and April 30. In reality, however, the beginning and the end of the freezing and thawing season varies both spatially and through time. Following

Karunaratne and Burn (2004), individual freezing and thawing seasons at each of the sites were defined using ground surface temperatures. Based on this methodology, the thawing season began when the mean daily ground surface temperature rose above 0°C for three consecutive days, and ended when the mean daily surface temperature dropped below 0°C for three consecutive days. Similarly, the freezing season began when the mean daily ground surface temperature fell below 0°C for three consecutive days, and ended when the mean daily surface temperature rose above 0°C for three consecutive days (Karunaratne and Burn, 2004).

Given that the ratio of ground surface to air temperature fluctuates over the course of both the freezing and thawing seasons, 9-day freezing and thawing factors were also computed for the study sites to examine sub-seasonal variability (Karunaratne and Burn, 2004).

2.3.3 Potential Incoming Solar Radiation Mapping

A number of maps of potential incoming solar radiation (PISR) were created for the Wolf Creek basin using the 'Solar Analyst' extension developed by Fu and Rich (1999). This extension generates an upward-looking hemispherical viewshed for each location on the DEM and merges these viewsheds together to produce a total PISR density map (MJ/m^2). The extension allows a number of user-defined conditions in relation to latitude, topographic shading, diffuse proportion based on cloud cover, and transmisivity. The model requires the input of a single latitude on which to base calculations. Following Lewkowicz and Ednie (2004), the centre of the basin was chosen as best representing that area, and the latitude was, therefore, set to 60.5° N. To examine seasonal changes in radiation patterns at each of the sites, total cumulative potential incoming solar radiation was calculated over both the freezing (Oct 1 – Apr 30) and thawing seasons (May 1 – Sep 30). An additional PISR density map was also created using the input conditions identified by Lewkowicz and Ednie (2004) for the Wolf Creek basin, including a slightly shorter thawing season (May 15 – Sep 30).

The amount of solar radiation received at the ground surface is greatly influenced by aspect, with PISR density on south-facing slopes nearly twice that on north-facing slopes during the snow-free period (Lewkowicz and Ednie, 2004). As the amount of solar radiation received at the ground surface is greatly influenced by cloud cover, the extension considers this factor in both direct and diffuse radiation calculations over the basin. Possible cloud cover proportions range from 0 to 1, where 0 corresponds to clear skies, and 1 corresponds to full cloud cover. Based on data collected from the Whitehorse Airport meteorological station (Environment Canada), the cloud cover model was given a value of 0.66 for the freezing season, and 0.55 for the thawing season. This means that, during the winter season, direct beam radiation is said to account for 34% of the total PISR, while the amount of diffuse radiation over the basin is 66% of the total. The difference between these proportions is slightly reduced during the summer season, with direct beam radiation representing 45%, and diffuse radiation accounting for the remaining 55%. An atmospheric transmisivity of 0.5 was used for both the freezing and thawing season model calculations.

In addition to the work described above, monthly maps of PISR were created for the months of June and July in order to incorporate the effects of solar radiation into the final air temperature model. Once again, the cloud cover model was based on data collected from the Whitehorse Airport meteorological station (Environment Canada), with values of 0.55 and 0.56 given for June and July respectively; an atmospheric transmisivity of 0.5 was used for both summer months. The effects of differential shading by vegetation and/or differing surface albedos were not considered as part of this study.

2.4 Air Temperature Modeling

This section summarizes the major steps used to develop a model of mean July air temperatures for the Wolf Creek basin. Air temperature data collected during July 2006 provided an opportunity to investigate the relationship between the 10°C July temperature transition and the physical location of treeline within the study area, as a means of verifying the accuracy of modeled July air temperatures.

2.4.1 Regression Analysis

A series of multiple linear regression analyses based on values of elevation, seasonal PISR and topographic position were performed using SPSS statistical software. Initial analysis was aimed at determining the appropriate neighbourhood size (ranging from 300 m to 3000 m) to be used for the TPI classification. The analysis also involved applying a a modification which involved the elimination of all positive values from the TPI dataset. Negative values indicate a location lower than the surrounding area, where the effects of air temperature inversions are expected to be greatest. Thus, the modified TPI values included only those sites likely to be affected by inversions. The results of this preliminary analysis indicated that future models should be focused on a modified TPI with a neighbourhood size of 500 m.

2.4.2 Modeling Mean July Air Temperatures

The ArcMap raster calculator was used to apply the selected regression equations to the projected DEM. The resultant values were displayed as mean July air temperature maps for the Wolf Creek basin and surrounding area.

2.4.3 Treeline Analysis

During an investigation of the basal temperature of snow (BTS) method of permafrost prediction in the basin, Ednie (2003) identified the presence of widespread permafrost in the confined valley on the west side of Coal Ridge at relatively low elevations, together with the presence of an inverted treeline along the valley side slopes. These findings suggest the presence of cold air drainage, resulting in temperature inversions within the valley. Ednie (2003) concluded that the presence of temperature inversions was likely to affect the distribution of permafrost on the valley floor, leading to greater distribution of permafrost than would be expected based on elevation and PISR alone.

The inverted treeline, identified through field observation and described by Ednie (2003) is not only absent from the NTS map sheets, but extends into areas well beyond the limits of treeline shown on the maps. Using high resolution Google Earth images, the position of treeline within a portion of the Wolf Creek basin was explored. The portion of the basin selected for this analysis includes an area of approximately 278 km^2, where image resolution is the highest. Given the superior quality of the imagery available over much of the study area, individual trees were easily identifiable under magnification.

The methodology for selecting individual trees involved a certain degree of subjectivity as a boundary line was drawn to separate forested and unforested areas.

Individual trees and groups of trees were circled, creating a series of polygons to represent the actual position of the treed areas within the study area. The polygons were then imported to ArcMap for comparison with the NTS-defined treeline and the modeled 10°C July temperature transition. Data obtained through GeoBase provided a shapefile of the NTS-defined treeline for use in the Arc environment.

2.4.4 Evaluation of the Model

The predicted position of treeline within the Wolf Creek basin was evaluated using a confusion matrix. The number of cells within each category was determined using zonal statistics. In order to evaluate the validity of the modeled mean July air temperatures, predicted temperatures from both models were compared with the presence or absence of trees in each cell. Misclassified cells were defined as treed cells with predicted July temperatures below 10°C and those with predicted temperatures above 10°C but without trees. The fact that the models are based on a single year of data, not long-term means, likely accounts for some degree of imprecision. The use of 10°C as a limit for tree growth introduces another source of inaccuracy.

3.0 AIR & GROUND SURFACE TEMPERATURE RELATIONS

3.1 Air Temperatures

The purpose of this section is to investigate air temperatures measured at the study sites between 2001 and 2006. Specifically, this section describes the air temperature regime at the existing monitoring stations by considering temperature trends over various time scales (i.e. daily, monthly, seasonal, annual), both at and among sites located throughout the Yukon.

3.1.1 Palsa valley site and Whitehorse Airport

Air temperatures measured at P9 (1254 m asl) between August 2001 and July 2006 were compared to air temperatures measured at the Whitehorse Airport (YXY) climatological station (706 m asl) over the same period. The average temperature at YXY (0.4°C) was 3.2°C warmer than at the palsa valley site (-2.8°C) over the five years. This closely approximates the expected difference of 3.6°C, based on a mean environmental lapse rate of 6.5°C/km, and an elevation difference of nearly 550 m. As shown in **Figure 10**, the separation between the winter and summer seasons is evident in the large amount of scatter at sub-zero temperatures, compared to that at higher temperatures, likely the result of the greater influence of winter temperature inversions.

Daily values show that, while P9 always experienced cooler air temperatures than Whitehorse during the summer, winter air temperatures were warmer than those measured at the airport for extensive periods between September and March, with peak frequency in the month of January (**Table 2**). On average, these periods redeveloped for 2.4 successive days, with some occurring for as many as 17 consecutive days (January-February 2004). In 2004, there were 27 days in January when air temperatures at P9 exceeded those recorded at the Whitehorse airport (**Figure 11**). As a result, mean monthly January temperatures at P9 exceeded those recorded at YXY in 2004 and 2005; monthly January averages measured at the sites are equal in the remaining three years of record (2002, 2003 and 2006).

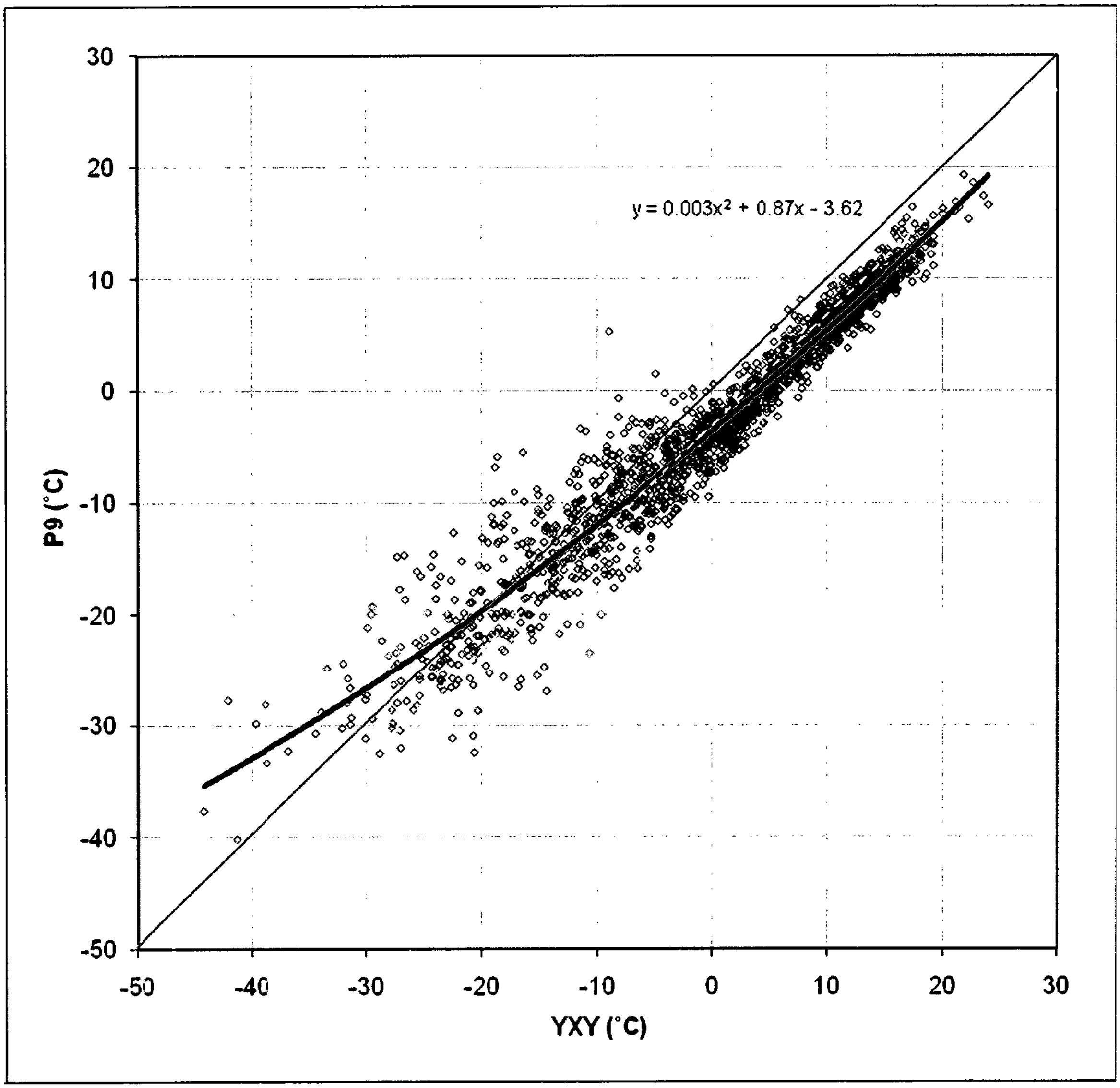

Figure 10: Relations between average daily air temperatures at the Whitehorse Airport (YXY) and P9 (August 2001 to August 2006). Note: The relationship between the two sites is not linear and does not parallel the 1:1 line (solid line). The dashed line represents the expected difference of 3.6°C, based on a mean environmental lapse rate of 6.5°C/km, and an elevation difference of nearly 550 m.

Table 2: Inversion episodes between YXY and P9 based on daily averages (2001-2006)

2001	Jan	Feb	Mar	Apr	May	Jun	Jul	Aug	Sep	Oct	Nov	Dec	Annual Total
Total number of days with inversions				0	0	0	0	0	0	0	6	17	23
Longest consecutive days with inversions				-	-	-	-	-	-	-	2	7	
Frequency (%)				-	-	-	-	-	-	-	0.19	0.57	0.08

2002	Jan	Feb	Mar	Apr	May	Jun	Jul	Aug	Sep	Oct	Nov	Dec	Annual Total
Total number of days with inversions	16	5	5	0	0	0	0	0	2	1	0	4	33
Longest consecutive days with inversions	6	2	3	-	-	-	-	-	2	1	-	2	
Frequency (%)	0.52	0.18	0.16	-	-	-	-	-	0.06	0.03	-	0.13	0.09

2003	Jan	Feb	Mar	Apr	May	Jun	Jul	Aug	Sep	Oct	Nov	Dec	Annual Total
Total number of days with inversions	17	11	5	0	0	0	0	0	0	1	7	12	53
Longest consecutive days with inversions	5	4	2	-	-	-	-	-	-	1	3	4	
Frequency (%)	0.55	0.39	0.16	-	-	-	-	-	-	0.03	0.23	0.40	0.15

2004	Jan	Feb	Mar	Apr	May	Jun	Jul	Aug	Sep	Oct	Nov	Dec	Annual Total
Total number of days with inversions	27	7	5	0	0	0	0	0	0	0	9	10	58
Longest consecutive days with inversions	17		3	-	-	-	-	-	-	-	3	3	
Frequency (%)	0.87	0.24	0.16	-	-	-	-	-	-	-	0.29	0.33	0.16

2005	Jan	Feb	Mar	Apr	May	Jun	Jul	Aug	Sep	Oct	Nov	Dec	Annual Total
Total number of days with inversions	26	4	1	0	0	0	0	0	0	1	6	7	45
Longest consecutive days with inversions	15	2	1	-	-	-	-	-	-	1	4	3	
Frequency (%)	0.84	0.14	0.03	-	-	-	-	-	-	0.03	0.19	0.23	0.12

2006	Jan	Feb	Mar	Apr	May	Jun	Jul	Aug	Sep	Oct	Nov	Dec	Annual Total
Total number of days with inversions	12	9	0	0	0	0	0	0					21
Longest consecutive days with inversions	4	3	-	-	-	-	-	-					
Frequency (%)	0.39	0.32	-	-	-	-	-	-					0.09

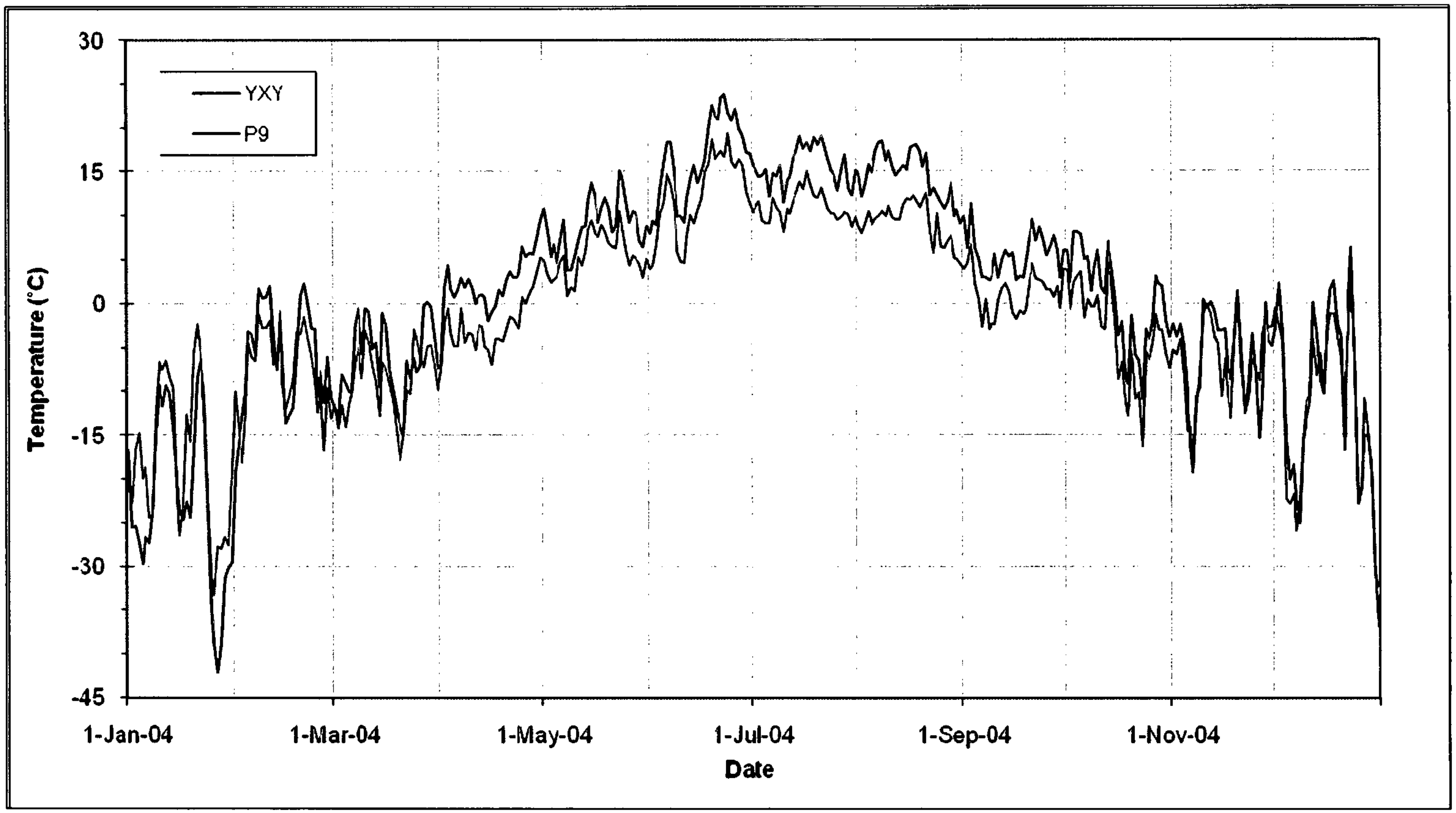

Figure 11: Average daily air temperatures at P9 and YXY in 2004

Day-to-day air temperatures were most variable during the winter season throughout the period of record (**Table 3**). Mean daily air temperatures were typically above 0°C from May to September, and below 0°C from October through April. Minimum daily winter temperatures occurred in mid-January 2005 at both sites, with temperatures dipping to -40.2°C at P9 and -44.2°C at Whitehorse. Day-to-day variability was considerably lower during the summer. Maximum daily summer temperatures were recorded at the end of June 2004, with temperatures exceeding 19°C at P9 and 23°C at the airport station.

Seasonal values computed for five thawing and five freezing seasons indicate that, despite the periods discussed above, air temperatures measured at Whitehorse are warmer than those recorded at P9 over both seasons (**Figure 12**), as expected based on a mean environmental lapse rate of 6.5°C. The degree to which Whitehorse is warmer varies seasonally, and is greater during the thawing season than during the freezing season, with average differences of 4.5°C and 2.2°C respectively. The coldest winter season during the period of study occurred in 2001-2002 at both the airport and valley bottom locations. The warmest winter season occurred the following year (2002-2003), with temperatures nearly 4°C warmer recorded at YXY. Seasonal air temperatures recorded at P9 over the same period are also the coldest on record, however, seasonal values computed for 2002-2003 and 2004-2005 are within the accuracy of the sensors (± 0.2°C) and cannot be considered significantly different. The coldest summer season is more difficult to determine, as seasonal values computed at both sites for 2001, 2002 and 2003 are within 0.1°C and are thus too similar to be determined. The warmest summer season occurred in

Table 3: Mean and standard deviation of air temperatures measured at YXY and P9 over five freezing and five thawing seasons (2001-2006)

	average seasonal air temperature		standard deviation	
	YXY	P9	YWY	P9
Thawing season 2001	10.5	5.8	4.1	4.3
Freezing season 2001-2002	-9.5	-11.5	9.3	8.1
Thawing season 2002	10.4	6.1	4.4	4.5
Freezing season 2002-2003	-5.4	-8.2	8.9	8.2
Thawing season 2003	10.3	6.0	4.6	4.5
Freezing season 2003-2004	-7.5	-9.1	10.4	7.9
Thawing season 2004	12.4	7.8	5.2	4.9
Freezing season 2004-2005	-6.5	-8.4	10.5	8.5
Thawing season 2005	11.5	7.1	3.4	3.2
Freezing season 2005-2006	-7.7	-10.5	9.2	8.4

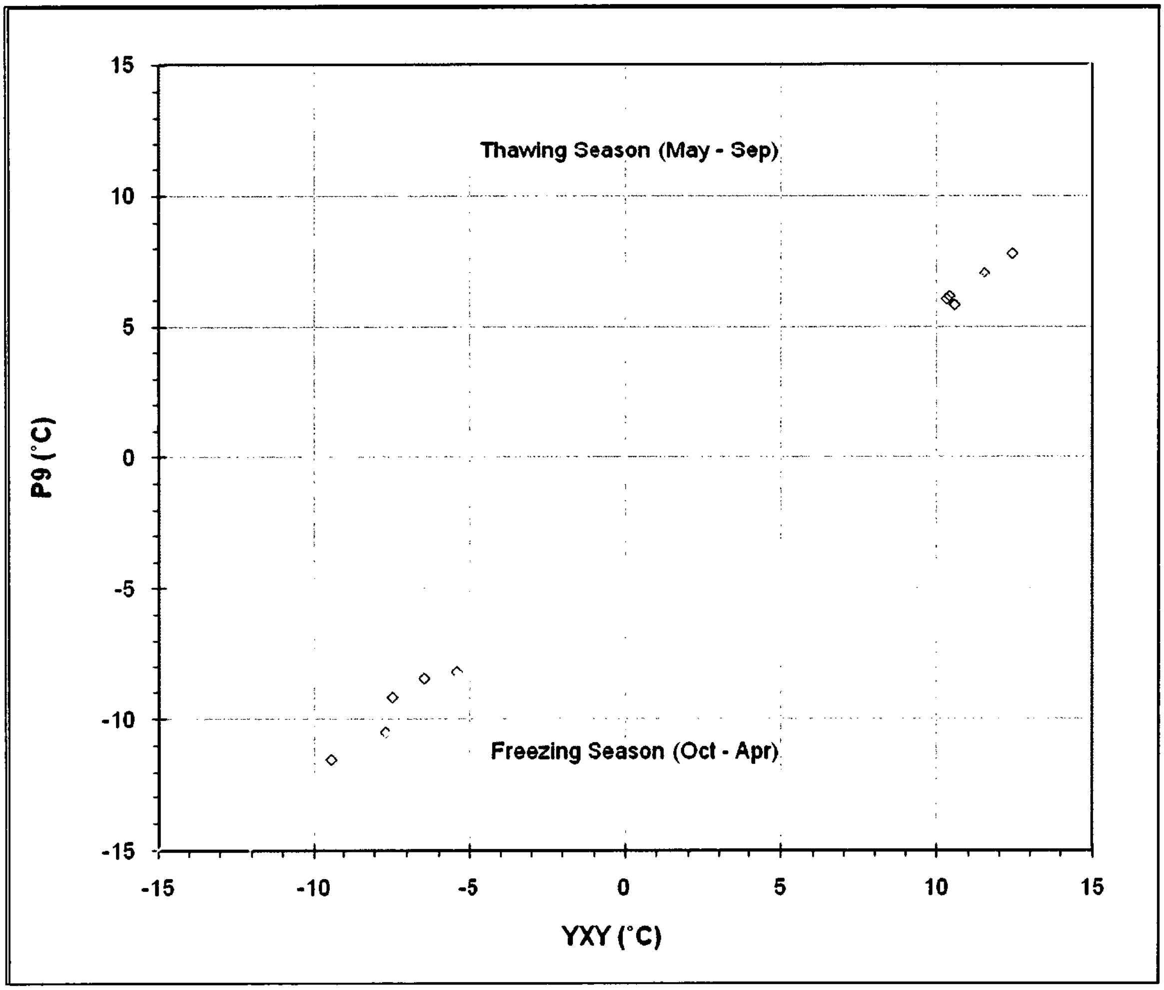

Figure 12: Relations between seasonal air temperatures at YXY and P9 (April 2001 to May 2006). Note: the dashed line represents the the expected temperature difference between YXY and P9 of 3.6°C (based on a mean environmental lapse rate of 6.5°C/km).

2004 at both Whitehorse and P9, with air temperatures recorded between May and September 2004 nearly 1°C higher at YXY, while those measured at P9 over the same period were only slightly warmer than those recorded in the following summer season (2005).

Although MAAT calculated for five consecutive years between August 2001 and July 2006 are all below 0°C at P9, those measured at the airport range from -1.0°C, in the first year, to more than 1.0°C in each of the following four years (**Figure 13**). Annual temperatures recorded at YXY were approximately 3.2°C warmer than those recorded at the palsa valley site. The coldest MAAT (-4.1°C) was measured during the first year of monitoring at P9 (2001-2002). The warmest annual temperature recorded at Whitehorse came in the following year (1.3°C), while the MAAT at P9 hovered around -2.0°C over three consecutive years between August 2002 and July 2005.

3.1.2 Coal Ridge Transect

Air temperatures were measured at five sites along the Coal Ridge transect between August 2003 and August 2006, including the valley bottom location (P9). Although two additional sites (CR5 and CR6) were installed at higher elevations along the transect after the initial set-up was completed, logger problems occurred at these sites. Air temperature data is available from CR5 from June 2004 to December 2004 and from mid-July to September 2005; there is currently no data available from CR6, which was installed in July 2005. Air temperatures collected from WC-Bowl, installed near Mount Granger in June 2004 are also included in this dataset.

Daily values indicate that, during both the freezing and thawing seasons, mean daily air temperatures measured along the transect frequently show a strong positive (inverted)

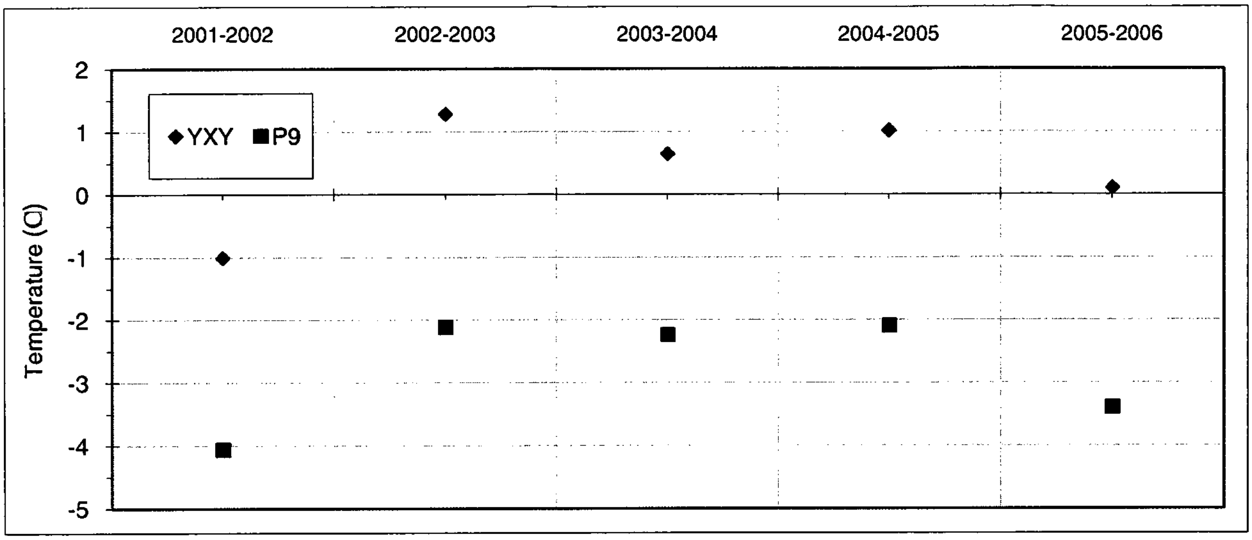

Figure 13: Mean annual air temperatures at P9 and YXY (August 2001 to July 2006)

gradient with elevation (**Figure 14**). Temperature inversions are known to occur in the main valleys of the Yukon (Wahl et al., 1987), and have also been shown to be frequent in the mountains (Lewkowicz and Smith, 2004). Daily values indicate that air temperature inversions are common in the palsa valley, occurring throughout the year and in all seasons (**Table 4**). Among the sites, daily temperature variations are greatest in winter, with differences of more than 10°C between P9 (1254 m) and CR4 (1457 m) on numerous occasions. The inversion episodes redeveloped over an average of 2.4 consecutive days, with some redeveloping over as many as 14 days (June-July 2004). In January 2006, there were 25 days when air temperatures at CR4 exceeded those recorded at P9. As shown in **Table 4**, daily data recorded in 2005 shows that inversions occurred in all months, on average 39% of the time. Inversions are most frequent and intense in the winter (58% in January) and least frequent in July and September (26% and 27%, respectively).

Day-to-day variability at each of the sites was considerably lower during the summer than during the winter, as observed at P9 over the same period (**Table 5**). Mean daily air temperatures were typically above 0°C from May to September, and below 0°C from October through to April. Minimum daily winter air temperatures were measured in January 2004 at the uppermost sites (CR3, CR4 and WC-Bowl), with temperatures below -31°C at all three locations. Minimum temperatures at the remaining sites were recorded during the same month the following year, when temperatures dipped below -40°C in the valley bottom. The highest daily summer temperatures were reached near the end of June 2004 at all of the palsa valley sites and WC-Bowl, ranging from 19.3°C at P9 to 21.6°C at CR4.

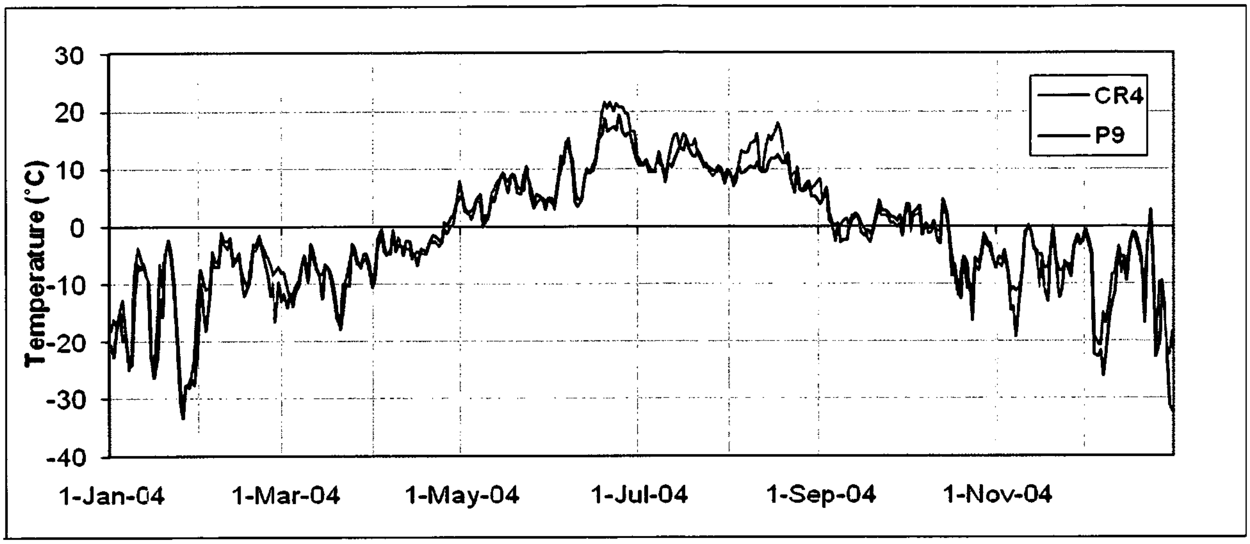

Figure 14: Mean daily air temperatures at P9 (1254 m) and CR4 (1457 m) in 2004.

Table 4: Inversion episodes along the Coal Ridge transect based on daily averages (2004-2006)

2004	Jan	Feb	Mar	Apr	May	Jun	Jul	Aug	Sep	Oct	Nov	Dec	Annual Total
Total number of days with inversions						16	13	19	7	8	13	19	95
Longest consecutive days with inversions						4	7	5	4	7	4	4	
Frequency (%)						0.53	0.42	0.61	0.23	0.26	0.43	0.61	0.44

2005	Jan	Feb	Mar	Apr	May	Jun	Jul	Aug	Sep	Oct	Nov	Dec	Annual Total
Total number of days with inversions	18	15	10	14	11	13	8	10	8	11	10	12	140
Longest consecutive days with inversions	7	5	3	5	6	4	2	9	3	4	11		
Frequency (%)	0.58	0.54	0.32	0.47	0.35	0.43	0.26	0.32	0.27	0.35	0.33	0.39	0.38

2006	Jan	Feb	Mar	Apr	May	Jun	Jul	Aug	Sep	Oct	Nov	Dec	Annual Total
Total number of days with inversions	25	15	15	8	4	5	10	5					87
Longest consecutive days with inversions	5	4	5	5	4	3	4	4					
Frequency (%)	0.81	0.54	0.48	0.27	0.13	0.17	0.32	0.16					0.36

Table 5: Mean and standard deviation of air temperatures measured along the Coal Ridge transect over three freezing and two thawing seasons (2003-2006)

	average seasonal air temperature						standard deviation					
	P9	CR1	CR2	CR3	CR4	BOWL	P9	CR1	CR2	CR3	CR4	BOWL
	1254m	1260m	1271m	1363m	1457m	1640m						
2003-2004	-9.1	-8.8	-8.9	-8.1	-7.6		7.9	7.7	7.5	7.3	7	
2004	7.8	8.0	7.7	8.4	8.6		4.9	5.0	5.3	5.7	5.9	
2004-2005	-8.4	-8.1	-8.4	-5.9	-7.0	-8.1	8.5	8.2	7.7	5.5	6.8	6.5
2005	7.1	7.2	6.7	6.9	7.5		3.2	3.2	3.3	4.1	3.6	
2005-2006	-10.5	-10.3	-10.1	-9.0	-8.7		8.4	8.1	7.5	7	6.9	

Seasonal values computed over three freezing and two thawing seasons the Coal Ridge sites indicate that the coldest winter during the study period occurred in 2005-2006, with average temperatures of approximately 1°C below those in the two previous freezing seasons. The warmest summer on record was 2004, with temperatures 0.5°C to 1.0°C higher than those measured in the following year (2005). Seasonal averages over the study period reflect the inverted daily temperature patterns discussed above (**Figure 15**). During the summer, differences in temperature between CR4 and P9 were <1.0°C, while temperatures recorded at CR4 during the winter were more than 1.5°C warmer. MAATs along the Coal Ridge transect calculated for three consecutive years between August 2003 and July 2006 were all below 0°C, and also show an overall inverted relationship between temperature and elevation (**Figure 16**). During the 2004-2005 year, for example, the mean value at the valley bottom site was -2.1°C, while 160 m higher on the Coal Ridge transect (CR4) the temperature was -1.0°C. Monthly air temperatures for the same period at the valley bottom site ranged from -15.7°C to 9.2°C, while CR4 had a range of -12.3°C to 11.2°C. In 2005-2006, although there was a steady increase in temperature from CR1 to CR4, P9 was actually warmer than CR1. In the previous two years, CR2 was colder than CR1, while CR4 was the warmest site in all three years (2003-2006).

3.1.3 Mount Sima Trail

Air temperatures were measured at five sites along the Mount Sima trail between June 2004 and August 2006. Air temperatures at the sites correlate closely with the Talmark monitoring station in the industrial part of Whitehorse, but there is considerably

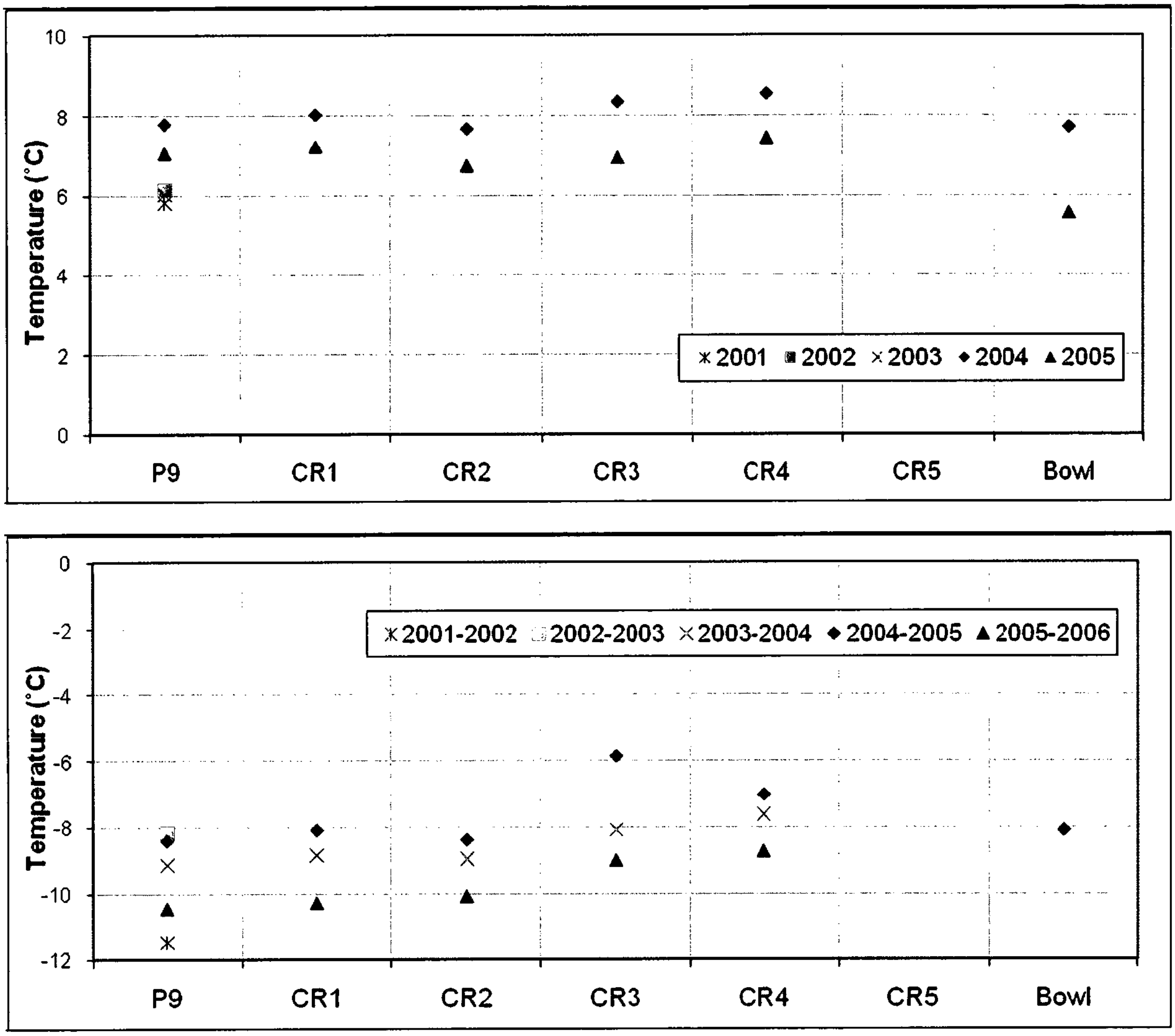

Figure 15: Average seasonal air temperatures along the Coal Ridge transect during five thawing (top) and five freezing (bottom) seasons (2001 to 2006). Note: Site elevation increases from left to right . Only P9 was operating in all years..

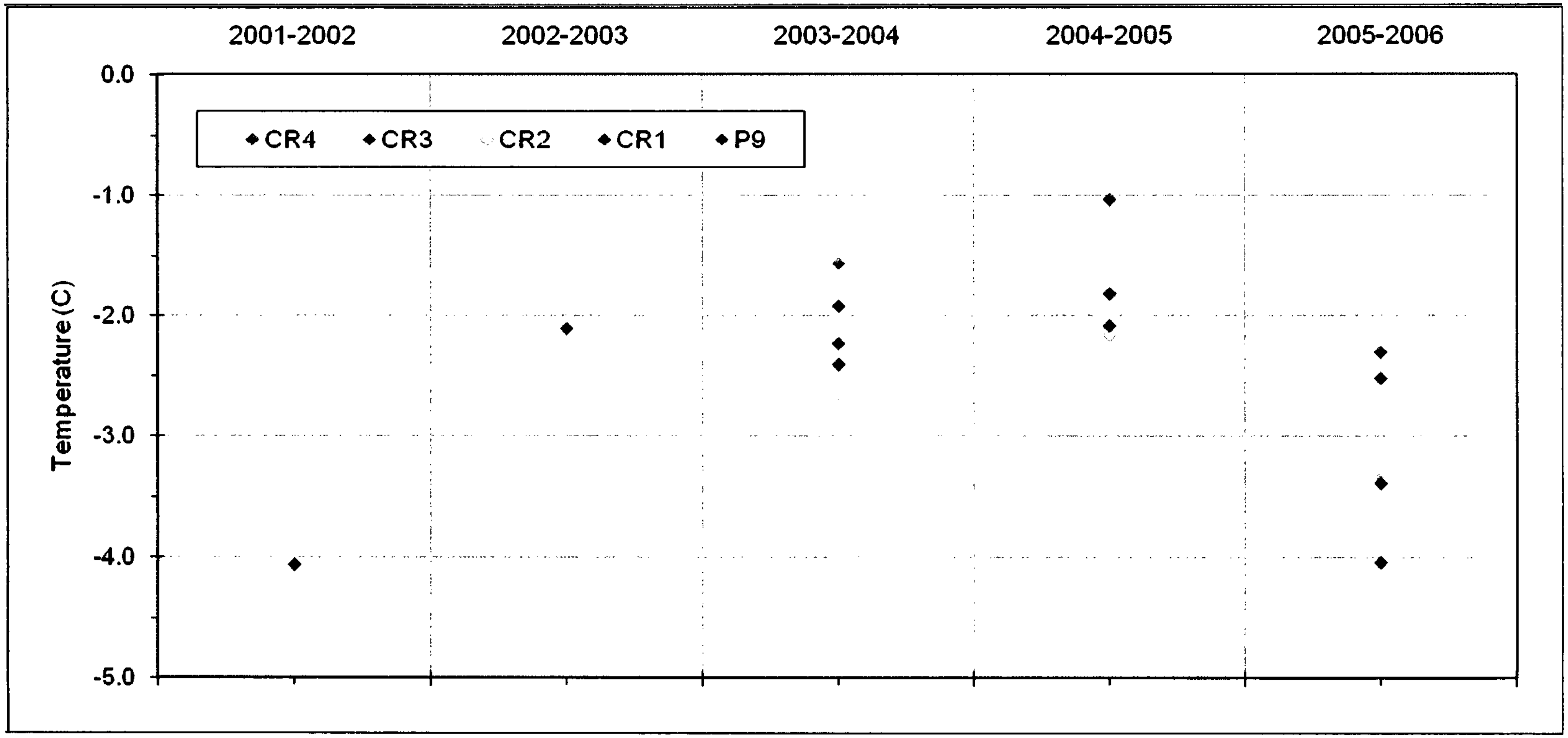

Figure 16: Mean annual air temperatures along the Coal Ridge transect (August 2001 to July 2006). Note: Only P9 was operating in all years.

more scatter when average daily temperatures are below 0°C than during the thawing season (**Figure 17**). Average daily summer temperatures measured at Talmark are significantly warmer than along the trail, with differences of approximately 2.0°C at T1, 3.0°C at T2, 3.5°C at T3 and nearly 5.0°C at T4. During the thawing season, the difference in daily air temperature between the sites typically follows the expected pattern of decreasing temperatures with increasing elevation, however, this pattern is reversed for periods of one day in both August and September 2004, with temperature increases of up to 1°C between T3 and T4. During the freezing season, average daily temperatures measured at Talmark are often significantly colder than along the trail, with differences occasionally approaching 10°C at T4. Daily air temperatures show a positive gradient with elevation along the trail for extensive periods between November and February (**Figure 18**), so much so that average monthly temperatures for this period often reflect these patterns (**Figure 19**). Daily inverted gradients occurred most frequently in the month of January and lasted an average of 2.5 days, with some lasting as little as one day and others as long as 8 days (December 2004). In 2006, there were 26 days in January when the air temperature at T4 exceeded those recorded at T3 (**Table 6**).

Day-to-day variability at each of the trail sites was considerably lower during the summer season than during the highly variable winter season (**Table 7**). Mean daily air temperatures were typically above 0°C from May to September, and below 0°C from October through to April. Minimum daily winter air temperatures occurred in mid-January 2005 at all but the Talmark location; the minimum temperature at this site was recorded at the end of January 2006, as data is missing for several months during 2005.

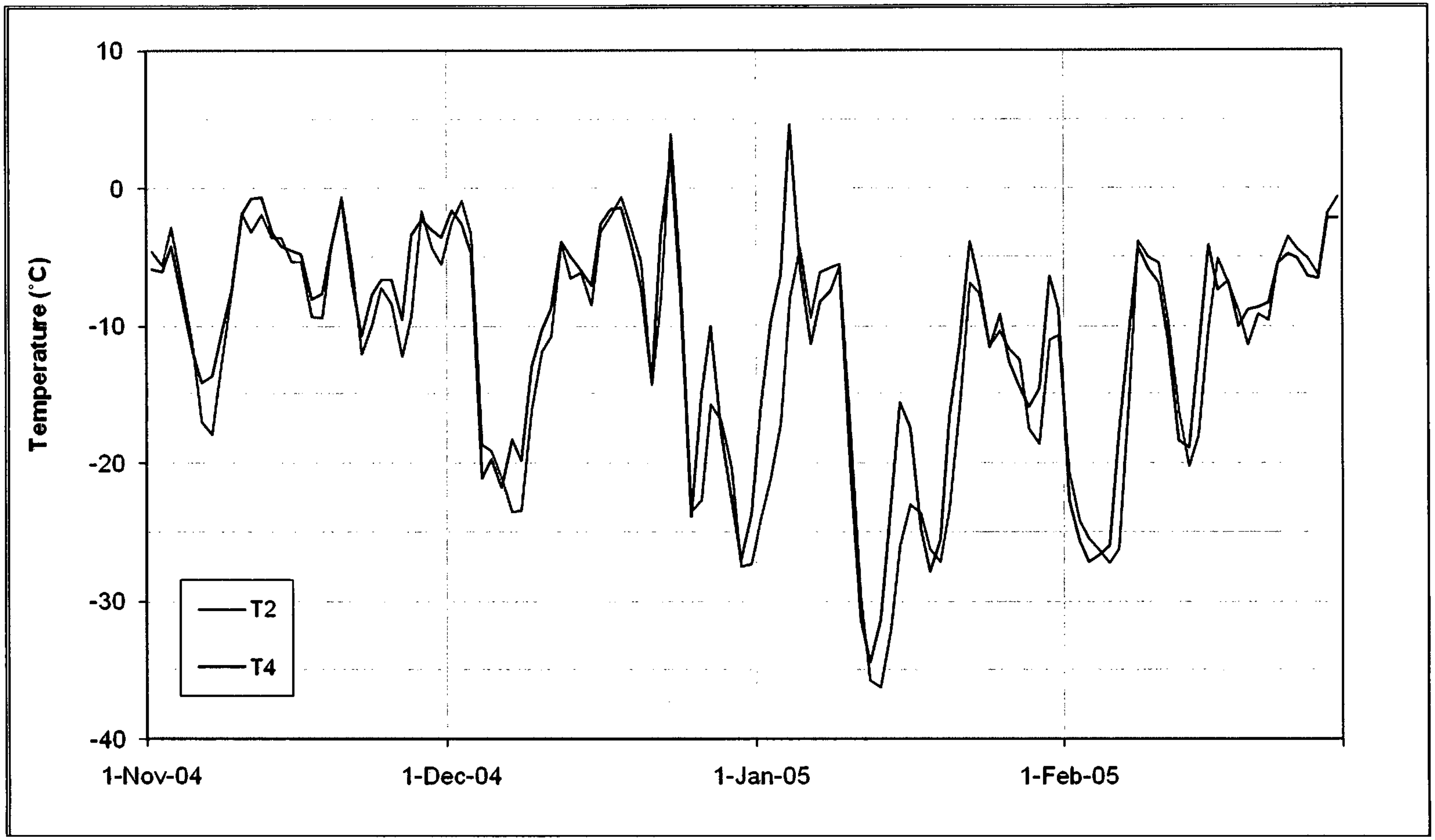

Figure 18: Mean daily air temperatures at T2(1011 m) and T4 (1290 m) (November 2004 to February 2005)

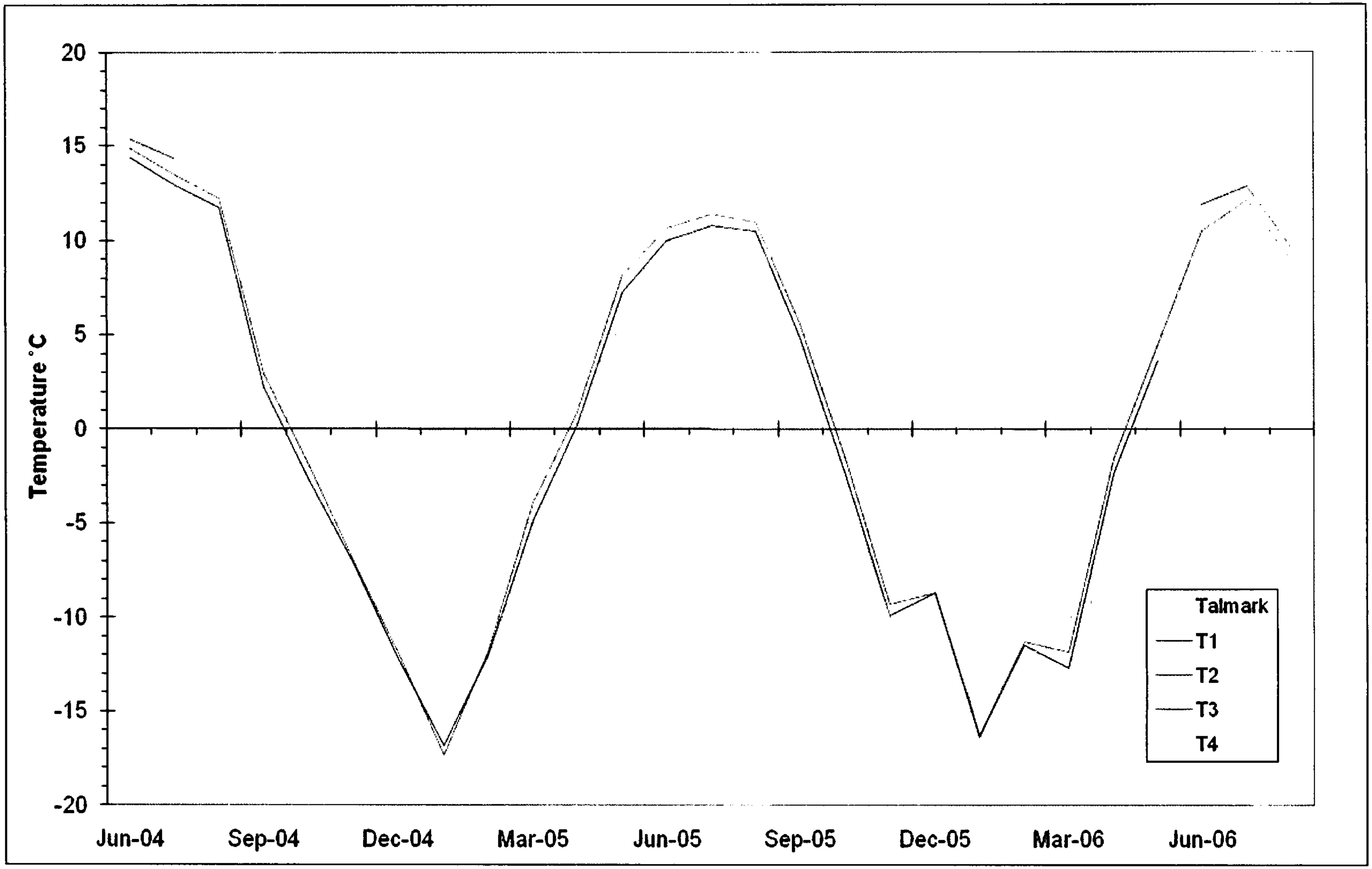

Figure 19: Mean monthly air temperature along the Mount Sima trail (June 2004 to August 2006). Note: During the winter, average monthly air temperatures often reflect daily inverted temperature gradient which occurs for extensive periods along the trail between November and February. As a result, T4 is often the warmest site during the winter months.

Table 6: Inversion episodes along the Mount Sima trail based on daily averages (2004-2006)

2004	Jan	Feb	Mar	Apr	May	Jun	Jul	Aug	Sep	Oct	Nov	Dec	Annual Total
Total number of days with inversions						0	0	0	2	9	20	20	51
Longest consecutive days with inversions						-	-	-	1	3	6	13	
Frequency (%)						0.00	0.00	0.00	0.07	0.29	0.67	0.65	0.24

2005	Jan	Feb	Mar	Apr	May	Jun	Jul	Aug	Sep	Oct	Nov	Dec	Annual Total
Total number of days with inversions	20	13	0	1	0	0	0	0	1	3	11	17	66
Longest consecutive days with inversions	7	4	-	1	-	-	-	-	1	2	7		
Frequency (%)	0.65	0.46	-	0.03	-	-	-	-	0.03	0.10	0.37	0.55	0.18

2006	Jan	Feb	Mar	Apr	May	Jun	Jul	Aug	Sep	Oct	Nov	Dec	Annual Total
Total number of days with inversions	25	11	3	0	0	MISSING DATA							39
Longest consecutive days with inversions	8		2	-	-								
Frequency (%)	0.81	0.39	0.10	-	-								0.26

Table 7: Mean and standard deviation of air temperatures measured along the Mount Sima trail over two freezing and two thawing seasons (2004-2006)

<table>
<tr><th rowspan="3"></th><th colspan="5">average seasonal air temperature</th><th colspan="5">standard deviation</th></tr>
<tr><th>Talmark</th><th>T1</th><th>T2</th><th>T3</th><th>T4</th><th rowspan="2">Talmark</th><th rowspan="2">T1</th><th rowspan="2">T2</th><th rowspan="2">T3</th><th rowspan="2">T4</th></tr>
<tr><th>630m</th><th>868m</th><th>1011m</th><th>1145m</th><th>1290m</th></tr>
<tr><td>2004-2005</td><td>-4.5</td><td rowspan="3">MISSING DATA</td><td>-7.6</td><td>-7.9</td><td>-7.7</td><td>7.8</td><td rowspan="3">MISSING DATA</td><td>9.0</td><td>8.8</td><td>7.8</td></tr>
<tr><td>2005</td><td rowspan="2">MISSING DATA</td><td>9.3</td><td>8.7</td><td>7.6</td><td rowspan="2">MISSING DATA</td><td>3.3</td><td>3.4</td><td>3.2</td></tr>
<tr><td>2005-2006</td><td>-8.7</td><td>-9.1</td><td>-9.2</td><td>8.1</td><td>8.1</td><td>7.5</td></tr>
</table>

The coldest daily winter air temperatures were recorded at T2 (-36.3˚C) and T3 (-37.3˚C) on January 13, 2005, while on the same day, the temperature measured at T4 was nearly 6˚C warmer. The highest daily summer air temperatures were reached near the end of June 2004 at all trail sites, including the Talmark location where the warmest temperature (25.1˚C) was recorded on June 23.

Seasonal values were computed for two freezing and one thawing season at the sites along the Mount Sima trail. Missing data prevents the calculation of seasonal values at Talmark during the 2005 summer and 2005-2006 winter seasons, while the limited data available from T1 prevents the calculation of any seasonal values. The winter of 2004-2005 recorded temperatures approximately 1˚C higher than during the following freezing season (2005-2006) (**Figure 20**). Seasonal air temperatures recorded at the trail sites indicate that Talmark is the warmest site, while temperature differences between T2, T3 and T4 are within the accuracy of the sensors (± 0.2˚C) and cannot be considered significant. However, since they span an elevation range of nearly 300 m, their similarity is important. Based on a mean environmental lapse rate of 6.5˚C /km, the expected temperature difference between T2 and T4 is 1.8˚C. The warmest summer season occurred in 2004, prior to the warm winter temperatures discussed above. Seasonal temperatures recorded between May and September 2004 were approximately 1.5˚C warmer than during the following summer season (2005) and show decreased temperature values with increased elevation.

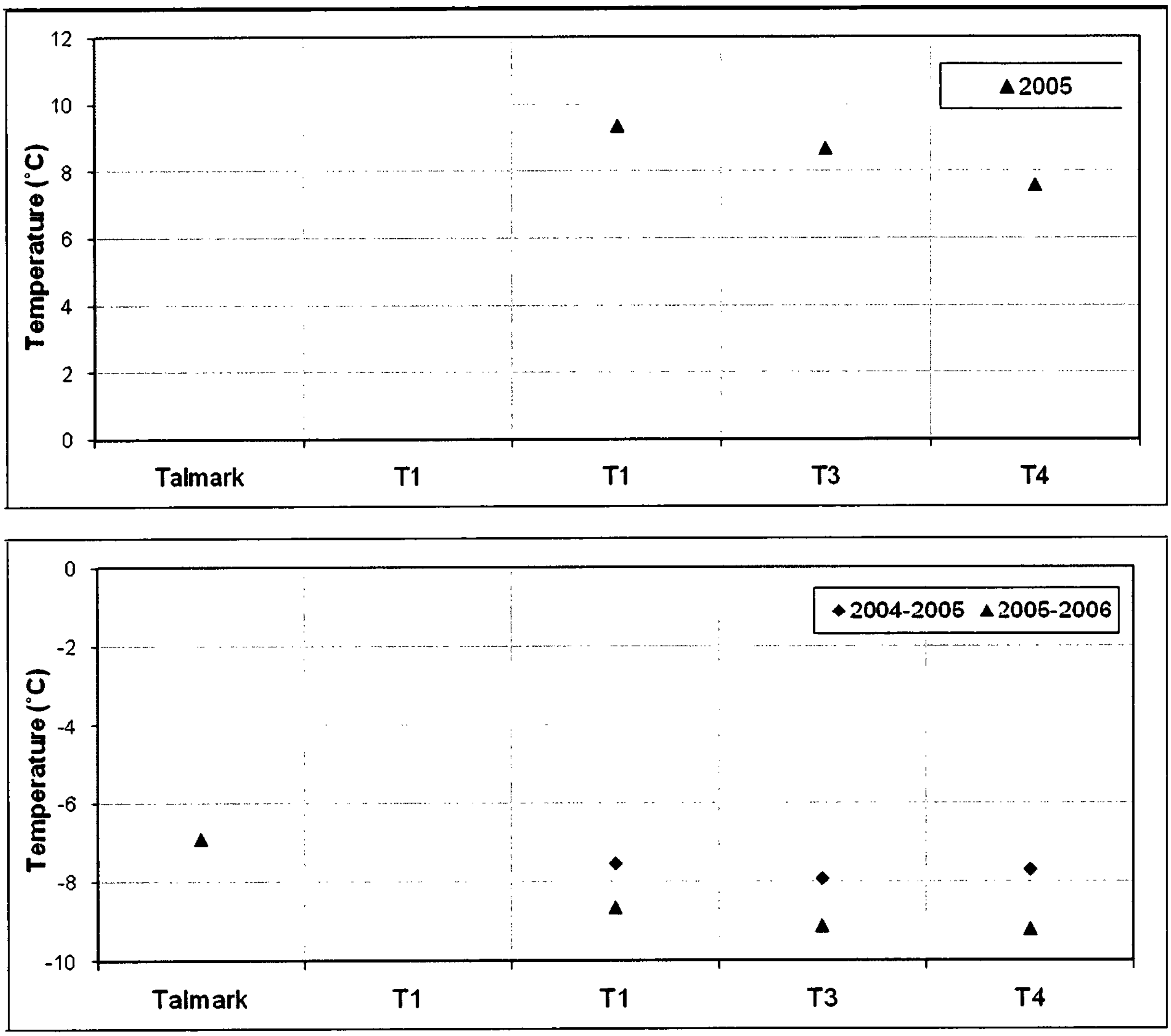

Figure 20: Average seasonal air temperatures along the Mount Sima trail during one thawing (top) and two freezing (bottom) seasons (2004 to 2006). Note: Site elevation increases from left to right.

Despite the inverted daily temperatures discussed above, air temperatures averaged over 2004-2005 show a normal temperature gradient with elevation (**Table 8**). The MAAT at Talmark was 2.9°C, while along the trail, temperatures measured -0.6°C at T2, -1.1°C at T3 and -1.4°C at the highest site (T4). Between August 2004 and July 2005, monthly air temperatures at the lowest available site (T2) ranged from -17.3°C to 12.2°C, while the highest site had a slightly smaller range of -14.5°C to 10.6°C. Although MAAT for the following year (2005-2006) were slightly cooler, ranging from 1.0°C at Talmark to -2.5°C at T4, monthly temperatures remained largely the same as the previous year.

3.1.4 Newly Installed Wolf Creek Sites

Daily values indicate that between June and August, air temperatures remained above 0°C at all but the Mount Granger site (WC2006-8), where temperatures fell below freezing on a number of occasions (**Figure 21**). Furthermore, average daily temperatures on the mountain top were below 10°C on all but three days during the summer season. Maximum daily summer temperatures were recorded during the second week of June, As shown in **Table 9**, monthly temperatures ranged from less than 4.0°C to nearly 12°C, with the majority of the sites recording mean monthly temperatures of approximately 9.0°C. Average monthly air temperatures for the month of July were approximately 1.0°C warmer than during the preceding month at all the sites. Mean air temperatures were above 0°C at all sites during this timeframe, with all but the Mount Granger site measuring above 8.5°C. The average temperature of 3.7°C recorded at that site was much lower than at the other sites, due to its high elevation (2066 m). The average temperature recorded at the exposed plain site (WC2006-1) was the warmest (9.7°C), while averages from the remaining sites all measured between 8.6°C and 9.0°C.

Table 8: Mean annual air temperatures along the Mount Sima trail (August 2004 to July 2006)

	T1	T2	T3	T4
2004 - 2005	-	-0.6	-1.1	-1.4
2005 - 2006	-	-1.4	-	-2.5

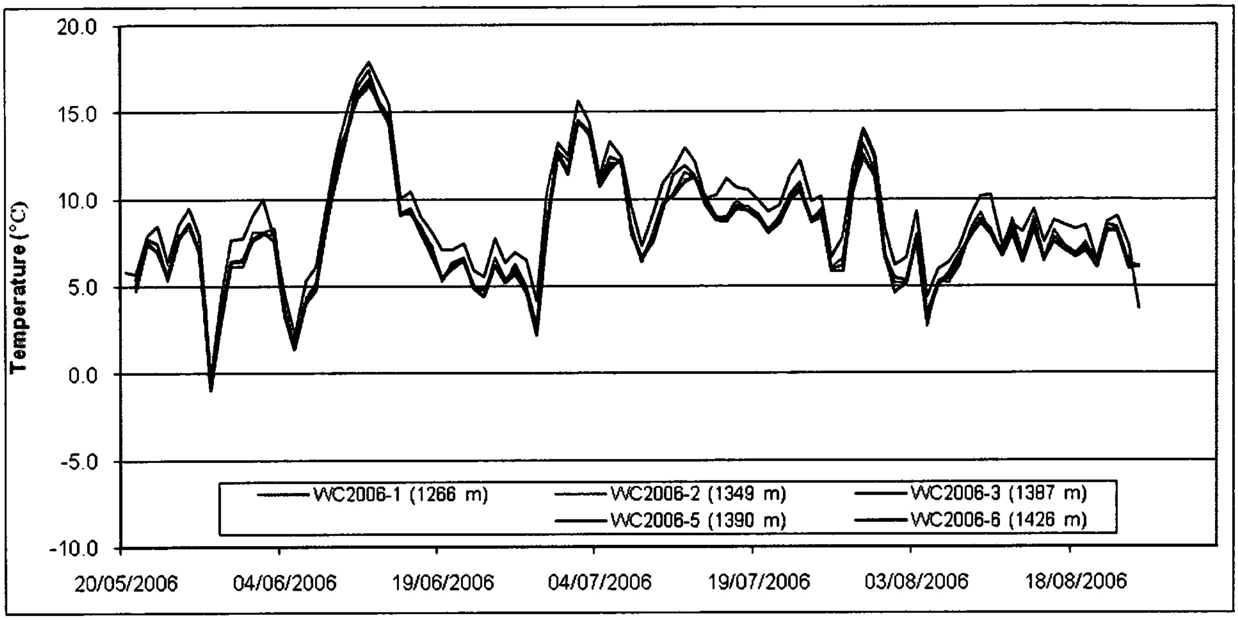

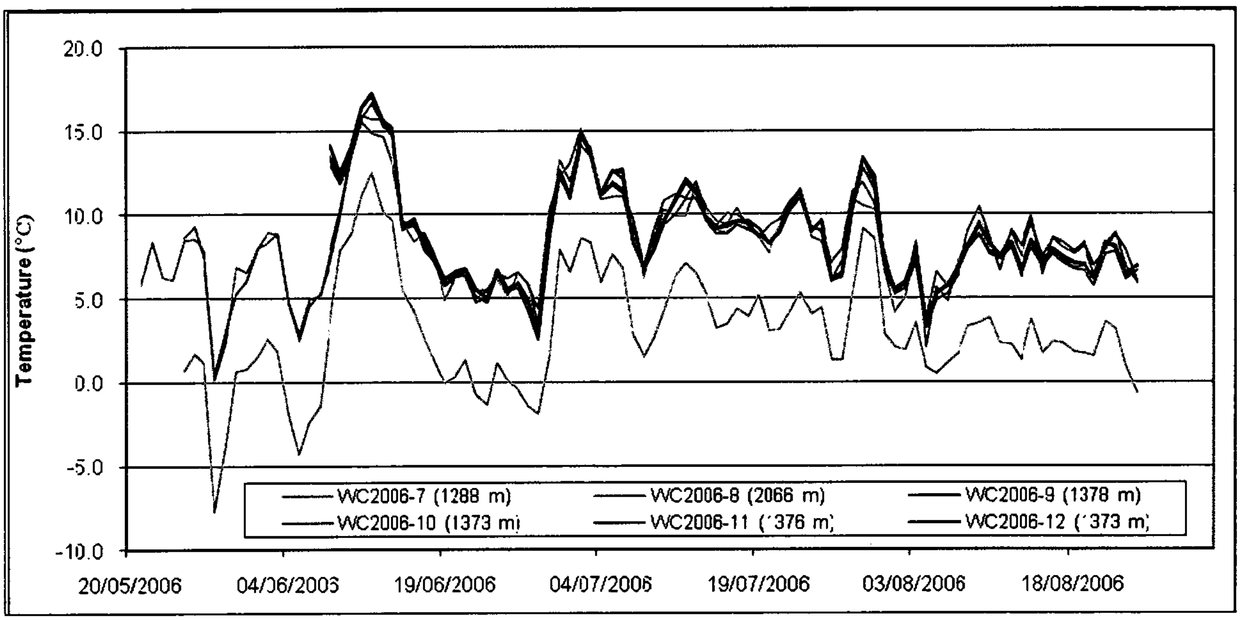

Figure 21: Mean Daily Air Temperatures at the Newly Installed Wolf Creek Valley Sites (May – August 2006)

Table 9: Average Air Temperature at the Newly Installed Wolf Creek Valley Sites (June and July 2006)

	June 2006	**July 2006**
WC2006-1	10.0	10.9
WC2006-2	8.9	9.9
WC2006-3	8.9	9.9
WC2006-4		
WC2006-5	8.9	9.8
WC2006-6	8.9	9.9
WC2006-7	8.9	9.8
WC2006-8	3.7	5.0
WC2006-9	9.1	10.0
WC2006-10	9.1	9.8
WC2006-11	9.3	10.1
WC2006-12	9.5	10.1
WC2006-DR	9.0	10.3

3.1.5 Climatic Regions of the Yukon

Ongoing research within the Yukon Territory provided an opportunity to collect additional temperature data which may be used to further evaluate climate-permafrost relations. During the 2006 spring and summer field season, 51 air and ground temperature monitoring stations were installed within four of the climatic regions of the Yukon, as identified by Wahl *et al.* (1987), as discussed in Section 2.2.4..

Analysis of summer air temperatures, measured during June and July, indicates that while the expected relationship between temperature and elevation is generally present, there are differences among the climate regions (**Figure 22**). At Keno, Johnson's Crossing and the Sa Dena Hes mine site, average monthly temperatures show a strong linear relationship with elevation in both months ($R^2 > 0.78$), despite the fact that the sites spanned a variety of TPI classifications. The relationship at Faro is somewhat weaker in both June ($R^2 = 0.72$) and July ($R^2 = 0.70$), while at Wolf Creek, there are marked differences in the relationship between the two summer months, with considerably more scatter in June ($R^2 = 0.68$) than in the following month ($R^2 = 0.87$). At sites where the relationship is less evident, other factors, such as air temperature inversions, vegetation, TPI and aspect likely play more important roles in regulating the relationship between elevation and temperature.

According to Wahl *et al.* (1987), mean daily air temperatures of between 10°C and 15°C are expected in all regions for both June and July, with the exception of Faro, where mean daily July temperatures are typically above 15°C. Temperatures recorded on a mountain top in Wolf Creek (2066 m) are significantly cooler than the other study sites in both June and July, recording monthly averages of 2.7°C and 5.0°C respectively. Average

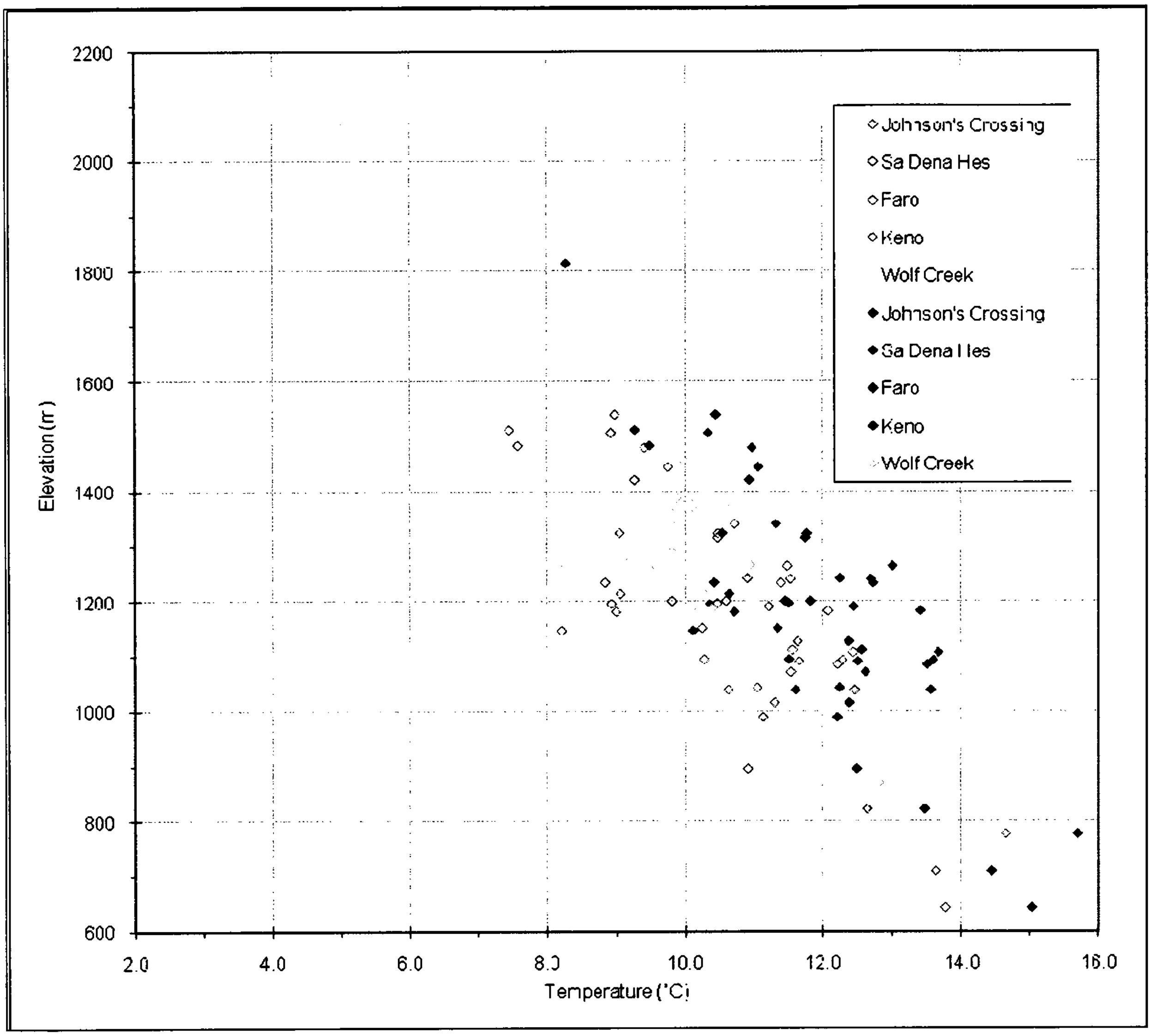

Figure 22: Relationship between elevation and air temperature within five climatic regions of the Yukon for June (outlined) and July (filled) 2006

June air temperatures at the remaining sites vary from 7.4°C on a mountain top in Johnson's Crossing (1512 m), to 14.7°C at a mid-slope ridge site in Keno (777 m). Mean July temperatures (**Table 10**) follow the same pattern but are approximately 1.5°C warmer, with temperatures ranging from 8.3°C at a newly installed site atop Keno Hill (1815 m), to 15.7°C at the mid-slope ridge site within the same region.

Overall, during the month of June (**Table 10**), the coldest temperatures were recorded at the Johnson's Crossing and Wolf Creek sites, where mean monthly temperatures were less than 10°C at all but two sites in each region. Average temperatures were less than 11°C at all but a single Wolf Creek site (T1), where an average of nearly 12°C was recorded. Faro was the warmest region, with all ten sites measuring temperatures of more than 10°C, including six sites with average temperatures greater than 12°C. Monthly temperatures recorded at both the Keno and Sa Dena Hes mine sites were all above 9°C, with the majority above 10°C. Furthermore, several sites in both regions recorded average temperatures of more than 11°C and temperatures at two low elevation Keno sites exceeded 13°C.

During the month of July, the coldest average temperatures were once again recorded at the Johnson's Crossing and Wolf Creek sites. In Johnson's Crossing, mean monthly temperatures were less than 11.0°C at all but two sites. Faro was once again the warmest region, with mean monthly air temperatures measuring more than 11°C at all ten sites, including eight sites with average temperatures greater than 12°C. A total of six sites recorded monthly averages greater than 13°C, with one plains site (644 m) measuring 15°C. Monthly temperatures recorded at the Sa Dena Hes mine sites were all above 10°C,

Table 10: Lapse rates

Region	Site	Elevation (m)	Aspect	TPI	June Lapse Rate	June Elevation Difference	June Expected T°	June Actual T°	June inversion Effect	July Lapse Rate	July Elevation Difference	July Expected T°	July Actual T°	July inversion Effect
Wolf Creek	WC2006-1	1266	W	plains	$0.0081 km^{-1}$	800	9.2	9.2	0.00	$0.0075 km^{-1}$	800	10.9	10.9	0.00
	WC2006-2	1349	E	U-shaped valley		717	8.5	8.2	-0.34		717	10.3	9.9	-0.44
	WC2006-3	1387	S	mid-slope ridge		679	8.2	8.1	-0.11		679	10.0	9.9	-0.16
	WC2006-4	1386	S	mid-slope ridge		680	8.2	failed			680	10.0	failed	
	WC2006-5	1390	S	mid-slope drainage		676	8.2	8.1	-0.06		676	10.0	9.8	-0.21
	WC2006-6	1426	S	open slope		640	7.9	8.0	0.17		640	9.7	9.9	0.14
	WC2006-7	1288	S	U-shaped valley		778	9.0	8.3	-0.75		778	10.8	9.8	-0.96
	WC2006-8	2066	Flat	mt. top		0	2.7	2.7	0.00		0	5.0	5.0	0.00
	WC2006-9	1373	N	mid-slope ridge		693	8.3	9.0	0.69		693	10.1	10.0	-0.15
	WC2006-10	1376	N	mid-slope drainage		690	8.3	9.0	0.73		690	10.1	9.8	-0.34
	WC2006-11	1378	N	mid-slope ridge		688	8.3	9.2	0.93		688	10.1	10.1	-0.03
	WC2006-12	1373	N	open slope		693	8.3	9.3	1.02		693	10.1	10.1	-0.01
	WC2006-DR	1225	Flat	U-shaped valley		841	9.5	8.3	-1.19		841	11.2	10.3	-0.92
	P9	1254	Flat	U-shaped valley		812	9.3	8.2	-1.10		812	11.0	9.5	-1.51
	CR1	1260	NW	U-shaped valley		806	9.2	8.2	-0.99		806	11.0	failed	
	CR2	1271	NW	U-shaped valley		795	9.1	7.6	-1.57		795	10.9	9.2	-1.70
	CR3	1363	NW	U-shaped valley		703	8.4	7.9	-0.48		703	10.2	9.8	-0.43
	CR4	1457	NW	mid-slope ridge		609	7.6	8.1	0.44		609	9.5	10.0	0.47
	CR5	1495	NW	mesa		571	7.3	failed			571	9.2	failed	
	CR6	1555	Flat	mesa		511	6.8	failed			511	8.8	failed	
	T1	868	NE	plains		1198	12.4	11.9	-0.55		1198	13.9	12.8	-1.11
	T2	1011	NE	open slope		1055	11.3	10.4	-0.83		1055	12.8	12.1	-0.75
	T3	1145	NE	open slope		921	10.2	failed			921	11.8	failed	
	T4	1290	NE	open slope		776	9.0	8.4	-0.55		776	10.8	10.3	-0.47
Johnsons Crossing	JC2006-1	1187	Flat	U-shaped valley	$0.0052 km^{-1}$	325	9.1	8.8	-0.30	$0.0035 km^{-1}$	325	10.4	10.1	-0.31
	JC2006-2	1187	E	plains		325	9.1	9.1	0.00		325	10.4	10.4	0.00
	JC2006-3	1196	W	plains		316	9.1	8.9	-0.15		316	10.4	10.3	-0.02
	JC2006-4	1234	SE	open slope		278	8.9	8.8	-0.04		278	10.2	10.4	0.18
	JC2006-5	1324	SE	mid-slope ridge		188	8.4	9.0	0.63		188	9.9	10.5	0.61
	JC2006-6	1512	N	mt. top		0	7.4	7.4	0.00		0	9.3	9.3	0.00
	JC2006-7	1483	N	upland drainage		29	7.6	7.6	-0.03		29	9.4	9.5	0.11
	JC2006-8	896	NW	n/a		616	10.6	10.9	0.27		616	11.4	12.5	1.06
	JC2006-9	1147	S	U-shaped valley		365	9.3	8.2	-1.13		365	10.5	10.1	-0.43
	JC2006-10	1181	S	U-shaped valley		331	9.2	9.0	-0.16		331	10.4	10.7	0.29
	JC2006-11	1214	S	open slope		298	9.0	9.1	0.07		298	10.3	10.6	0.33
	JC2006-12	1095	NE	n/a		417	9.6	10.3	0.67		417	10.7	11.5	0.78
	JC2006-13	1129	S	plains		383	9.4	failed			383	10.6	failed	
Sa Dena Hes	SDH2006-1	1073	E	open slope	$0.0054 km^{-1}$	433	11.3			$0.0046 km^{-1}$	433	12.3		
	SDH2006-2	1112	E	U-shaped valley		394	11.1	11.6	0.50		394	12.1	12.6	0.42
	SDH2006-3	1200	E	mid-slope drainage		306	10.6	10.6	0.01		306	11.7	11.8	0.09
	SDH2006-4	1200	SE	mid-slope drainage		306	10.6	9.8	-0.77		306	11.7	11.5	-0.28
	SDH2006-5	1506	Flat	mt. top		0	8.9	8.9	0.00		0	10.3	10.3	0.00
	SDH2006-6	1420	NE	mt. top		86	9.4	9.3	-0.13		86	10.7	10.9	0.20
	SDH2006-7	1315	E	mid-slope ridge		191	10.0	10.5	0.51		191	11.2	11.7	0.54
	SDH2006-8	1241	NE	open slope		265	10.4	10.9	0.54		265	11.5	12.2	0.69
	SDH2006-9	1126	S	canyon		380	11.0	11.6	0.65		380	12.1	12.4	0.30
	SDH2006-10	988	SW	U-shaped valley		518	11.7	11.1	-0.59		518	12.7	12.2	-0.50
	SDH2006-11	1014	N	U-shaped valley		492	11.6	11.3	-0.29		492	12.6	12.4	-0.20
	SDH2006-12	988	S	plains		518	11.7	failed			518	12.7		
	SDH2006-13	821	SW	plains		685	12.6	12.6	0.00		685	13.5	13.5	0.00
Faro	F2006-1	1038	SW	upper slope	$0.0060 km^{-1}$	158	11.4	12.5	1.04	$0.0064 km^{-1}$	158	12.5	13.5	1.04
	F2006-2	1538	SE	mt. top		data not available					data not available			
	F2006-3	1405	S	open slope										
	F2006-4	1340	S	open slope										
	F2006-5	644	W	plains		552	13.8	13.8	0.00		552	15.0	15.0	0.00
	F2006-6	1196	S	plains		0	10.5	10.5	0.00		0	11.5	11.5	0.00
	F2006-7	1151	N	U-shaped valley		45	10.7	10.2	-0.49		45	11.8	11.3	-0.45
	F2006-8	1190	NE	mid-slope drainage		6	10.5	11.2	0.72		6	11.5	12.4	0.90
	F2006-9	1093	SW	open slope		103	11.1	12.3	1.20		103	12.2	13.6	1.44
	F2006-10	1182	S	mid-slope ridge		14	10.5	12.1	1.52		14	11.6	13.4	1.82
	F2006-11	1043	W	canyon		153	11.4	11.1	-0.33		153	12.5	12.2	-0.25
	F2006-12	1085	N	open slope		111	11.1	12.2	1.08		111	12.2	13.5	1.29
	F2006-13	1107	Flat	mid-slope ridge		89	11.0	12.4	1.44		89	12.1	13.7	1.60
Keno	K2006-1	1478	SW	open slope		data not available				$0.0056 km^{-1}$	337	10.2	11.0	0.81
	K2006-2	1443	SE	upper slope							372	10.4	11.1	0.71
	K2006-3	1240	SE	open slope							575	11.5	12.7	1.21
	K2006-4	1323	E	mid-slope drainage							492	11.0	11.8	0.75
	K2006-5	1039	Flat	canyon							776	12.6	11.6	-0.99
	K2006-6	1071	S	canyon							744	12.4	12.6	0.19
	K2006-7	1264	Flat	mid-slope ridge							551	11.4	13.0	1.66
	K2006-8	1091	NW	U-shaped valley							724	12.3	12.5	0.19
	K2006-9	1233	N	open slope							582	11.5	12.7	1.21
	K2006-10	777	Flat	mid-slope ridge							1038	14.1	15.7	1.64
	K2006-11	709	Flat	plains							1106	14.4	14.4	0.00
	K2006-12	1815	Flat	ridge							0	8.3	8.3	0.00

Note: 'Elevation Difference' refers to the difference in elevation between a given site and the upper exposed control site while averages at the Keno sites were above 11°C at all but the highest Keno Hill site (8.3°C). Several sites in both regions recorded average temperatures of more than 12°C and temperatures at two low elevation Keno sites exceeded 14°C.

3.1.6 Lapse Rates

Lapse rates were calculated for each region based on the exposed control sites, which were used to estimate the monthly air temperature for all remaining sites based on elevation alone (**Table 10**). Inversion-prone sites were identified as having lower air temperatures than predicted from the control site values, while taking potential measurement errors into account. Therefore, only those sites with temperatures 0.4°C cooler (or more) than predicted were considered inversion-prone. Inversion-prone sites were predominantly situated in U-shaped valleys, although open slopes, mid-slope ridges and plains were also identified. Thus, while almost all sites that were more than 0.4°C cooler than predicted were classified according to the TPI as canyons or U-shaped valleys, not all sites falling into this classification were inversion-prone.

Based on the first two months of data, Wolf Creek is the most inversion-prone region, with a total of nine sites showing lower than predicted values for both summer months, including six U-shaped valley sites (P9, CR1, CR2, CR3, WC2006-DR and WC2006-7), two open slopes (T2 and T4) and a single plains site (T1). A tenth valley bottom site (WC2006-2) was considered inversion-prone only during the month of July. Of these sites, four recorded temperatures more than -0.9°C cooler than predicted in June (P9, CR1, CR2 and WC2006-DR) and five in July (P9, CR2, T1, WC2006-DR and WC2006-7). In Faro, five sites recorded cooler than predicted temperatures during the month of June, including two U-shaped valley/canyon sites (F2006-7 and F2006-11), two plains sites (F2006-5 and F2006-6) and an upper slope site (F2006-1). All but the upper slope site remained inversion-prone in July, with temperatures more than 0.9°C cooler than predicted at the plains and valley bottom sites. In Keno, four sites were considered inversion-prone in July, including 3 U-shaped valley/canyon sites (K2006-5, K2006-6 and K2006-8) and a plains site (K2006-11). Temperatures recorded at these sites were all more than 0.9°C cooler than predicted. A June lapse rate could not be calculated for the Keno sites because the exposed mountain top site (K2006-12) was not installed until the end of June. Individual U-shaped valley sites showed a tendency for inversions in both summer months at Johnsons Crossing (JC2006-1 and JC2006-9); two additional plains sites (JC2006-2 and JC2006-3) were also considered inversion prone in July. At Sa Dena Hes, a U-shaped valley (SDH2006-10) and mid-slope drainage site (SDH2006-4) were identified in June, but only the valley site remained prone to inversions a month later.

3.2 Ground Surface Temperatures

In the previous section, it was shown that air temperatures are more variable during the winter, when air temperature inversions within the Wolf Creek basin are especially large and persistent. Inversion episodes are common year-round and have the potential to affect permafrost distribution in the region. The purpose of this section is to investigate ground surface temperatures measured at the study sites between 2001 and 2006. Specifically, this section describes the ground surface temperature regimes at the existing monitoring stations by considering temperature trends over various time scales (i.e. daily, monthly, seasonal, annual), both at and among the study sites.

3.2.1 Coal Ridge Transect

Ground surface temperatures are strongly influenced by soil conditions, vegetation and snow cover, and do not, therefore, show the same trends in day-to-day variability as air temperatures (**Table 11**). In most cases, variability at the Coal Ridge and WC-Bowl sites was higher during the summer than in winter, when the ground surface is typically insulated by seasonal snow cover (see section 3.3.2). Surface temperatures at the sites typically began to increase in late-April and early-May, and became similar as air temperatures rose above 0°C. During the snowmelt season, surface temperatures remained just below 0°C for a period of approximately one week at P9 and WC-Bowl, and two weeks at the other sites along the transect. Maximum daily summer surface temperatures occurred at the end of June 2004 at all the sites, and corresponded closely with maximum daily summer air temperatures (**Figure 23**). Surface temperatures at the sites generally fell below 0°C in early-October and remained below freezing until snow-melt began the following spring. Minimum daily winter surface temperatures were more variable, occurring on different dates at each of the sites. Winter minima did not correspond with the minimum air temperatures, and were nearly 15°C warmer on the same date. The coldest daily surface temperature was recorded at WC-Bowl in January 2004, when a temperature of -18.7°C was measured. Along the Coal Ridge transect, minimum daily surface temperatures ranged from -17.5°C (CR1) to -12.0°C (P9), several degrees warmer than the daily air temperatures recorded on the same dates, and >20.0°C warmer than the lowest recorded daily air temperatures measured at these sites.

Table 11: Mean and standard deviation of ground surface temperatures measured along the Coal Ridge transect over three freezing and two thawing seasons (2003-2006)

	average seasonal ground surface temperature						standard deviation					
	P9	CR1	CR2	CR3	CR4	BOWL	P9	CR1	CR2	CR3	CR4	BOWL
	1254m	1260m	1271m	1363m	1457m	1640m						
2003-2004	-4.1	-4.3	-3.6	-6.0	-5.4		2.3	2.3	2.3	3.7	2.8	
2004	7.8	7.1	6.2	7.9	7.2		4.8	4.8	4.0	5.2	5.2	
2004-2005	-2.1	-2.8	-2.6	-3.3	-3.6	-4.9	1.4	1.7	1.6	2.1	1.7	2.9
2005	7.7	6.3	6.9	6.4	6.3		2.5	3.6	3.2	3.4	3.3	
2005-2006		-5.7	-4.2	-4.9	-4.3			3.4	2.2	2.6	2.2	

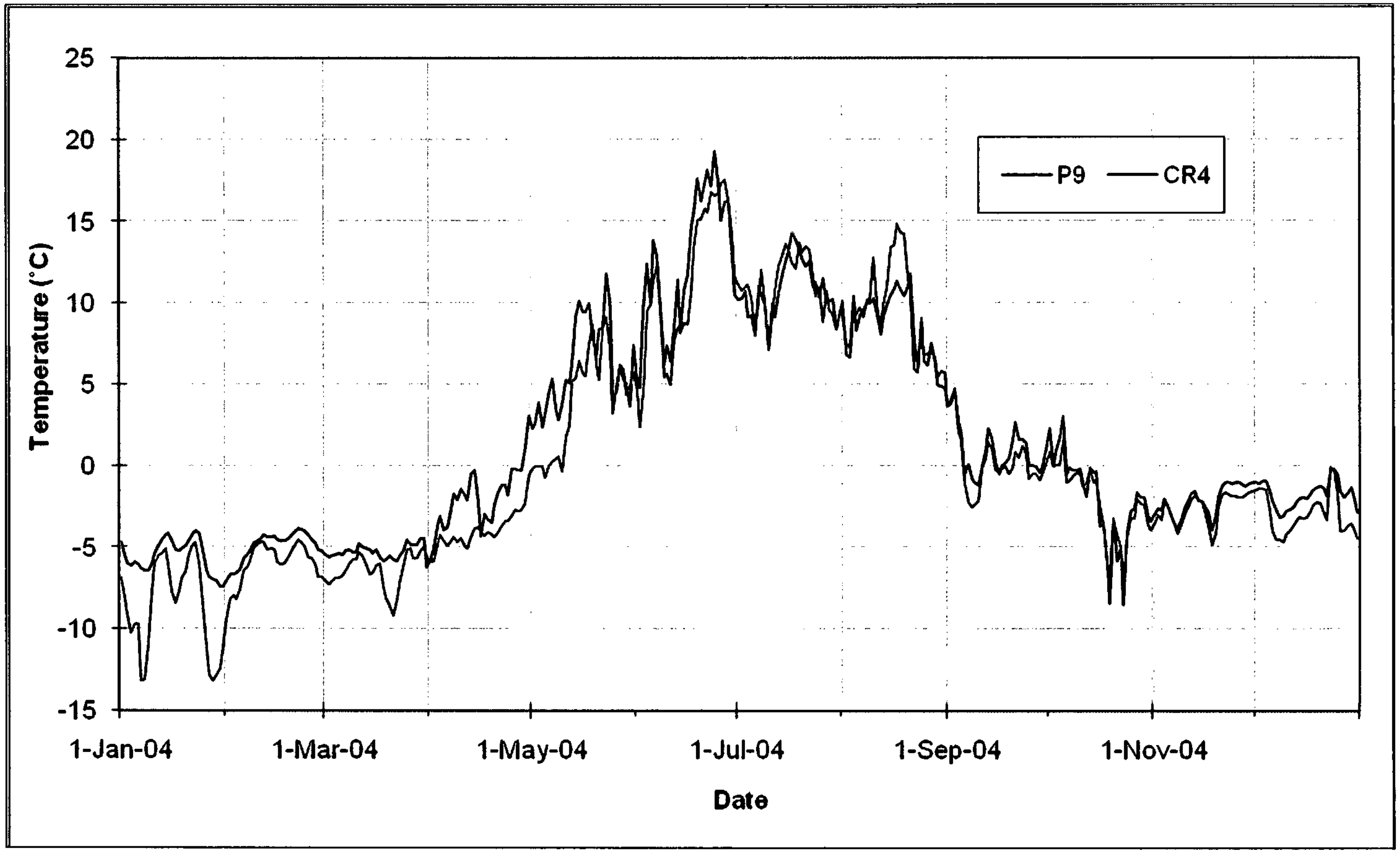

Figure 23: Mean daily ground surface temperatures at P9 and CR4 (2004)

Seasonal values were computed for three freezing seasons and two thawing seasons along the Coal Ridge transect, and for two additional freezing and thawing seasons at the valley bottom site (**Figure 24**). Given that the warmest seasonal air temperatures were recorded in summer 2004, ground surface temperatures recorded over the same period were also the warmest. The coldest winter season is more difficult to determine, demonstrating the importance of snow accumulation to winter ground surface temperatures. While the coldest air temperatures along the transect were recorded during the 2005-2006 winter season, ground surface temperatures measured at the sites over the same period do not all represent the coldest seasonal values. Although seasonal minima recorded at CR1 and CR2 correspond to minimum seasonal air temperatures, the coldest ground surface temperatures were recorded at P9, CR3 and CR4 during earlier winter seasons; the limited data available from P9 and WC-Bowl over the 2005-2006 winter season prevents the calculation of seasonal values during that period.

MAGST calculated for three consecutive years between August 2003 and July 2006 are generally <1.0°C, and do not show an inverted relationship between temperature and elevation except during the 2005-2006 year (**Figure 25**). During the 2004-2005 year, for example, the mean value at the valley bottom site was 1.2°C, while 160 m higher on the Coal Ridge transect (CR4) the temperature was 0.4°C. This is the only year where annual temperatures were above 0°C at all the sites, except at WC-Bowl where a temperature of -0.8°C was recorded. Monthly ground surface temperatures for the same period at the valley bottom site ranged from -2.7°C to 9.4°C, while the highest site (CR4) had a slightly smaller range (-5.3°C to 9.4°C) (**Figure 26**).

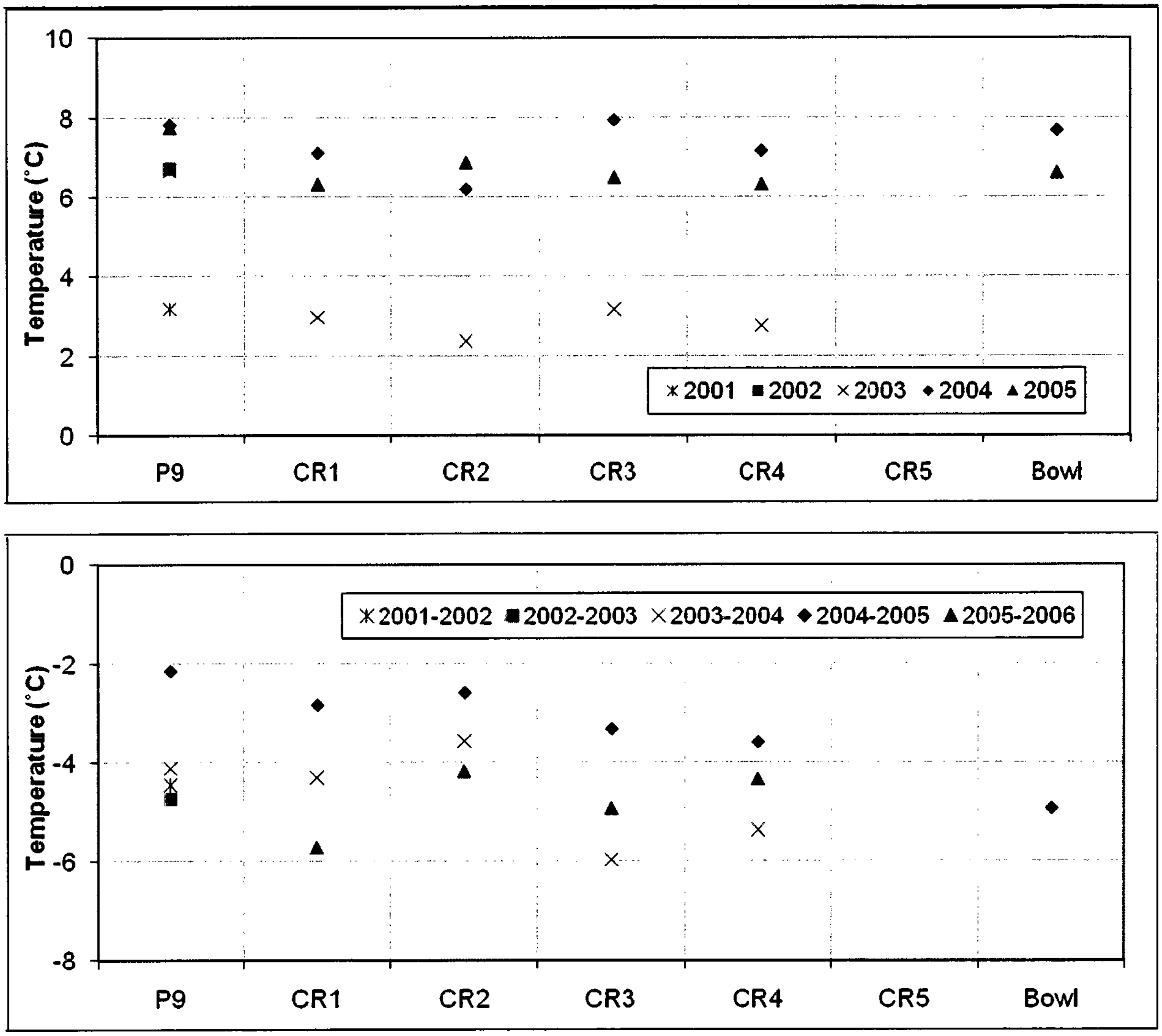

Figure 24: Average seasonal ground surface temperatures along the Coal Ridge transect during five thawing (top) and five freezing (bottom) seasons (2001 to 2006). Note: Site elevation increases from left to right. . Only P9 was operating in all years.

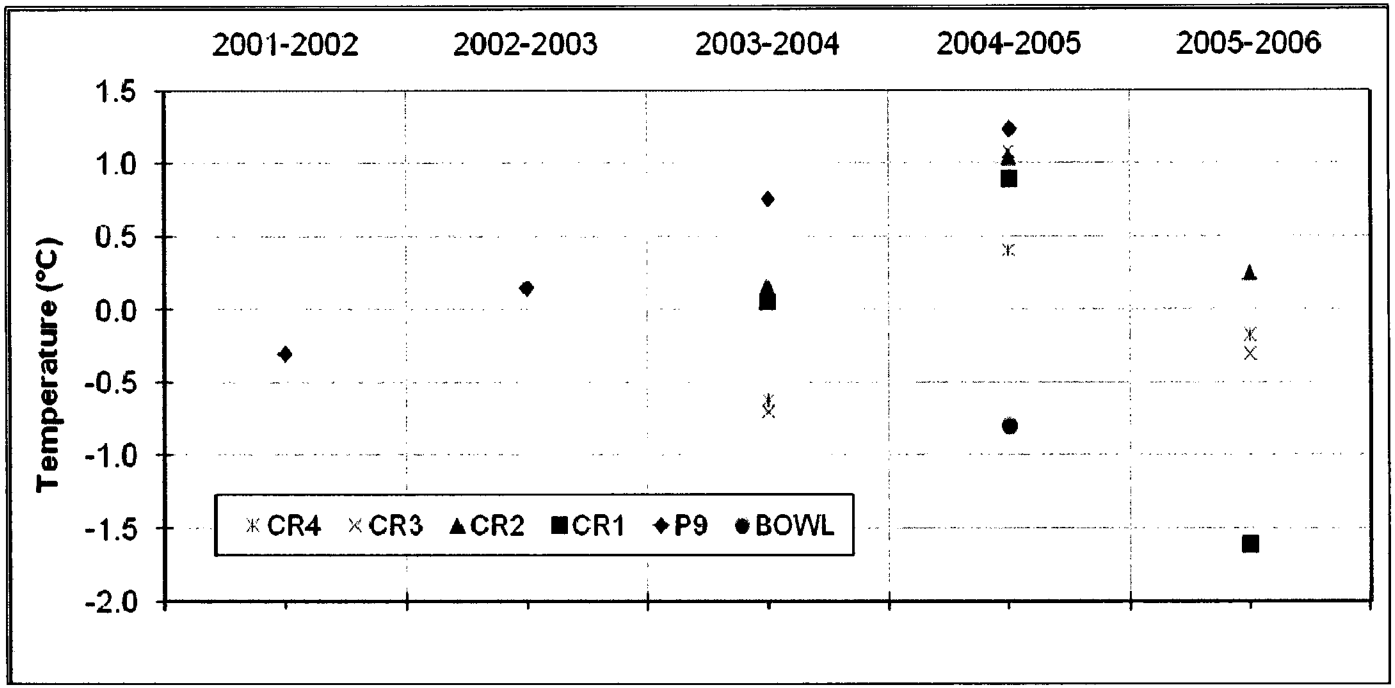

Figure 25: Mean annual ground surface temperatures along the Coal Ridge transect (August 2001 to July 2006). Note: Elevation increases along the transect from P9 (1254 m), CR1 (1260 m), CR2 (1271 m), CR3 (1363 m), CR4 (1457 m) to BOWL (1640 m)

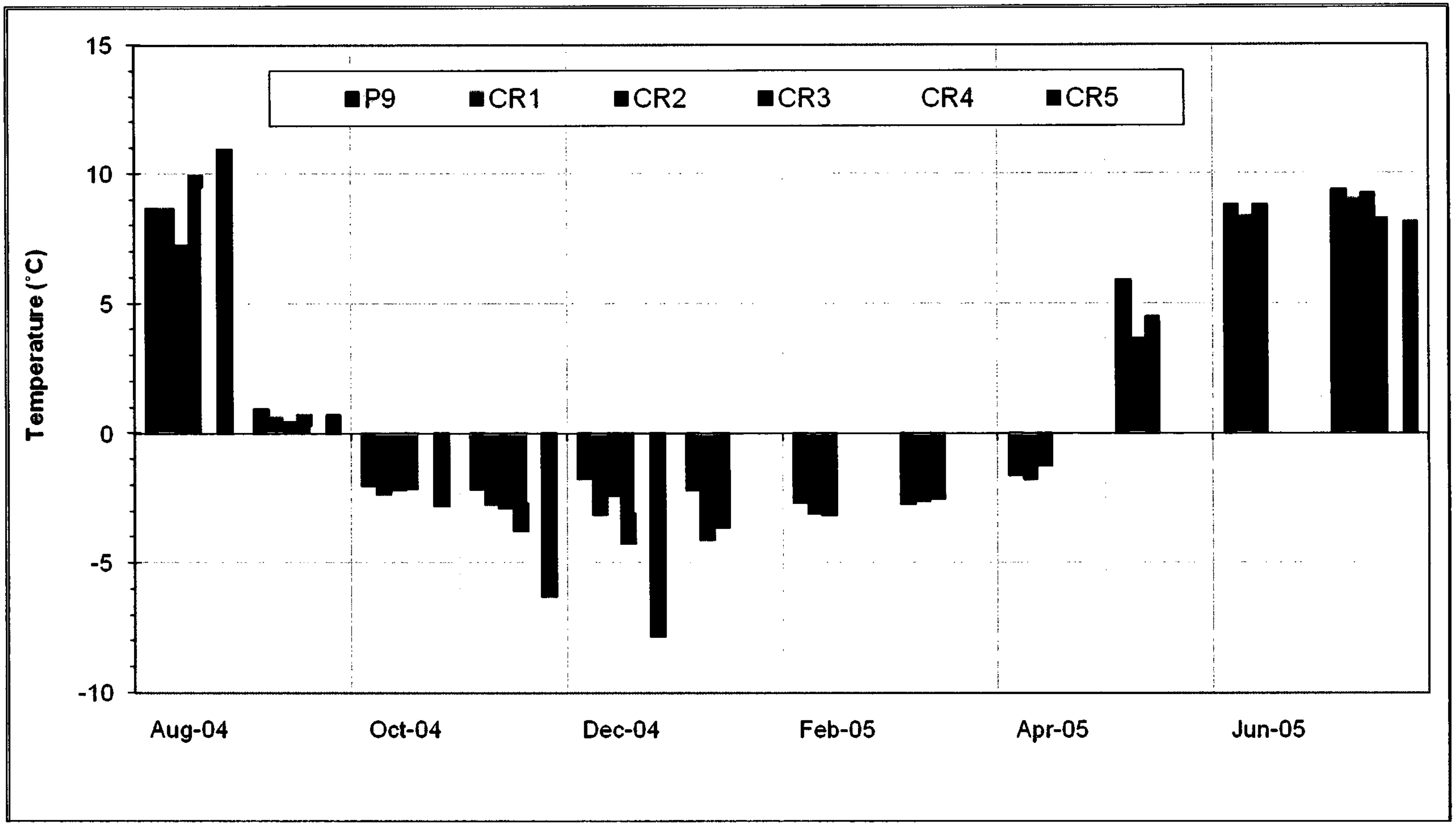

Figure 26: Mean monthly ground surface temperatures along the Coal Ridge transect (August 2005 to July 2006). Note: inversion in air temperatures in winter months not not generally result in inverted ground surface temperatures

3.2.2 Mount Sima Trail

Ground surface temperatures recorded along the Mount Sima trail do not include Talmark and T1, as the former site is only instrumented to measure air temperatures and limited data available from the latter prevents analysis. In most cases, ground surface temperatures measured along the trail are less variable during the winter than in summer (**Table 12**). Surface temperatures at the sites typically began to increase in late-April and early-May, and became similar as air temperatures rose above 0°C. During the snowmelt season, surface temperatures remained just below 0°C for a period of approximately two weeks as the snow ablated, particularly at the highest transect site (T4). Maximum daily summer surface temperatures correspond closely with maximum daily summer air temperatures (**Figure 27**), occurring at the end of June 2004 at each of the trail sites. Surface temperatures at the sites generally fell below 0°C in early-October and remained frozen until snow-melt began. Minimum daily winter surface temperatures are less fixed and occur on different dates at the sites. These minima do not correspond with minimum air temperatures, which were all >20°C colder on the same dates. Along the Mount Sima trail, minimum daily surface temperatures ranged from -12.5°C (T2) to -5.7°C (T4).

Seasonal values computed for two freezing and two thawing seasons along the trail show that the warmest seasonal surface temperatures were recorded in summer 2004, when air temperatures at the sites were also the warmest (**Figure 28**). Winter 2005-2006 exhibited temperatures approximately 1.0°C to 2.0°C cooler than 2004-2005 at all of the stations, and corresponded to the coldest seasonal air temperatures. MAGST calculated for two consecutive years between August 2004 and July 2006 are all >0°C (**Figure 29**).

Table 12: Mean and standard deviation of ground surface temperatures measured along the Mount Sima trail over two freezing and two thawing seasons (2004-2006)

	average seasonal ground surface temperature				standard deviation			
	T1	T2	T3	T4	T1	T2	T3	T4
	868m	1011m	1145m	1290m				
2004		10.5	9.3	8.6		5.6	5.1	5.0
2004-2005		-2.1	-0.9	-1.8		1.7	0.6	1.0
2005		8.7	7.6	6.4		3.4	4.1	3.7
2005-2006		-4.3	-3.2	-3.1		3.2	2.2	1.1

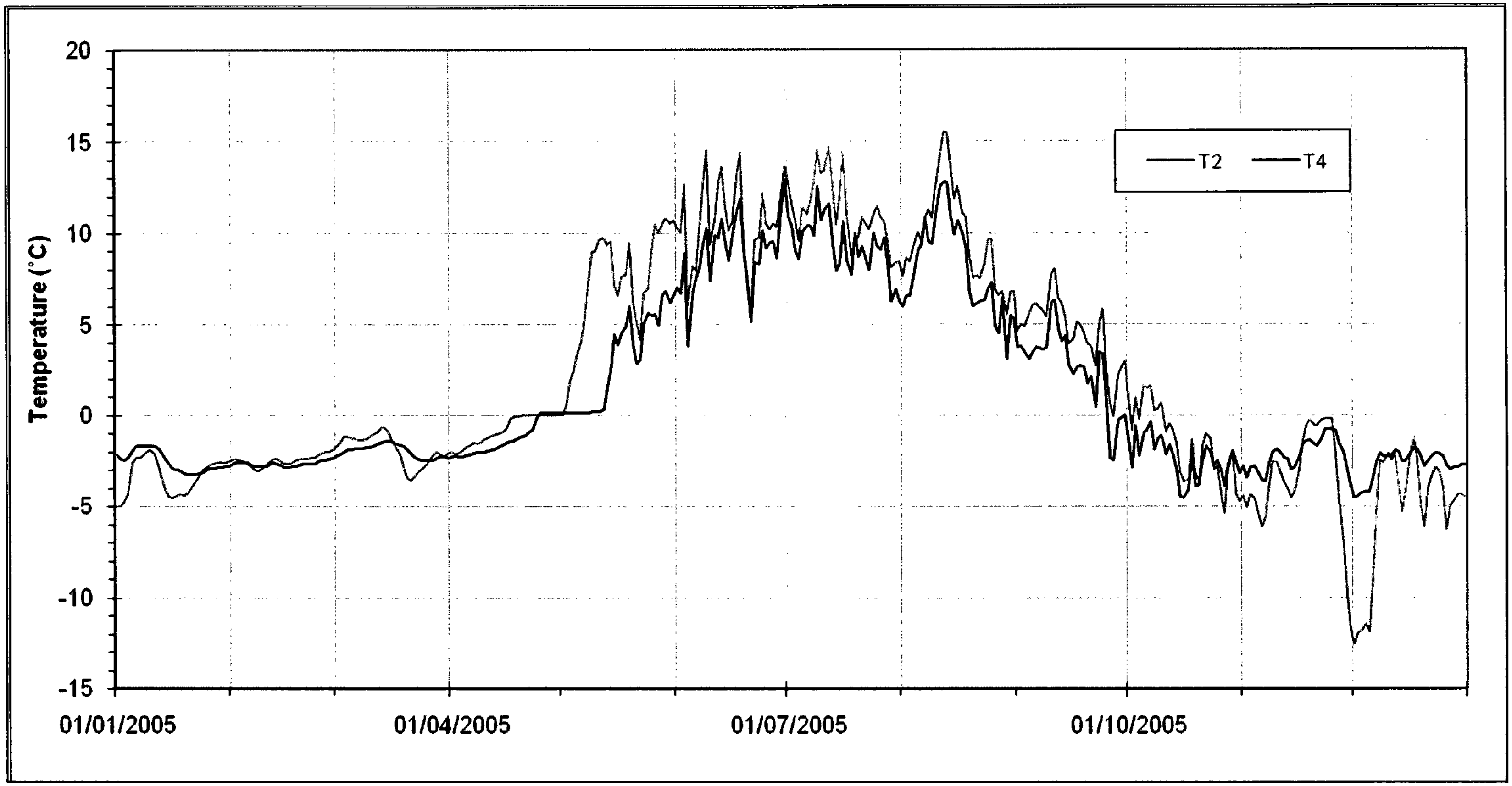

Figure 27: Mean daily ground surface temperatures at T2 and T4 (2005).

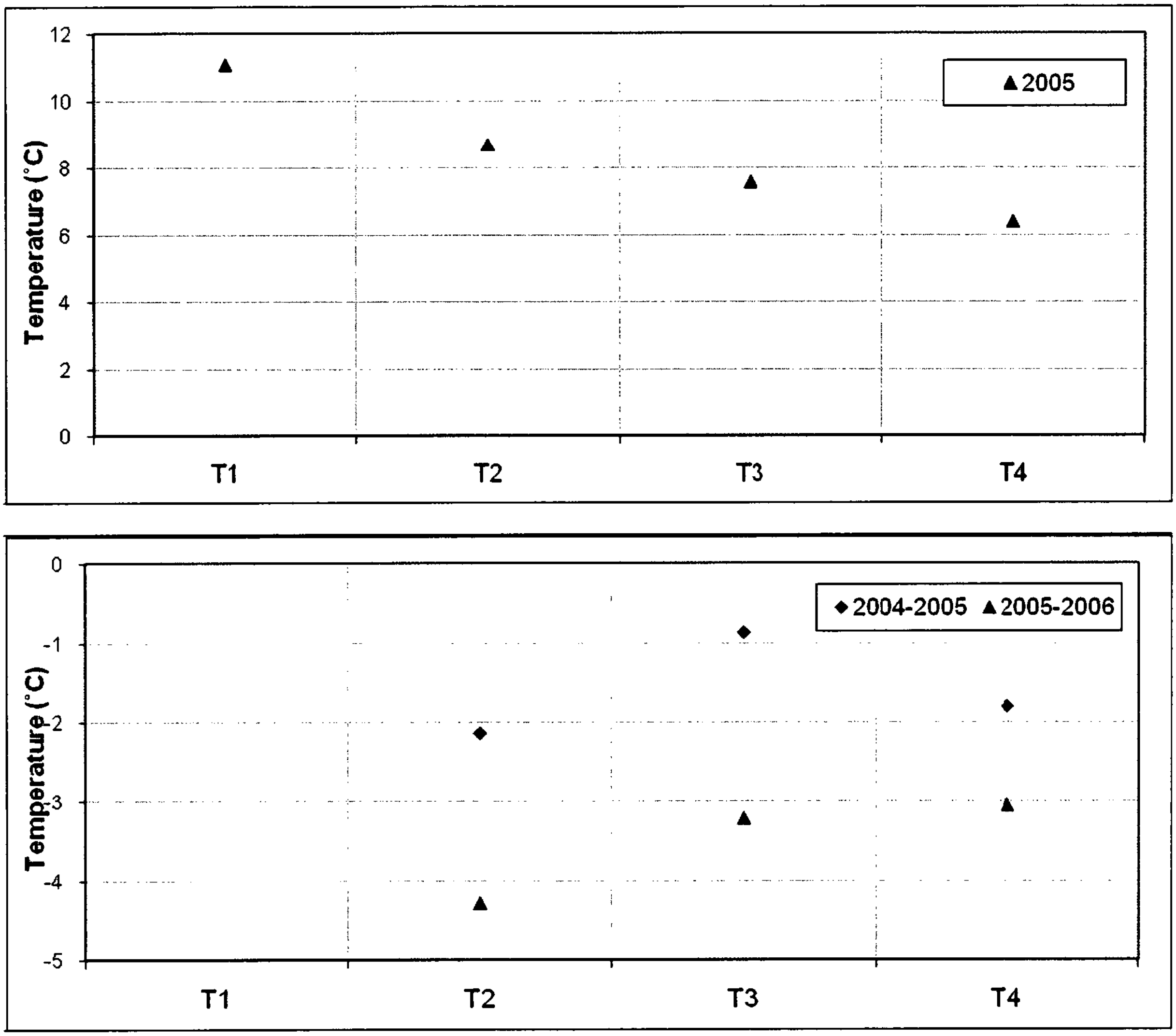

Figure 28: Average seasonal ground surface temperatures along the Mount Sima trail during one thawing (top) and two freezing (bottom) seasons (2004 to 2006)

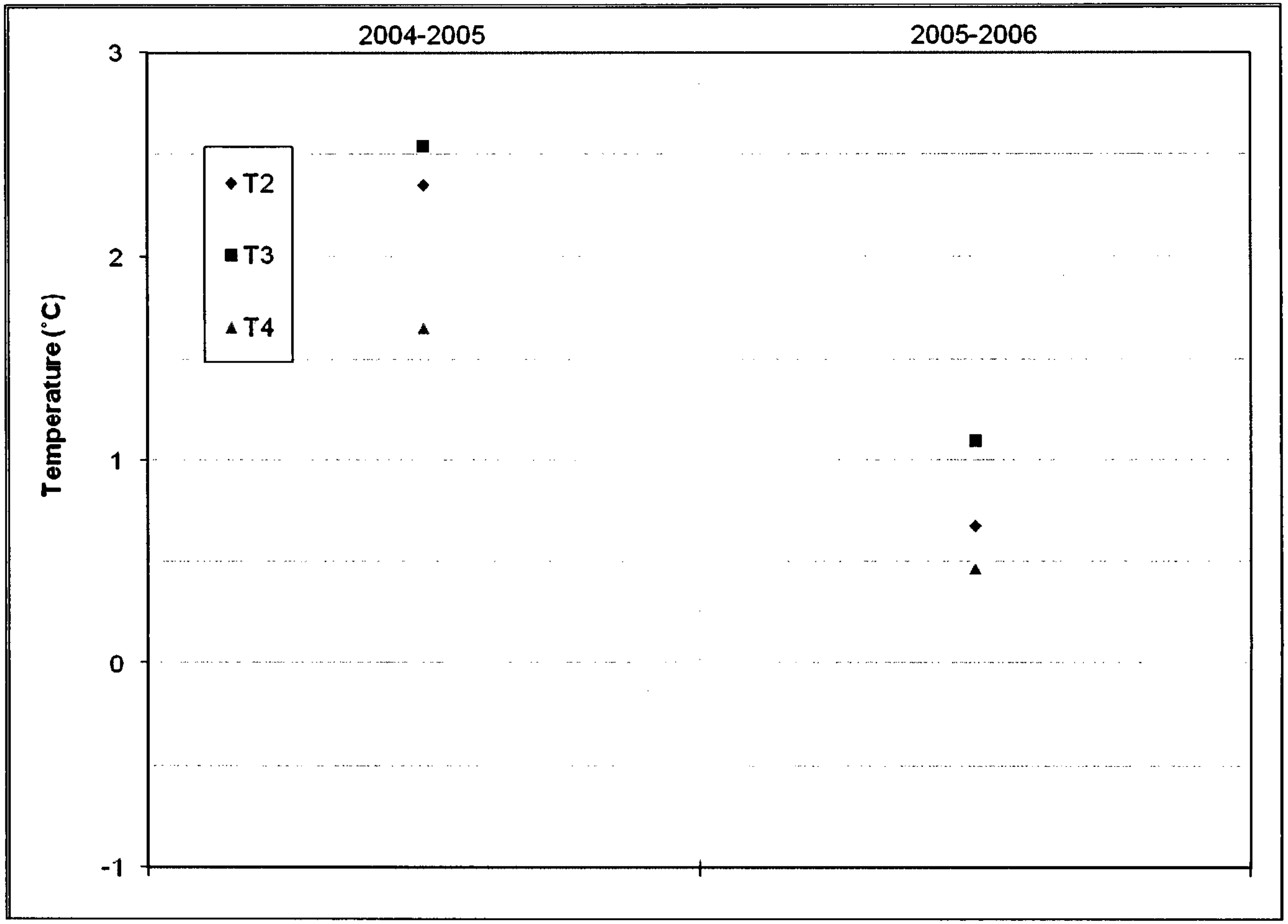

Figure 29: Mean annual ground surface temperatures along the Mount Sima trail (August 2004 to July 2006)

Monthly ground surface temperatures at T2 ranged from -7.9°C to 10.9°C, a much larger range than that of T4 (-4.3°C to 9.5°C) (**Figure 30**).

3.2.3 Newly Installed Wolf Creek Sites

Daily values indicate that between June and August 2006, ground surface temperatures remained above 0°C throughout the period of record at all but the Mount Granger site, where temperatures fell below freezing on a number of occasions (**Figure 31**). Maximum daily summer surface temperatures occurred in mid-June, and correspond closely with maximum daily summer air temperatures at all the sites. During the month of June, mean ground surface temperatures at the sites ranged from less than 5.0°C, atop Mount Granger, to approximately 12°C, at the exposed plain site; the remaining sites recorded mean monthly temperatures of between 7.5°C and 11.0°C (**Table 13**). Average temperatures remained relatively unchanged during July at a number of sites, with the greatest difference recorded at the newly re-vegetated drained lake site. Mean ground surface temperatures were above 0°C at all sites, with the lowest average recorded at the Mount Granger site (4.7°C). Average temperatures recorded at the drained lake and exposed plain sites were the warmest, measuring 10.4°C and 11.4°C respectively. Ground surface temperatures measured at the remaining sites averaged between 7.6°C and 9.3°C.

3.3 Air and Ground Surface Temperature Relations

The purpose of this section is to investigate the relationship between air and ground surface temperatures, to describe trends in potential incoming solar radiation, vegetation cover, and winter snow accumulation, and to examine the influence of these site-specific conditions (with the exception of TPI effects) on the temperature relations both at and

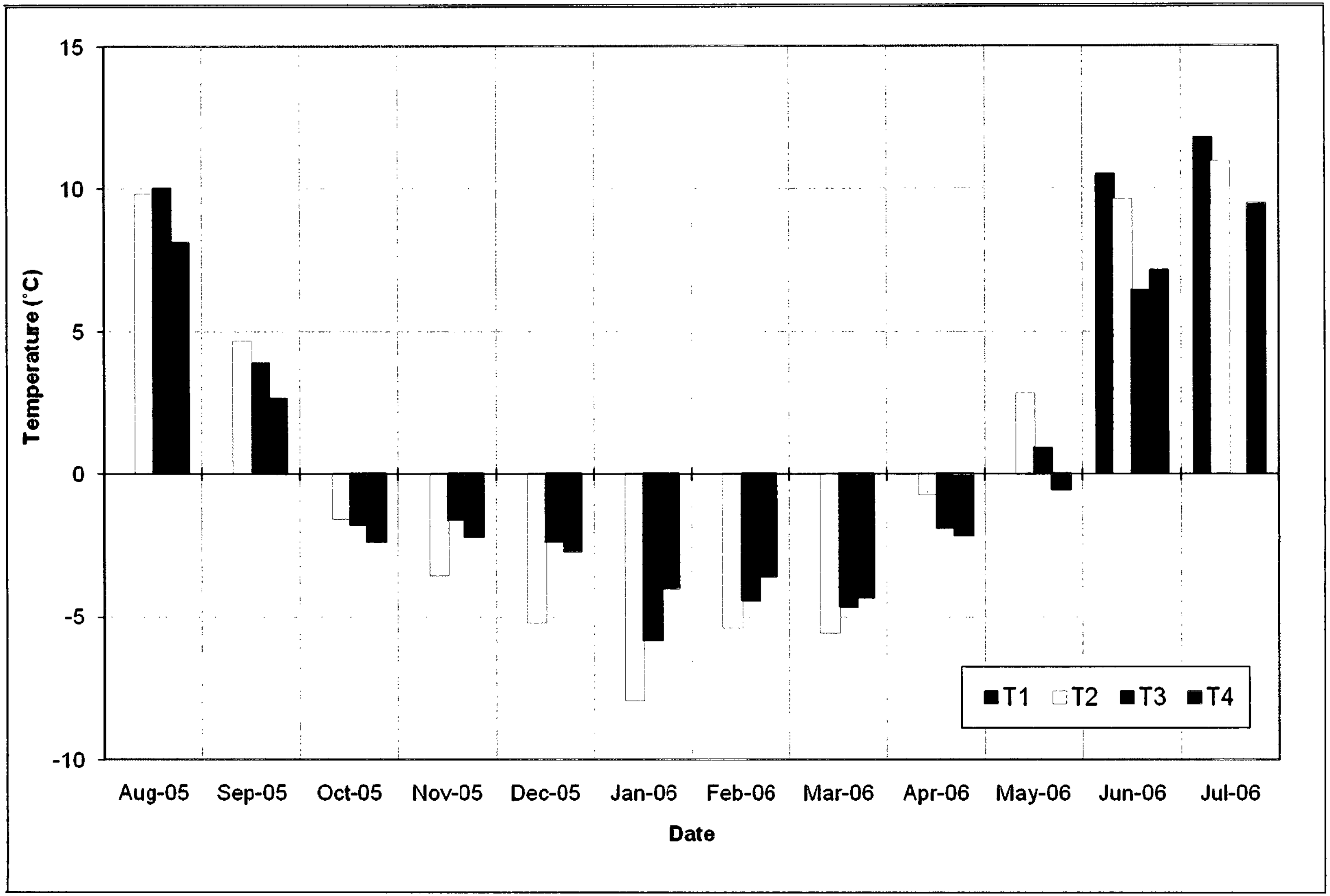

Figure 30: Mean monthly ground surface temperatures along the Mount Sima trail (August 2005 to July 2006)

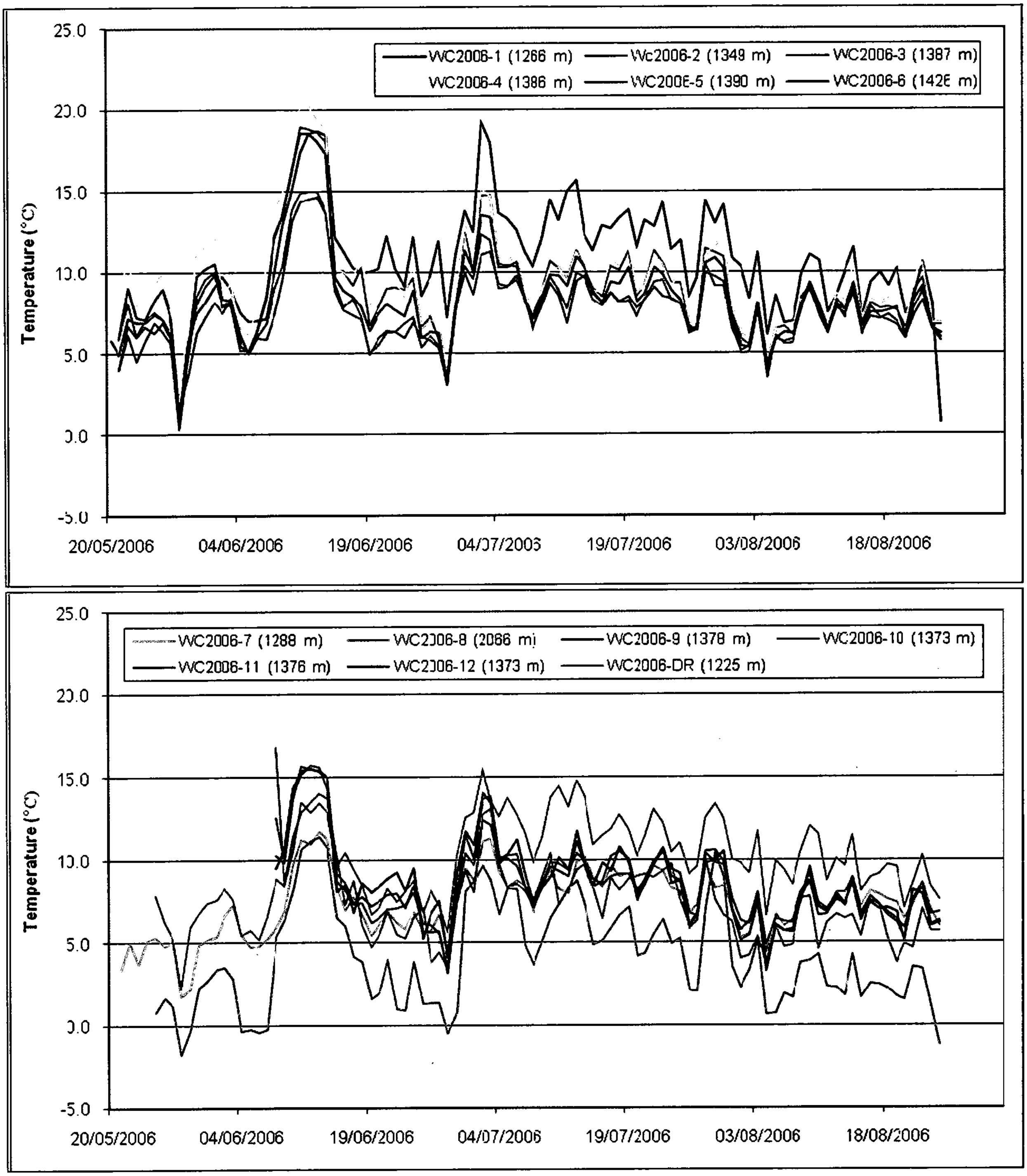

Figure 31: Mean Daily Ground Surface Temperatures at the Newly Installed Wolf Creek Valley Sites (May – August 2006)

Table 13: Average Ground Surface Temperatures at the Newly Installed Wolf Creek Valley Sites (June and July 2006)

	June 2006	July 2006
WC2006-1	12.2	13.0
WC2006-2	8.6	8.7
WC2006-3	10.9	10.0
WC2006-4	11.5	10.2
WC2006-5	8.4	8.6
WC2006-6	10.2	9.5
WC2006-7	7.6	8.8
WC2006-8	4.8	6.3
WC2006-9	9.2	9.4
WC2006-10	8.4	8.6
WC2006-11	9.3	9.4
WC2006-12	9.8	9.6
WC2006-DR	9.4	12.2

among the study sites, as summarized by the surface offset and calculated seasonal n-factors.

3.3.1 Potential Incoming Solar Radiation

During the freezing season, modeled PISR density at the study sites ranges from a minimum of 441 MJ/m^2 to a maximum of 682 MJ/m^2, with a mean of 567 MJ/m^2 and a standard deviation of 68 MJ/m^2 (**Figure 32**). Over this period, PISR density at the temperature measurement sites is lowest mid-way along the Coal Ridge transect (CR3) and highest at the tundra sites (T4, CR5 and CR6). At the remaining Coal Ridge sites, predicted values of PISR density are also low, while forested sites situated along the Mount Sima trail receive relatively high levels of PISR. It should be noted that modeled PISR does not include vegetation, shading effects or differences in albedo, all of which affect insolation reaching the ground surface. Seasonal changes in radiation density patterns are evident across the basin, with predicted totals during the 5-month thawing season more than twice as great as in the 7-month freezing season. PISR values over the latter period range from a minimum of 1046 MJ/m^2 to a maximum of 1633 MJ/m^2, with a mean of 1430 MJ/m^2 and a standard deviation of 173 MJ/m^2. Trends in PISR density over this period remain fairly consistent with winter values, with maximum values at the tundra sites, and minimum values mid-way along the Coal Ridge transect.

3.3.2 Snow Accumulation

As outlined in Section 2.2.4, the effects of snow cover on ground surface temperatures at each of the sites, snowpack development was tracked over the 2005-2006 winter season using the iButton stakes installed during the previous summer's fieldwork

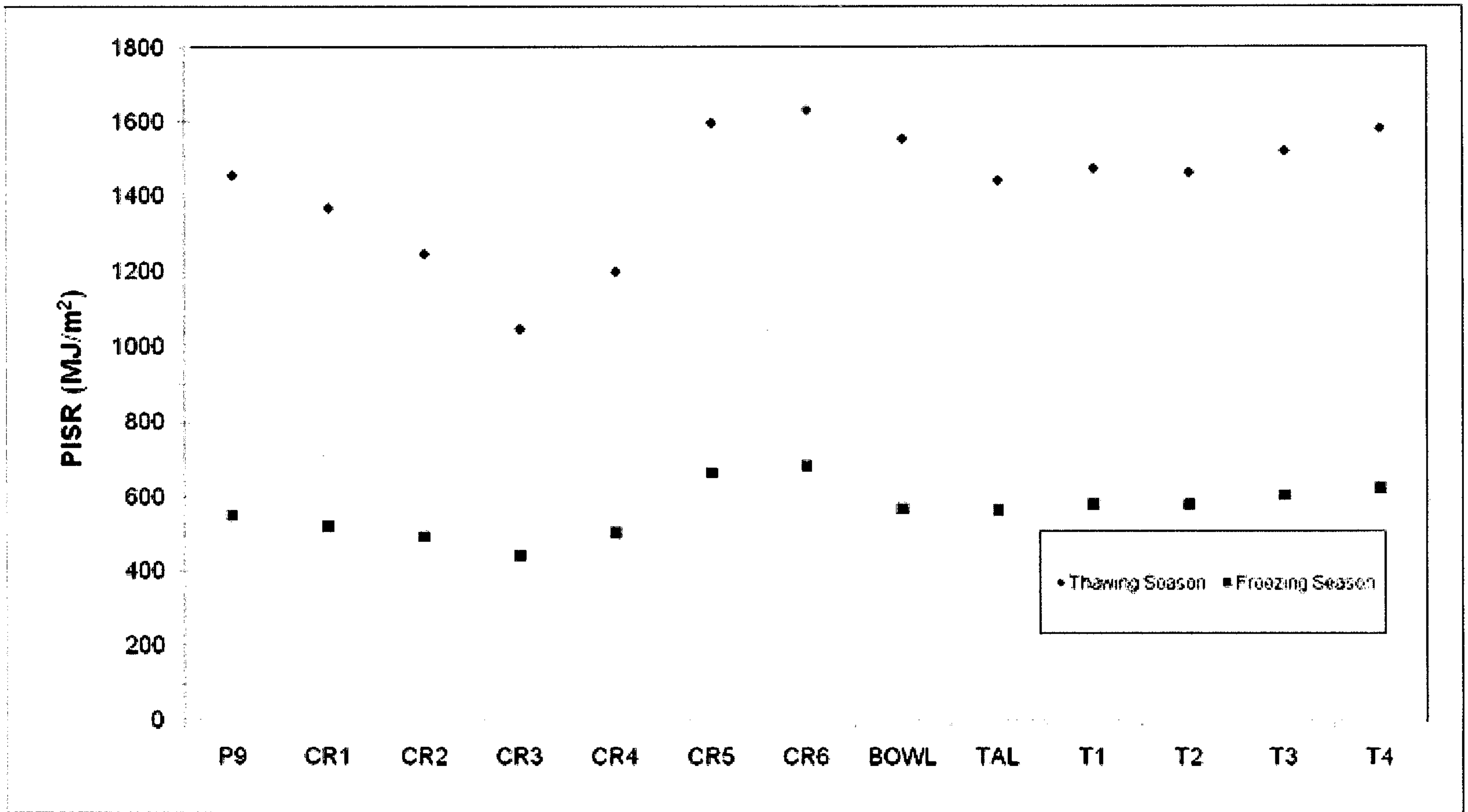

Figure 32: Potential incoming solar radiation density at the study sites for both the freezing and thawing seasons

(**Table 14**). Since the temperature sensors are installed at 10 cm intervals (see Section 2.2.4), the analysis of temperature differences along the stake offers an approximation of snow depth within a range of values (e.g. 10-20, 20-30, 30-40, 40-60, 60-80 cm).

Snow accumulation data from the Whitehorse airport shows that the first snowfall occurred in early October 2005 with more than 10 cm recorded during a single event (**Figure 33**). While increased temperatures at the end of the month resulted in a reduced snow cover at the site, the warming was short-lived and accumulation continued to increase until a maximum depth of 23 cm was reached in mid-November. Snow depths fell below 5 cm in December and February, while depths of approximately 20 cm were recorded in both January and March. Over a two-week period in April, snow depth continued to vary, fluctuating from exposed ground to accumulations of up to 17 cm, and culminating in complete snow melt by months end. According to the *Yukon Snow Survey* (Environment Yukon, 2006), accumulations in the Whitehorse area were above average during the month of April, with YXY receiving three times more snow than the normal for that period. Across much of the Yukon, a combination of increased precipitation and below average melt resulted in above normal snowpack conditions in early May.

Along the Mount Sima trail, snow accumulation began in early October at all four sites, and depths continued to increase in subsequent weeks to more than 20 cm at the lower three sites (T1, T2 and T3) and more than 30 cm at T4 in early November (**Figure 34**). Despite mid-season melt periods in December, January and March, which reduced snow depths significantly along the trail, accumulations continued to increase following a similar pattern to that of YXY throughout the winter season. Maximum depths were recorded between the end of March and mid-April at each of the sites, increasing with

Table 14: Maximum snow depth at the study sites over the 2005-2006 freezing season

Study Sites	Maximum Snow Depth (mm)
T1	40-60
T2	60-80
T3	60-80
T4	80-100
P9	40-60
CR1	60-80
CR2	40-60
CR3	40-60
CR4	30-60

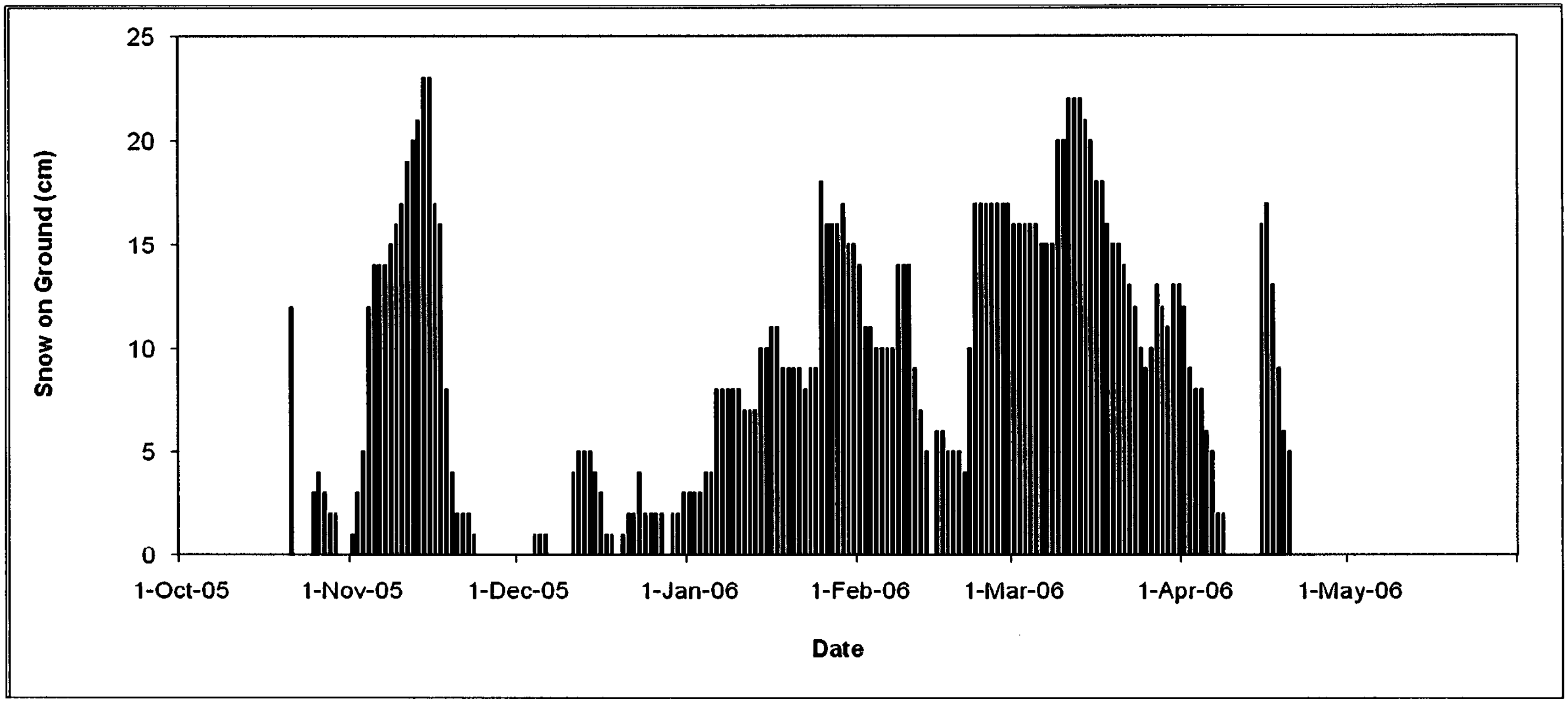

Figure 33: Daily snow on the ground at the Whitehorse airport (October 2005 – April 2006). Source: Environment Yukon, 2006. *Yukon Snow Survey*

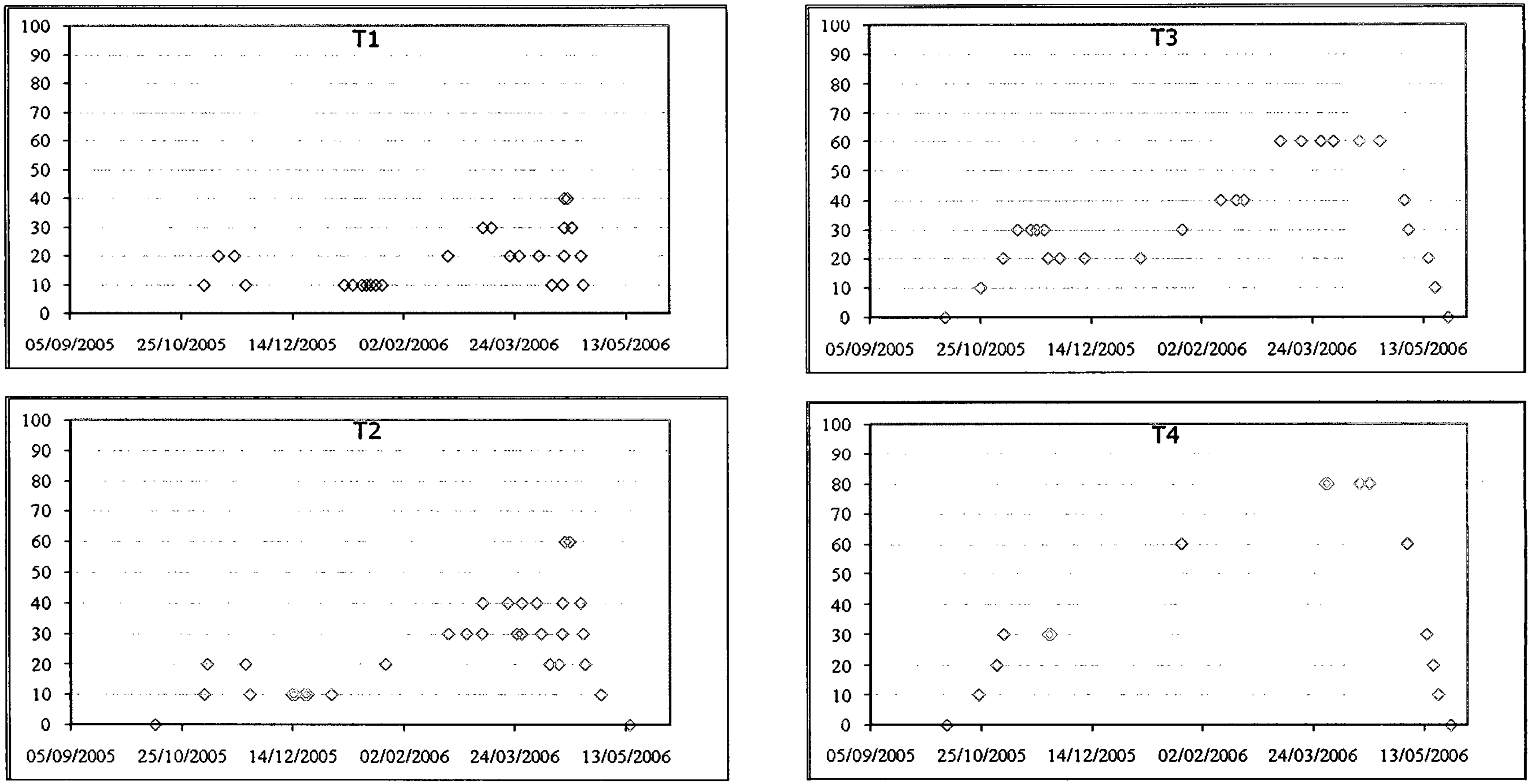

Figure 34: Snow on the ground along the Mount Sima trail (October 2005 – May 2006)

elevation along the trail. The accumulation was greatest at the uppermost sub-alpine taiga site (T4), where between 80 and 100 cm of snow was recorded. Maximum accumulation at the lowest boreal forest site (T1) was between 40 and 60 cm, while depths of between 60 and 80 cm were measured at the remaining forested sites (T2 and T3). The spring melt period began shortly after these maximums were reached. The ground surface was first exposed between the middle and end of May at all of the sites, with T2 being the first exposed and T4 the last, more than two weeks after the ground at YXY became snow-free.

Along the Coal Ridge transect, the first snowfall occurred in early October and snow depths continued to increase in subsequent weeks to more than 20 cm at the lower three sites (P9, CR1 and CR2) in early November (**Figure 35**). Accumulation continued to increase along the transect throughout the winter period, with maximum depths reached near the end of January, except at CR3 where a maximum snow depth of 40 cm was reached just prior to the spring melt in April. Maximum accumulation at the lowest Coal Ridge site (CR1) was between 60 and 80 cm, while depths of between 40 and 60 cm were measured at the remaining sub-alpine taiga sites (P9, CR2 and CR3). Although snow depth at the lone alpine tundra site (CR4) reached at least 30 cm, failure of the 40 cm sensor limits the ability to determine whether this represents the maximum accumulation at the site. Snow depths remained relatively constant over several weeks between January and the late March at all of the sites, until the beginning of the spring melt period in mid-April; the ground surface was first exposed between the middle and end of May at all of the sites.

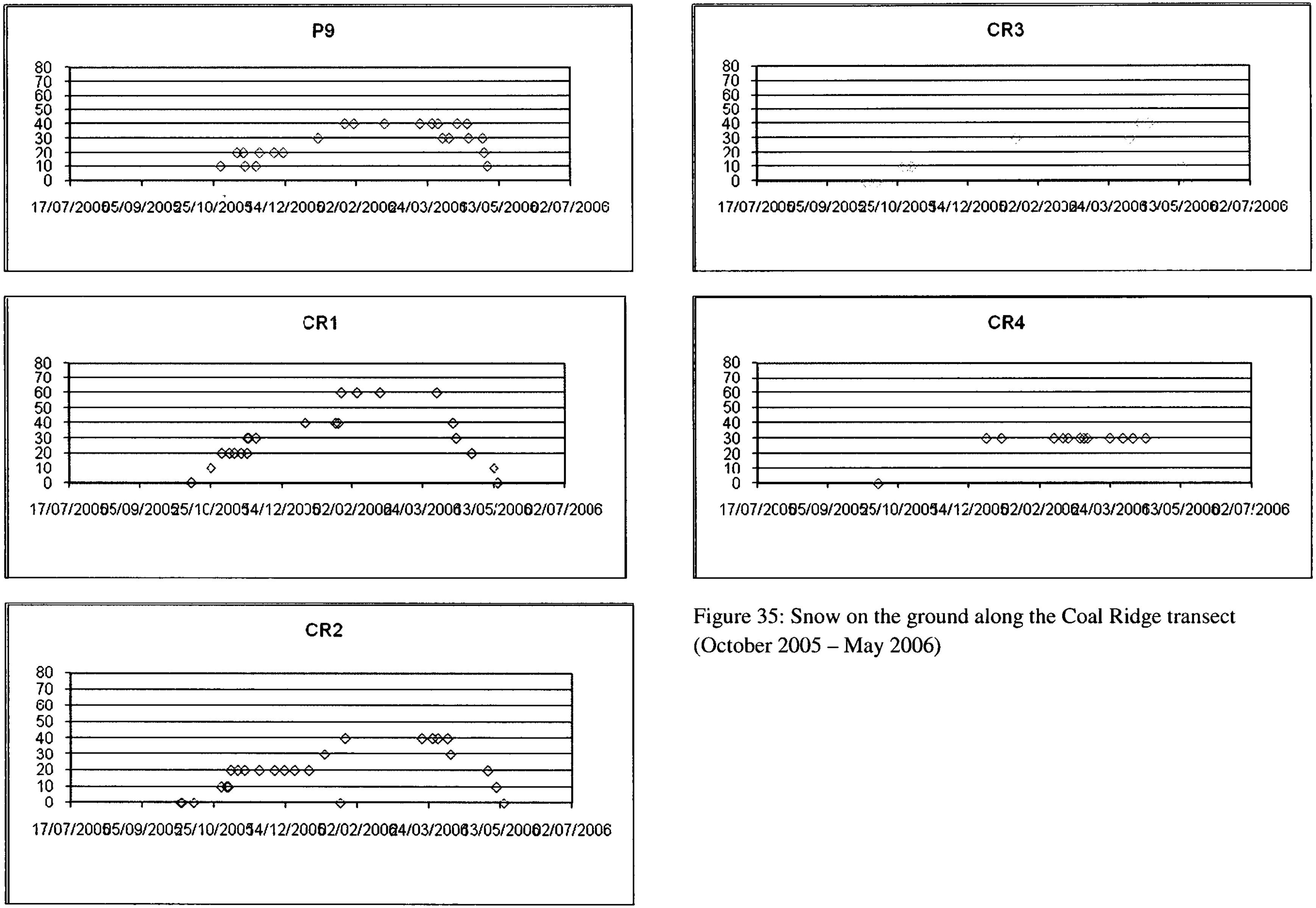

Figure 35: Snow on the ground along the Coal Ridge transect (October 2005 – May 2006)

3.3.3 The Relationship between Air and Ground Surface Temperatures

Throughout the study area, temperature differences between the air and the ground surface were typically highest in the middle of the freezing season, when the ground was insulated by seasonal snow cover (**Figure 36**). The low thermal conductivity of snow restricts ground heat loss, resulting in mean daily ground surface temperatures which are typically much warmer than corresponding air temperatures. Daily minima averaged more than 20°C warmer than the lowest recorded daily air temperatures measured at the each of the study sites. In January 2004, mean monthly ground surface temperatures measured along the Mount Sima trail all averaged more than 12°C warmer than their corresponding air temperatures, while 2005 temperatures averaged approximately 10°C warmer. The lowest three sites along the Coal Ridge transect averaged more than 11°C warmer than their corresponding air temperatures in January 2004 and 2005, while the two uppermost sites were between 6°C and 7°C warmer.

During the thawing season, temperature differences between the air and the ground were generally small (less than 2°C), with the smallest differences typically recorded at the alpine tundra sites. Air and ground surface temperatures at these sites were closely related, with surface temperatures either equal to or greater than measured air temperatures. At the remaining sites, located within the sub-alpine taiga and boreal forest, air temperatures exceeded ground surface temperatures for the majority of the summer season, presumably due to vegetative shading of the ground. The smallest differences were measured during the shoulder seasons, when daily air and ground surface temperatures were both close to freezing.

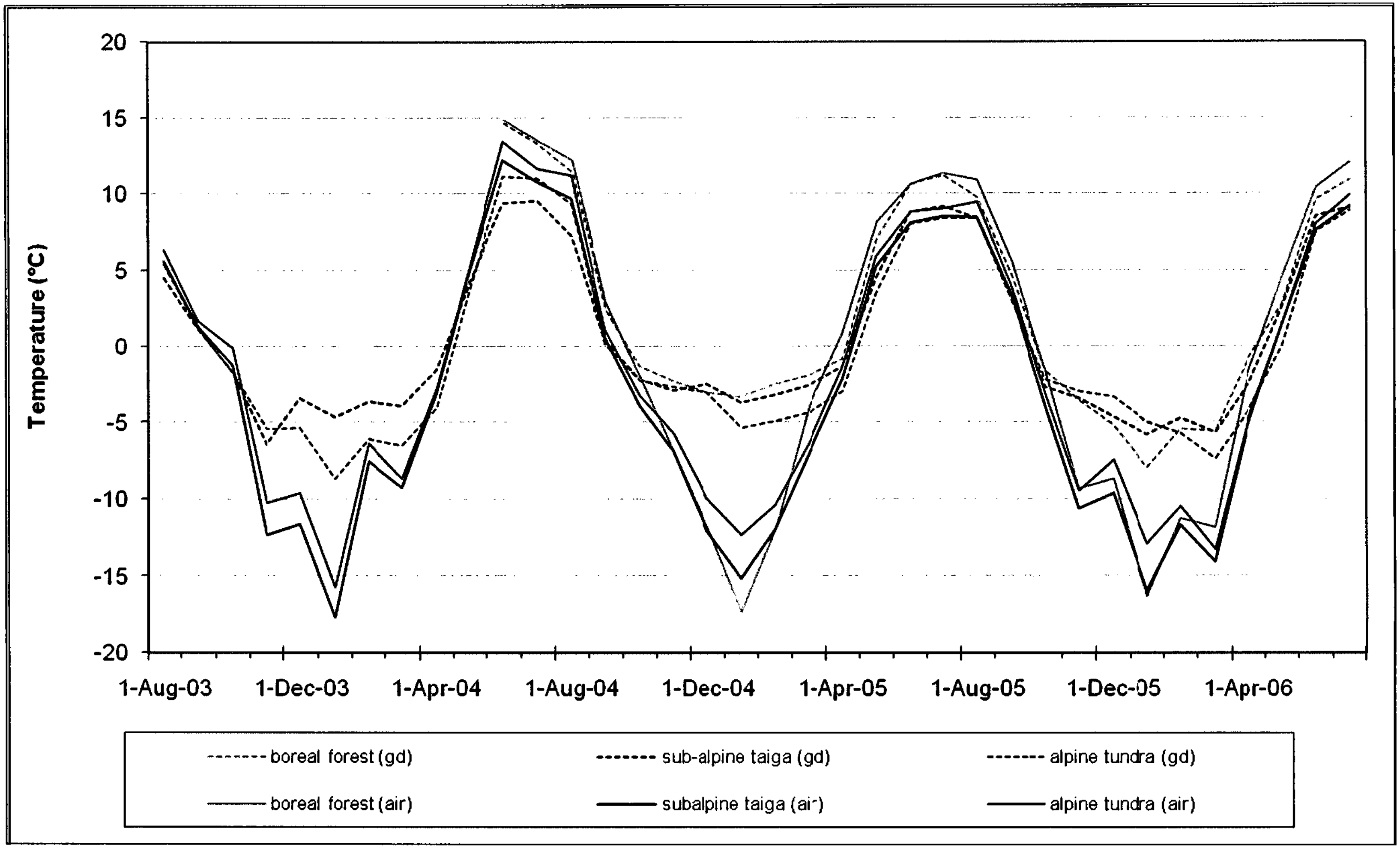

Figure 36: Mean monthly air and ground surface temperatures at T2 (boreal forest), CR3 (sub-alpine taiga), and CR4 (alpine tundra) over three years (August 2003 – July 2006)

3.3.4 The Surface Offset

As shown above, the relationship between air and ground surface temperatures varied at and among the study sites throughout both the freezing and thawing seasons. The surface offset summarizes this relationship on an annual basis, representing the difference between MAGST and MAAT. In general, temperatures measured at the ground surface were higher than air temperatures during the freezing season and during the thawing season. Annually, ground surface temperatures exceeded air temperatures at each of the study sites, resulting in positive surface offset values and confirming the overriding influence of winter snow conditions on the annual surface temperatures. Over the study period, the surface offset varied among the sites, with values ranging from a minimum of 0.4°C at an alpine tundra site, to a maximum of 3.6°C within the boreal forest zone (**Table 15**). While surface offset values measured at the sub-alpine taiga sites (1.0 to 3.6) cover almost the entire range of values, those recorded at the forested (2.1 to 3.6) and alpine tundra sites (0.4 to 2.1) were less variable and fall within the high and low parts of the overall range, respectively. The smallest range in values was recorded at the forested sites (1.5°C), slightly smaller than at the alpine tundra sites (1.7°C), where snow accumulation is typically lowest. It is notable that there was virtually no overlap in values between the alpine tundra and forested sites. At sites where snow cover was similar, differences in the offset values were attributed to variations in subsurface temperatures, and the approximation of snow depth within a range of values. In the future, the analysis of data measured by additional I-Button sensors (at 5 cm, 50 cm and 100 cm) and of ground temperature data measured at the top of permafrost (TTOP) may help to explain these differences, both at and among the study sites.

Table 15: Annual surface offsets (Aug 2001 – Jul 2006)

		P9	CR1	CR2	CR3	CR4	Bowl	T2	T3	T4
2001-2002	**MAAT**	-4.1								
	MAGST	-0.3								
	Surface Offset	3.8								
2002-2003	**MAAT**	-2.1								
	MAGST	0.1								
	Surface Offset	2.3								
2003-2004	**MAAT**	-2.2	-2.4	-2.7	-1.9	-1.6				
	MAGST	0.8	0.1	0.2	-0.7	-0.6				
	Surface Offset	3.0	2.5	2.8	1.2	0.9				
2004-2005	**MAAT**	-2.1	-1.8	-2.2	0.1	-1.0	-3.0	0.6	-1.1	-1.4
	MAGST	1.2	0.9	1.0	1.1	0.4	-0.8	2.4	2.5	1.7
	Surface Offset	3.3	2.7	3.2	1.0	1.4	2.2	2.9	3.6	3.1
2005-2006	**MAAT**	-	-4.0	-3.3	-2.5	-2.3	-	-1.4	-	-2.5
	MAGST	-	-1.6	0.3	-0.3	-0.2	-	0.7	1.1	0.5
	Surface Offset	-	2.4	3.6	2.2	2.1	-	2.1		3.0

3.3.5 The N-Factor

Empirically-derived n-factors are used to relate air and surface temperatures by establishing the ratio between air and surface freezing (winter) and thawing (summer) degree-days, thus summarizing the surface energy balance on a seasonal basis. In previous sections, standard dates were used to define the freezing and thawing seasons in order to facilitate seasonal and inter-annual variability both at and among the study sites. In reality, however, the beginning and end of the freezing and thawing season varies both spatially and through time. The actual seasonal dates for each of the study sites are presented in **Table 16.**

Freezing factors (*nf*) over the study period ranged from 0.12, at a forested site, to 0.73, at a site located within the sub-alpine taiga zone (**Table 17**). The distribution of n-factors shown in **Figure 37** demonstrates that there is a broad relationship with both elevation and vegetation, particularly during the freezing season. Values of *nf* calculated for the forested sites were all below 0.40, ranging from 0.12 to 0.36, while those calculated for the tundra sites were all above 0.50 with a range of 0.51 to 0.70 over the study period. Freezing factors for the sub-alpine taiga zone point to the role of variable vegetation cover close to and below tree-line, with values ranging from 0.23 to 0.73 at these sites. The insulating effects of snow are also strongest in the sub-alpine taiga zone, as snow accumulation reaches a peak close to tree-line. Values of *nf* measured at individual sites exhibited significant inter-annual variability with increases of more than 0.20 at some sites between 2004-2005 and 2005-2006. In the years between 2001 and 2005, freezing factors at P9 varied by more than 0.10 annually. Snow accumulation

Table 16: Seasonal dates used to determine n-factors at each of the study sites

Season		P9	CR1	CR2	CR3	CR4	Bowl	T2	T3	T4
nf	2001-2002	Sep 26 - May 6								
nt	2002	May 7 - Oct 7								
nf	2002-2003	Oct 8 - Apr 25								
nt	2003	Apr 26 - Oct 7								
nf	2003-2004	Oct 8 - Apr 28	Oct 7 - May 7	Oct 8 - Apr 28	Oct 8 - Apr 28	Oct 8 - May 6				
nt	2004	Apr 29 - Oct 5	May 8 - Oct 5	Apr 29 - Oct 5	Apr 29 - Oct 5	May 7 - Oct 5				
nf	2004-2005	Oct 6 - Apr 26	Oct 6 - May 10	Oct 6 - Apr 30	Oct 6 - failed	Oct 6 - May 8	Sep 6 - Apr 24	Oct 16 - Apr 27	Oct 6 - May 10	Oct 6 - Apr 24
nt	2005	Apr 27 - failed	May 11 - Sep 24	May 1 - Sep 30	failed - Sep 30	May 9 - Sep 30	Apr 25 - failed	Apr 28 - Oct 10	May 11 - Sep 30	Apr 25 - Sep 25
nf	2005-2006	failed	Sep 25 - May 16	Oct 1 - May 14	Oct 1 - May 18	Oct 1 - May 21	failed	Oct 11 - May 3	Oct 1 - May 20	Sep 26 - May 25

Table 17: Freezing season n-factors (2001-2006)

	P9	CR1	CR2	CR3	CR4	Bowl	T1	T2	T3	T4	Snow Depth*(cm)
2001-2002	0.39										125
2002-2003	0.57										75
2003-2004	0.45	0.49	0.40	0.73	0.70						90
2004-2005	0.26	0.36	0.31	-	0.52	0.60	-	0.29	0.12	0.23	156
2005-2006	-	0.56	0.41	0.55	0.51	-	-	0.49	0.36	0.35	109

*Historical snow depth data from YXY provided by R. Janowicz, Yukon Department of Environment. Data collected February-May.

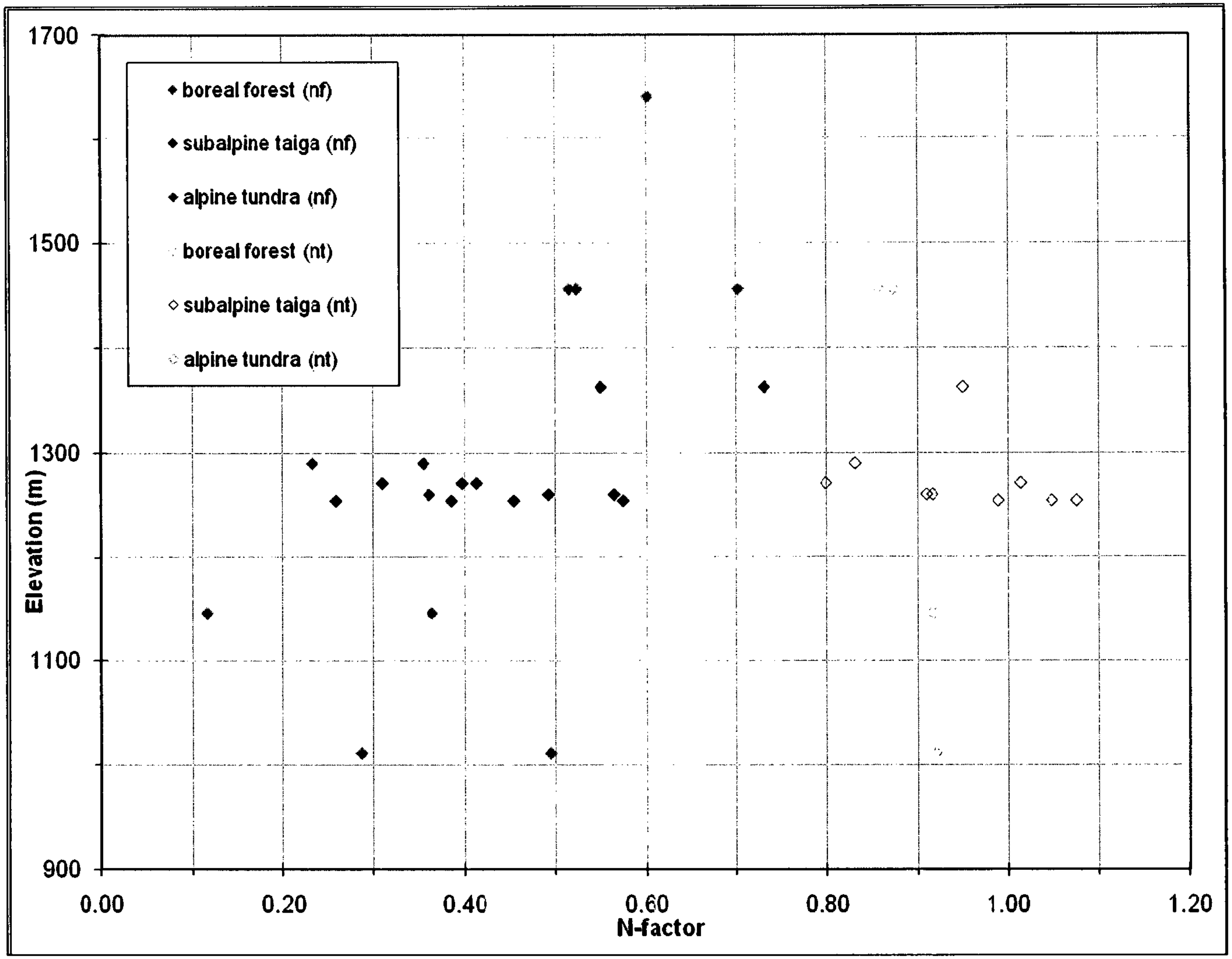

Figure 37: The relationship between elevation, vegetation and seasonal n-factors at the study sites (2001-2006). Freezing (filled) and thawing (outlined) n-factors are shown for the boreal forest (green), sub-alpine taiga (blue) and alpine tundra (orange) vegetation zones. Note: elevation has been placed on the y-axis to aid visualization, and not because it is a dependent variable.

differences likely account for this pattern. It is hypothesized that a decrease in snow accumulation over the 2005-2006 winter season resulted in higher values of *nf*, while deeper snow cover during the previous winter season (2004-2005) produced lower freezing factors. During the 2005-2006 winter season, the forested sites (T2 and T3) received between 60 and 80 cm of snow and had higher values of *nf* than the sub-alpine taiga site (T4), where snow accumulation was thicker (between 80 and 100 cm). The Whitehorse Airport recorded a maximum of 47 cm of snow on the ground in 2004-2005 compared to 22 cm in 2005-2006 (Environment Canada, 2008). The continued collection of data will facilitate a further examination of the relationship between *nf* and snow conditions, taking into consideration long-term patterns and seasonal anomalies.

Thawing factors (*nt*) ranged from 0.80 to 1.08 for the study period (**Table 18**), with both the highest and lowest values recorded at sub-alpine taiga sites (CR2 and P9, respectively). Values of *nt* calculated for the forested sites over the study period were both 0.92 (T2 and T3), slightly above those calculated for the tundra site, at 0.86 and 0.87. Sites where *nt* was greater than 1.0 were all situated above 1200 m, and all are located within the alpine taiga zone. Thawing factors calculated for P9 were above 1.0 during two consecutive seasons (2002 and 2003), and only slightly below 1.0 in the following year (2004), when above-average air and ground surface temperatures were recorded and inversion episodes along the Coal Ridge transect were most frequent. Values of *nt* measured at individual sites remained relatively constant from one year to the next (typically ±0.01), with one significant exception. During the 2005 season, a thawing factor above 1.0 was recorded at CR2, representing an increase of more than 0.20 from the previous year. Along the Mount Sima trail, there is a clear transition in *nt*

Table 18: Thawing season n-factors (2002-2005)

	P9	CR1	CR2	CR3	CR4	T1	T2	T3	T4
2002	1.05								
2003	1.08								
2004	0.99	0.91	0.80	0.95	0.86				
2005	-	0.92	1.01	-	0.87	-	0.92	0.92	0.83

associated with tree-line, with thawing factors at the two forested sites (T2 and T3) nearly 0.10 higher than at the sub-alpine site (T4) in 2005.

The n-factor is typically used to define the relationship between air and ground temperatures on a seasonal basis, but can also be calculated on a daily or sub-seasonal basis in order to examine variability over both the freezing and thawing seasons (Karunaratne and Burn, 2004). While changes in the relationship between air and ground surface temperatures are summarized by the seasonal n-factor values, the daily ratio fluctuates considerably. Following Karunaratne and Burn (2004), 9-day freezing and thawing n-factors were computed for each of the study sites and were then compared to the seasonal values (**Figure 38**).

Throughout the freezing season, the 9-day ratio fluctuated around the seasonal value; mid-season *nf* were closest to the seasonal values, while early season and late season values were typically high. The high daily values of *nf* during the early season declined relatively quickly as air temperatures dropped and the ground began to freeze. Higher values (>1.0) also typically developed during the late season when the air was warming but the snowpack was still present. While the 9-day ratio of *nt* were also closest to the seasonal values during the mid-season; values during the early and late season were generally both below the seasonal average. Generally, values gradually increased during the early season as they approached 1.0 and declined during the late season. Overall, values of *nt* are highly dependent on the length of the mid-thawing season, and values of *nt* are, therefore, higher when the length of this period is greater.

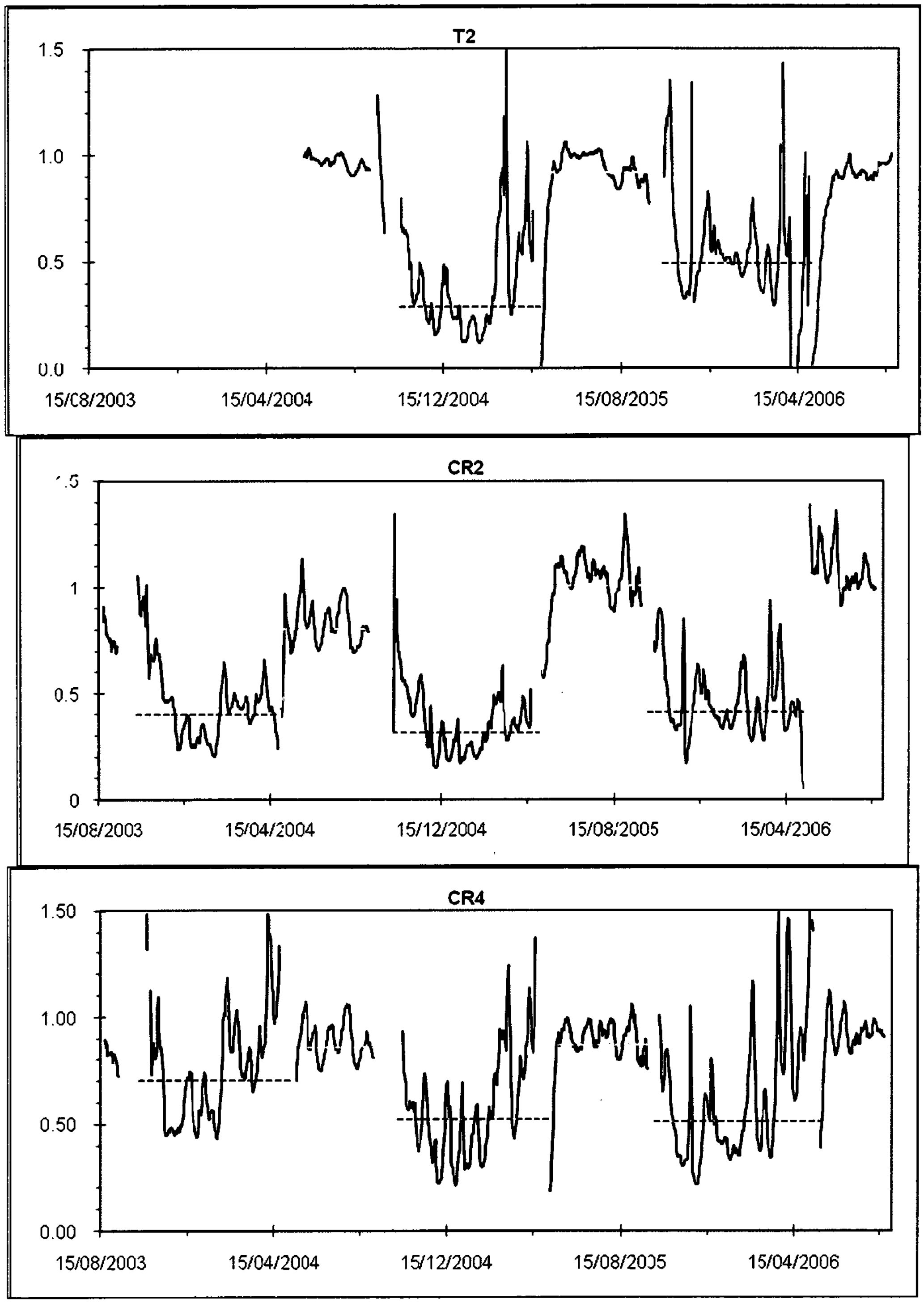

Figure 38: Calculated 9-day freezing(blue) and thawing (red) n-factors for sites located within the boreal forest (T2), sub-alpine taiga (CR2), and alpine tundra (CR4) ecological zones (August 2003 – July 2006). Note: The dashed line represents the seasonal n-factor.

4.0 AIR TEMPERATURE MODELING

4.1 Regression Analysis

The development of an empirical-statistical model to predict mean monthly air temperatures for July involved performing a multiple linear regression based on elevation, topographic position and PISR. Such a model uses regression functions to generate average temperatures in each grid cell of the DEM based on actual air temperature measurements at the study sites.

The development of the air temperature model involved the use of measured air temperature values collected at the study sites during the month of July 2006. Air temperature values were correlated with elevation, PISR and TPI, as described above. Once again, analysis involved applying a negative modification to TPI values at an appropriate neighbourhood size.

An initial linear regression model was created using elevation and mean monthly air temperatures collected at 22 study sites during July 2006 (**Table 19**). The resultant model produced a statistically significant fit with an R^2 value of 0.92 and the following equation:

[6] $$T_a = 19.123 + (-0.007)(\text{elevation})$$

In order to examine the role of topographic position and solar radiation, a second linear regression model was created using the modified TPI (mTPI500) and PISR values in addition to mean monthly July air temperatures and elevation (**Table 20**). The resultant model produced a statistically significant fit with an R^2 value of 0.97 and the following equation:

[7] $$T_a = 20.928 + (-0.007)(\text{elevation}) + (0.030)\ \text{mTPI500} + (0.001)(\text{PISR})$$

Despite a significance level of 0.048, given the very small PISR coefficient for the month of July, this variable was eliminated from further analysis and the model was rerun with the remaining variables (**Table 21**). The resultant model produced a statistically significant fit with an R^2 value of 0.96 and the following equation:

[8] $$T_a = 19.423 + (-0.007)(\text{elevation}) + (0.025)\ \text{mTPI500}$$

The above stated equation demonstrates that elevation and modified TPI values may be used to predict average July air temperatures in the Wolf Creek basin and the surrounding area. Of the linear equations described above, it is evident that topography exerts a major influence on local climate and plays a key role in the development of temperature variations in complex terrain. In mountainous areas, the amount of incoming solar radiation can vary significantly within short distances as a result of changes in elevation and topographic shading. Here, the relationship between elevation and temperature is also highlighted, with a best-fit lapse rate of 6.8°C km^{-1}.

Table 19: Summary of coefficients in the linear regression equation that includes elevation (Equation 6)

$R^2 = 0.92$ Adjusted $R^2 = 0.92$	Coefficient	Standard Error	Significance
Intercept	19.123	0.619	0.000
Elevation	-0.007	0.000	0.000

Table 20: Summary of coefficients in the linear regression equation that includes elevation, topography and PISR (Equation 7)

$R^2 = 0.97$ Adjusted $R^2 = 0.96$	Coefficient	Standard Error	Significance
Intercept	20.928	0.813	0.000
Elevation	-0.007	0.000	0.000
Modified TPI500	0.030	0.006	0.000
PISR	-0.001	0.000	0.048

Table 21: Summary of coefficients in the linear regression equation that includes elevation and topography (Equation 8)

$R^2 = 0.96$ Adjusted $R^2 = 0.96$	Coefficient	Standard Error	Significance
Intercept	19.423	0.452	0.000
Elevation	-0.007	0.000	0.000
Modified TPI500	0.025	0.006	0.001

4.2 Modeled Mean July Air Temperatures

The ArcMap raster calculator was used to apply the regression equations developed in Section 4.1 to the projected DEM. The resultant values are displayed as a mean July 2006 air temperature maps for a portion of the Wolf Creek basin and the surrounding area – one based on elevation alone (**Figure 39**), and the other incorporating the effects of topographic position along with elevation (**Figure 40**).

Based on the elevation model, temperatures within the selected area are slightly cooler than those predicted by the final temperature model, ranging from approximately 6°C to below 15°C. Within this range of temperatures, the number of cells within each temperature class is evenly distributed between those predicted to be below 10°C (40%), those between 10°C and 11°C (20%) and those above 10°C (40%). When topography is considered, predicted temperatures within the study area are all above 7°C, although the maximum temperature remains below 15°C. Unlike the elevation model, the distribution of cells is uneven, with 30% predicted to be below 10°C, 20% between 10°C and 11°C, and 50% above 11°C. Overall the elevation model appears more generalized, with smooth contours between temperature transitions.

4.3 Evaluation of the Model

Over the next several decades, the location of the treeline transition zone is expected to shift in response to global climate change. Without accurate mapped data, changes in local vegetation conditions cannot be measured and reliable predictions of future conditions cannot be made. While the location of treeline within the Wolf Creek basin and surrounding areas is defined on the NTS sheets (**Figure 41**), previous research

Figure 39: Modeled Mean July Air Temperature - Elevation Model (Equation 6)

Figure 40: Modeled Mean July Air Temperature - Final Temperature Model (Equation 8)

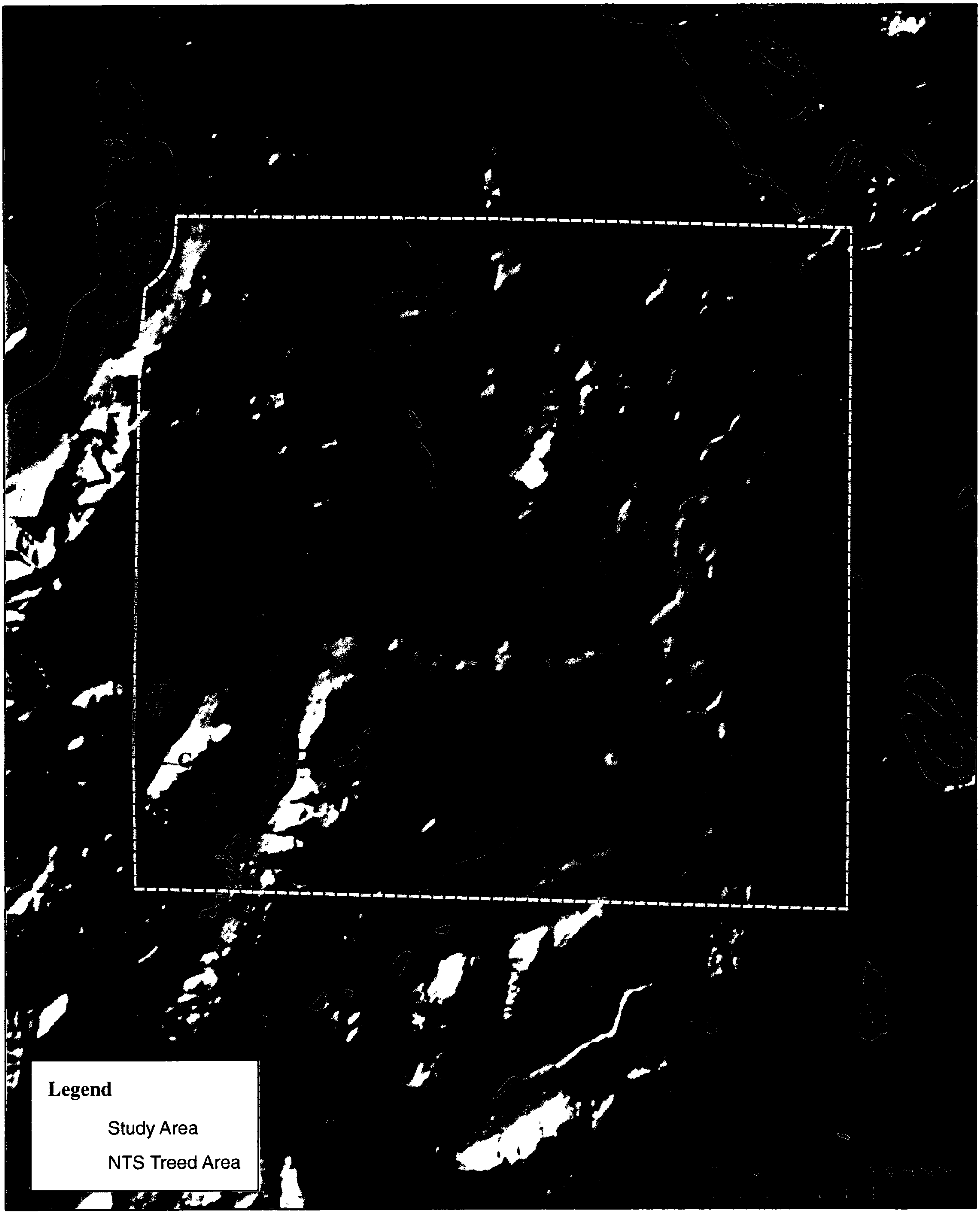

Figure 41: Location of treed area according to NTS map sheets

combined with recent field observations indicate that many areas of the basin shown to be above treeline are in fact quite densely treed. According to the NTS map sheets, treeline within the Wolf Creek basin corresponds roughly with 1200 metres elevation.

Based on the methodology described in Section 2.4.3, the location of treeline was defined for the selected portion of the basin using high resolution Google Earth images (**Figure 42**). The interpreted treeline differs significantly from the NTS sheets, with the treed area extending along the lakes and within the palsa valley, including the inverted treeline on the valley side slopes (**Figure 43**). The role of topographic drainages is more visible when mapped using the final temperature model and the location of the 10°C July temperature transition more closely resembles the interpreted treeline, including the recreation of the double-treeline along Coal Ridge.

In an error-free modeling environment, treeline would correspond to exactly 10°C. If the 2006 results are representative of the long-term, the optimum predictions would be 0% in all categories less than 10°C and 100% in all categories with temperatures greater than 10°C. **Figure 44** shows the number of cells within each temperature category for four pairings of data:

a) the NTS treeline compared to the modeled July air temperatures using the preliminary elevation model;
b) the NTS treeline compared to the modeled July air temperatures using the final temperature model;
c) the interpreted treed area compared to the modeled July air temperatures using the preliminary elevation model;

Figure 42:

Treed Area as Interpreted from Google Earth Images

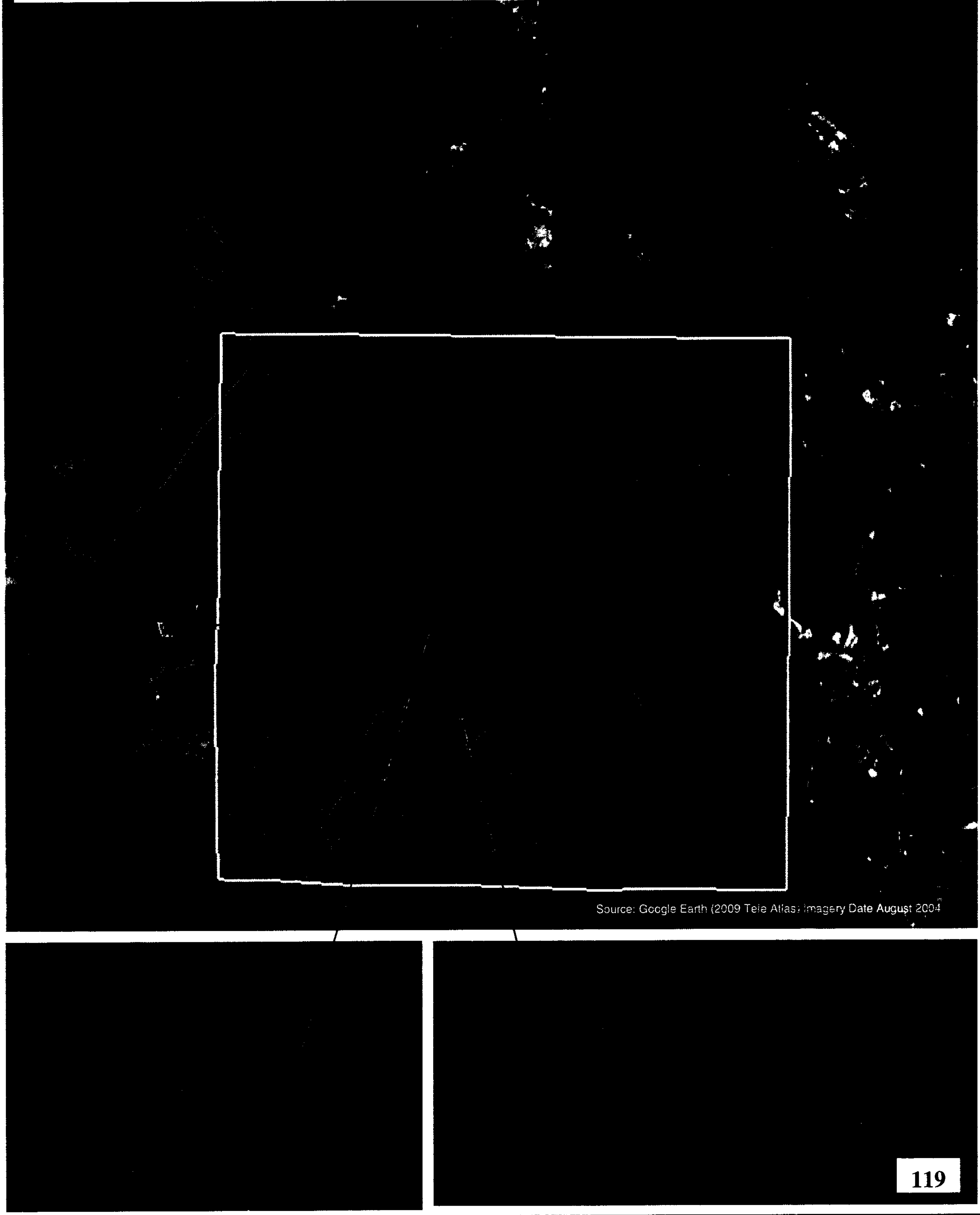

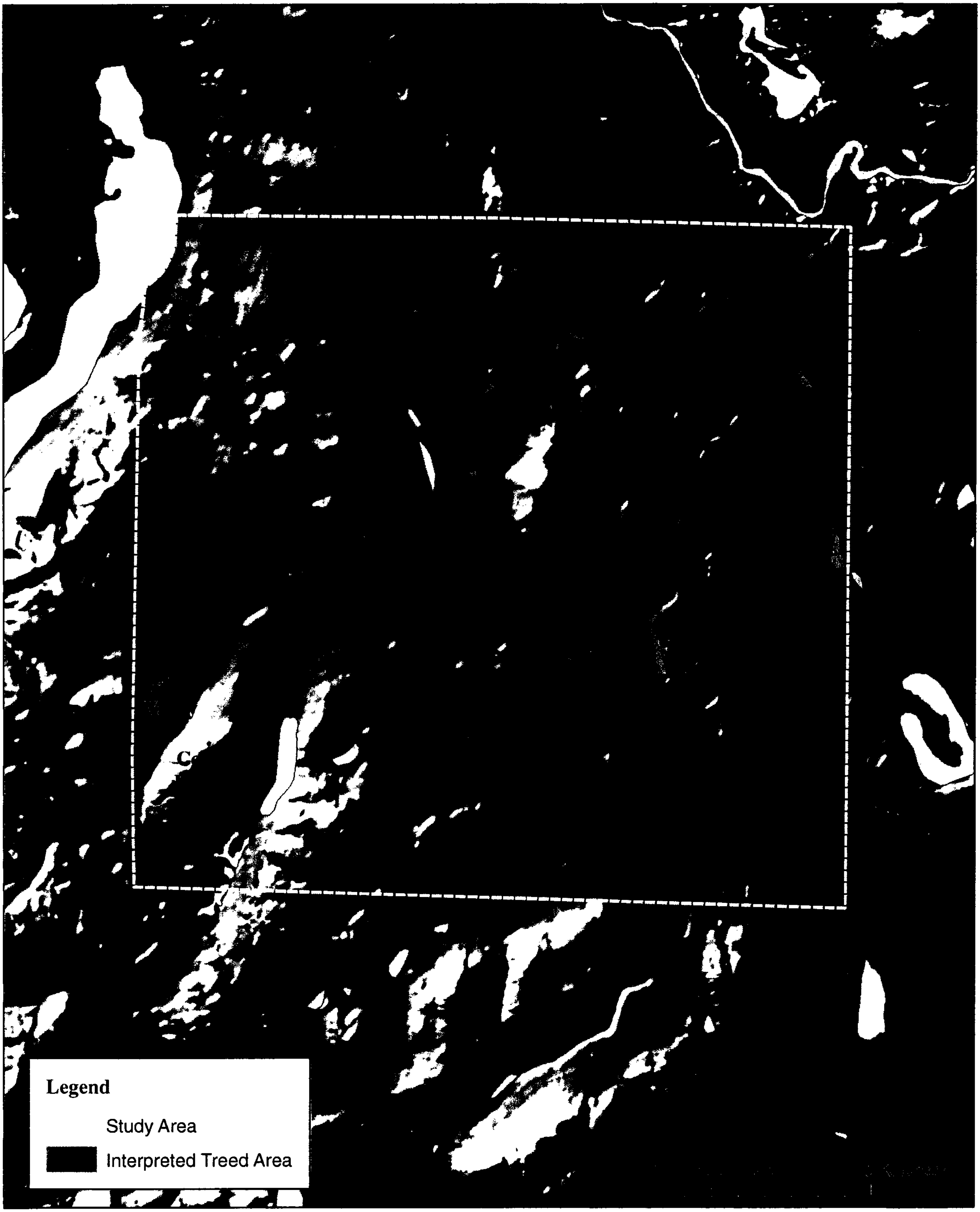

Figure 43: Location of treed area as interpreted from Google Earth images

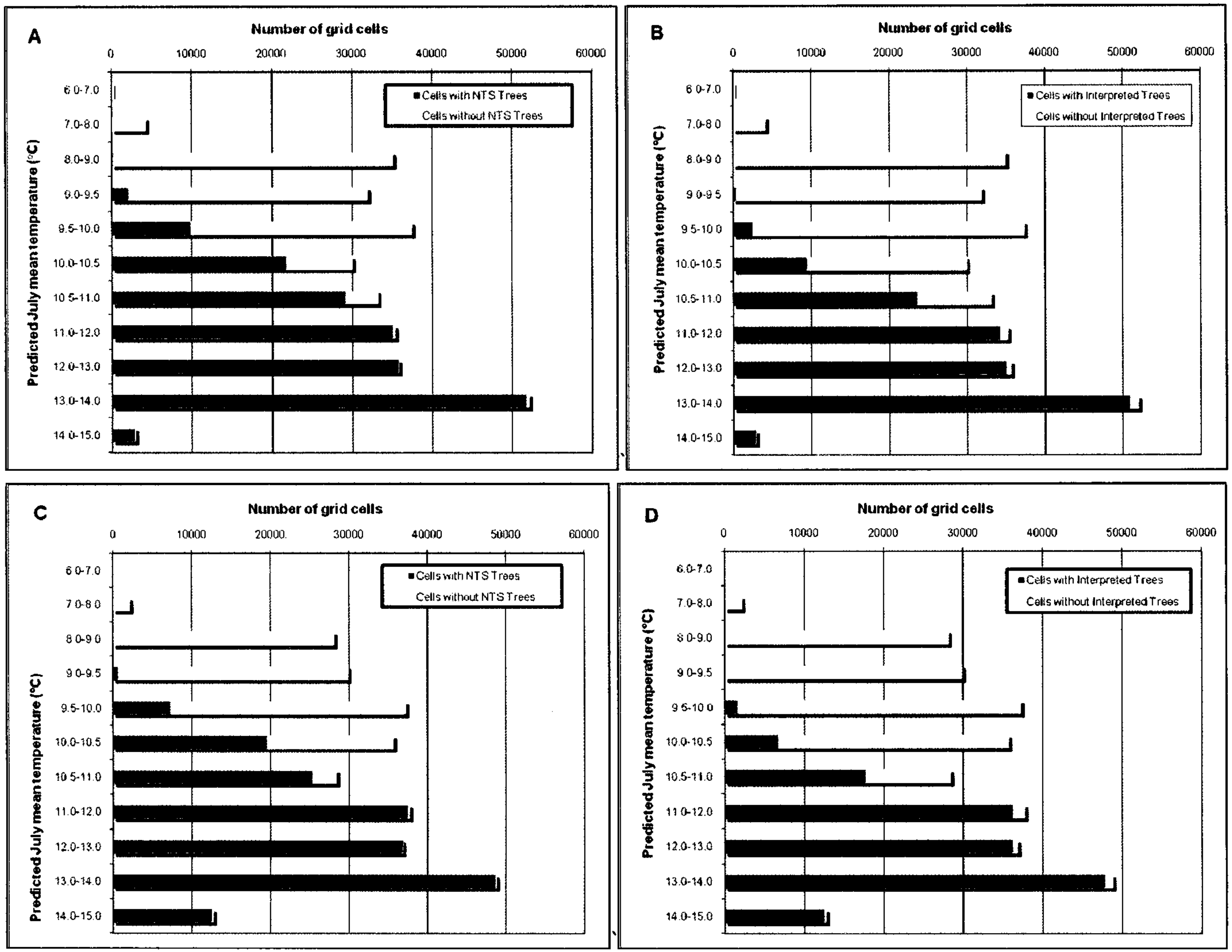

Figure 44: Evaluation of the Model based on (a) NTS treeline and (b) interpreted treeline compared to the preliminary elevation model; and (c) NTS treeline and (d) interpreted treeline compared to the final temperature model. Note: Below 10°C the green cells are the misclassified cells, above 10°C the yellow cells are the misclassified cells

d) the interpreted treed area compared to the modeled July air temperatures using the final temperature model.

As shown in **Figure 44**, both the preliminary elevation model (Equation 6) and the final temperature model (Equation 8) perform better when combined with the Google-interpreted treeline than with the NTS map data, particularly in the lower temperature ranges within the treeline transition zone. Using the interpreted treeline, the final temperature model misclassifies 9.3% of cells, while the elevation model misclassifies 8.3%. When the NTS-defined treeline is used, misclassification increases to 11.7% for the elevation model and 14.6% for the final temperature model. Misclassifications include those cells with predicted temperatures below 10°C classified as treed, as well as those cells with predicted temperatures above 10°C where no trees are present. Based on this evaluation of the model the following conclusions can be reached:

- The preliminary elevation model and the final temperature model using the interpreted treeline both provide more accurate interpretations of treeline in the selected portion of the basin than the NTS map sheets, with fewer misclassified cells overall. Visually, the fit is also better, with the 10°C temperature transition extending into the valleys, which corresponds to the location of the treed area as observed both in the field and on the Google Earth images.

- Using the interpreted treeline, temperature predictions using the final temperature model may be too warm, with virtually all the cells predicted to be below 10°C and the majority of the cells with predicted temperatures between 10°C-11°C classified as being without trees. The elevation model is also likely too warm, however, it is slightly cooler than the final temperature model. As a result, while it has a higher accuracy in the 10°C-11°C range, the model starts to develop trees in cells which are predicted to be below 10°C. Neither model sharply differentiates at 10°C between above and below treeline. This likely indicates that other factors, such as drainage, vegetation type and PISR play a role in the 10°C predictions.

- Although the R^2 value is higher for the final temperature model, the predicted temperatures from the elevation model generally correspond more closely to the true distribution of trees in the basin, with fewer misclassified cells overall. However, along the valley side slopes on Coal Ridge, the final temperature model produces a double treeline that is not generated by the elevation model, but can be observed both in the field and on the Google Earth images. This suggests that, while elevation is the simplest predictor of the position of treeline, topography (through the TPI) also plays a role in determining local vegetation patterns in complex terrain, particularly in areas where cold air drainage may be present.

5.0 DISCUSSION AND CONCLUSIONS

5.1 Discussion

5.1.1 Air Temperature Inversions

Temperature inversions are common in the main valleys of the Yukon and are a known factor in the maintenance of subzero surface temperatures (Wahl et al., 1987; Harris, 1981). Within the discontinuous permafrost zone, where average surface temperatures are often close to zero, even a relatively small change in temperature could have a widespread impact on permafrost distribution (Lewkowicz and Smith, 2004; Lovatt and Lewkowicz, 2009). Despite the critical role of air temperature inversions in the distribution and occurrence of permafrost, inversion presence has often been overlooked in permafrost studies. Lovatt and Lewkowicz (2009) estimate that the overall impact of regular low-level inversions in the Yukon River Valley (1956-2003) results in an average reduction of 3.4°C near the ground surface. Simply stated, in the absence of surface based temperature inversions, the average annual ground surface temperature at Whitehorse (-0.7°C) would exceed 1°C and permafrost existence could not be maintained.

The current research presents the preliminary linkages between air and ground surface temperatures collected along altitudinal transects close to Whitehorse and the presence of surface-based inversions. While MAGST measured at the study sites are generally below 1.0°C, in the absence of surface based temperature inversions, average annual ground surface temperatures within the Wolf Creek basin and surrounding area would also likely exceed the threshold for permafrost existence. Changes in inversion impact in the context of future climate change are likely to result in significant changes on permafrost distribution in the basin and throughout the Yukon.

Following an analysis of twice-daily radiosonde data from the Whitehorse airport, Lovatt and Lewkowicz (2009) found that, at the daily scale, surface-based inversions occurred 46% of the time, with average inversion frequencies ranging from 52% in October to above 80% in December and January. Previous work by Lewkowicz and Smith (2004) found that within the palsa valley inversions occur on average 42% of the time in all months. The current research supports these findings, with air temperature data collected at the study sites (2001-2006) indicating that inversions are common in the palsa valley, occurring throughout the year and in all seasons, with peak frequency in January. Along the Coal Ridge transect, differences in daily temperatures are greatest during the winter, with increases of more than 10°C between P9 and CR4 on numerous occasions. Daily air temperatures show a positive gradient with elevation along the Mount Sima trail for extensive periods between November and February, so much so that average monthly temperatures for this period often reflect these patterns.

5.1.2 N-Factors

The relationship between the surface offset, n-factors, elevation and vegetation within the Wolf Creek basin and the surrounding area described in the current research demonstrate that trends previously identified in relation to latitudinal treeline also apply to altitudinal treeline.

Trends in the summer n-factors determined by Klene et al. (2001) indicate a relationship with land cover classification. Values from bare ground and wet tundra sites were highest, while lower values were determined for sites located within shrublands and water tracks (Klene et al., 2001). Similarly, Taylor (1995) used data collected from the Mackenzie Valley active layer monitoring transect to calculate preliminary n-factors for sites with similar forest classifications. Calculated values of *nt* were highest at open sites and lowest at shaded sites, predominantly those located within the forest where low near-surface thermal diffusivity is an important influence on *nt* (Taylor, 1995).

Over the study period, freezing factors (*nf*) exhibit a broad relationship with both elevation and vegetation. Values for the forested sites were all <0.40, ranging from 0.12 to 0.36, while those calculated for the tundra sites were all >0.50. Freezing factors for the sub-alpine taiga point to the role of variable vegetation and snow cover close to and below treeline, with values ranging from 0.23 to 0.73 at these sites. Thawing factors (*nt*) ranged from 0.80 to 1.08, a much smaller range than for *nf*. Values of *nt* calculated for the forested sites over the study period were both 0.92, slightly above those calculated for the tundra site (0.86 and 0.87). Sites where *nt* was greater than 1.0 were all situated above 1200 m, and all are located within the sub-alpine taiga zone. Along the Mount Sima trail, there is a clear transition in *nt* associated with tree-line, with thawing factors at the two forested sites (T2 and T3) nearly 0.10 higher than at the sub-alpine site (T4) in 2005.

The current research also supports the findings of Karunaratne and Burn (2004) and others, who concluded that snow depth is the most important variable influencing *nf*. During the winter, the low thermal conductivity of snow cover restricts heat losses to the atmosphere, resulting in a warmer ground surface, despite cold winter air temperatures (e.g. Smith, 1975; Goodrich, 1982). Thin snow cover results in low surface temperatures, more closely related to the winter air temperatures, while the insulating effects of a thick snow cover results in higher surface temperatures (Karunaratne and Burn; 2004). Thus, values of *nf* are high at sites with low snow accumulation, and low at sites with a deeper snow cover. Within the Wolf Creek basin and surrounding areas, the insulating effects of snow are strongest in the sub-alpine taiga zone where snow accumulation reaches a peak close to treeline. Values of *nf* measured at individual sites exhibited significant inter-annual variability, with increases of more than 0.20 at some sites between 2004-05 and 2005-06. Snow accumulation differences likely account for this pattern. Whitehorse recorded a maximum of 47 cm of snow on the ground in 2004-05 but a maximum of only 22 cm in 2005-06 (Environment Canada, 2008).

5.1.3 Modeling Mountain Permafrost

Research currently underway to generate detailed permafrost probability models over large areas of the North American Cordillera suggests that improvements to the modeling process are necessary to increase the accuracy of such models. Although previous studies indicate that elevation and PISR are the two leading factors contributing to the existence of permafrost at a given location (Lewkowicz and Ednie, 2004; Lewkowicz and Bonnaventure, 2008; Bonnaventure and Lewkowicz, 2008), additional factors may also contribute significantly to the existence of mountain permafrost. These factors include vegetation cover, snow accumulation and the degree to which individual mountain landscapes are prone to air temperature inversions, as discussed in the current research. Further research is needed to determine exactly how and when these factors will be incorporated into future permafrost probability models.

As discussed previously, the assumption that air temperature decreases with elevation is frequently incorrect and, as such, the presence of temperature inversions presents a unique challenge to permafrost probability mapping in mountainous terrain, including the Wolf Creek basin (Lewkowicz and Ednie, 2004). While elsewhere the existence of permafrost can be linearly related to elevation, the presence of frequent inversions within the basin violates this assumption, affecting permafrost distribution in ways that the basal temperature of snow (BTS) modeling cannot predict at present, and resulting in anomalously extensive permafrost on the palsa valley floor (Lewkowicz and Ednie, 2004). In order to improve the validity of the modelled predictions, modeling efforts have looked specifically at valley bottom locations to identify inversion-prone locations. The current research suggests that, while inversion prone sites within the Wolf Creek basin are predominantly situated in U-shaped valleys and canyons, open slopes and plains sites may also be affected. Permafrost probability may, therefore, be significantly higher in these areas and, as a result, existing probability mapping may underestimate the area underlain by permafrost in the basin. Furthermore, the current study indicates that elevation and topography are also key factors in determining local vegetation patterns in complex terrain, particularly in areas where air temperature inversions may be present.

Within the Wolf Creek basin and surrounding areas, the insulating effects of snow have been shown to minimize the effects of cold winter temperatures on the ground, which may significantly affect whether permafrost will be present or absent at a given location. Although the presence of permafrost is much more likely in low-snow areas, particularly at high elevations, these areas cannot be sampled using the BTS method. Inter-annual variations introduce additional uncertainty into the creation of permafrost probability models, particularly those using the BTS method (Etzelmüller et al., 2001). As shown by the current research, inter-annual variability in snow accumulation can result in significant variability in ground surface temperature, with seasonal differences in *nf* of more than 0.20 recorded at some sites in the basin.

5.2 Conclusions

This thesis explored the relationship between air and ground surface temperatures through altitudinal treeline within the Wolf Creek basin and surrounding area between 2001 and 2006. As a result of this research, the following conclusions can be reached:

1) The relationship between the surface offset, n-factors, elevation, snow accumulation and vegetation in the study area demonstrates that trends previously identified in relation to latitudinal tree-line also apply to altitudinal tree-line:

   - Values of *nt* may relate to land cover, as suggested by Klene et al. (2001), who obtained the highest values on bare ground and wet tundra sites. Similarly, Taylor (1995) calculated the highest values of *nt* at open sites and lowest at shaded sites, predominantly those located within the forest. Along the Mount Sima trail, there is a clear transition in *nt* associated with tree-line, with thawing factors at the two forested sites nearly 0.10 higher than at the sub-alpine site. Sites where *nt* was greater than 1.0 were all situated above 1200 m, and all are located within the sub-alpine taiga zone.

   - The current research supports the findings of Karunaratne and Burn (2004) and the modeling of Smith and Riseborough (2002) who showed that snow depth is the most important variable influencing *nf*. The insulating effect of a thick snow cover results in higher surface temperatures, while thin snow cover results in low surface temperatures more closely related to the winter air temperatures. Within the study area, values of *nf* are high at sites with low snow accumulation, and low at sites with a deeper snow cover. Likewise, surface offsets were lowest in the tundra, highest in the forest and most variable in the shrub zone where wind-blown snow is particularly heterogeneous. This research is among the first to describe these trends in relation to complex mountainous terrain.

2) Topography exerts a major influence on local climate and plays an important role in the development of temperature variations in alpine regions (Harris, 1986; Wahl *et al.*, 1987, Whiteman, 2000). This thesis demonstrates that the Topographic Position Index (TPI) is an effective tool for classifying the landscape according to slope position and landform categories. Results obtained for sites across the Yukon indicate that the TPI can be used to compare site characteristics and monitoring data across different topographic positions and in a number of climate regions.

3) The calculation of regional lapse rates based on topographic control sites, as described in this thesis, is a practical method for estimating average monthly air temperatures for sites located within a variety of topographic positions within a given region. Sites identified as having lower air temperatures then predicted can be considered inversion-prone. At sites across the Yukon Territory, inversion-

prone sites were predominantly situated in U-shaped valleys, although open slopes, mid-slope ridges and plains were also identified.

4) Temperature inversions likely contribute to the distribution and occurrence of permafrost within the discontinuous zone, particularly at sites where mean annual air temperatures are close to 0°C. The current research supports the finding of Lovatt and Lewkowicz (2009) that, in the absence of surface based temperature inversions, average annual ground surface temperatures within the Wolf Creek basin and surrounding area would likely exceed the threshold for permafrost existence. Within the Wolf Creek basin and surrounding area, inversion episodes have a measurable effect on local air temperatures, occurring during the fall and winter seasons along the Mount Sima trail, and year-round in the palsa valley. Changes in inversion impact in the context of future climate change are, therefore, likely to result in significant changes on permafrost distribution in the basin and throughout the Yukon.

5) Mean July air temperature mapping suggests that, while elevation is the simplest predictor of the position of treeline, topography (through the TPI) also plays a role in determining local vegetation patterns in complex terrain, particularly in areas where cold air drainage may be present. Along the valley side slopes on Coal Ridge, the final temperature model produces a double treeline that is not generated by the elevation model, but can be observed both in the field and on the Google Earth images.

5.3 Future Research

Growing concerns over the effects of potential climate warming on permafrost conditions, coupled with the difficulties involved in predicting the response of ground stability to seasonal and potential future changes in air temperature, underlines the need to expand the number of known n-factors for natural surfaces. The application of n-factor modeling techniques within the permafrost region, and the verification of these techniques for a range of natural surfaces, is essential to the determination of the thermal and physical response to potential climate warming in permafrost regions. Likewise, there is a need for n-factor studies to be extended to a wider range of vegetation and soil types, in a variety of northern climate zones. The compilation of a database of seasonal n-factors will facilitate accurate prediction of the limits and continuity of permafrost in Canada in relation to variable climatic and environmental conditions. These values, in conjunction with field observations, are critical to the understanding of climate-permafrost relations.

Given that much of this thesis is based on a single summer of data, the results presented should be considered preliminary. Inter-annual variability plays an important role in the determination of representative n-factors, as changes in temperature trends and snow distribution patterns may have significant impacts. While sites with similar forest classifications and site descriptions exhibit similar n-factor values, data collection over several years will lead to increased confidence and will facilitate the assessment of n-factor variability from site to site, and from year to year at the same site.

Ongoing data collection at the study sites will also provide additional insight into the role of snow accumulation, the thermal offset, cold air drainage and topography in the permafrost-climate relationship:

- Additional I-Button sensors, installed at each of the study sites (5 cm, 50 cm and 100 cm) in August 2006 will yield more accurate interpretations of the data and provide a better idea of the snow accumulation patterns at and among the study sites, particularly at the beginning and end of the season, and at sites where snow depths are greatest. Depth of snow cover is a critical factor in determining permafrost distribution and occurrence in the discontinuous zone.

- The thermal offset controls permafrost occurrence at the limit of the discontinuous zone. Previous research indicates that the TTOP model has potential in ground temperature modeling in complex terrain. Each of the study sites is equipped with a second external thermistor which measures the ground temperature as close as possible to the top of permafrost (TTOP). Data collected since August 2006 may provide details on heat transfer within the active layer and underlying permafrost. This is particularly relevant in areas where mean annual surface temperatures are greater than 0°C.

The inclusion of air temperature data obtained over multiple summer seasons will likely result in more accurate predictions of treeline in the Wolf Creek basin using both the final temperature model and elevation model. The methods developed here have potential applicability in other regions of the Yukon, particularly those where inversions are present.

6.0 REFERENCES

Anquetin, S., Guilbraud, C., and Chollet, J.P., 1998. The formation and destruction of inversion layers within a deep valley. *Journal of Applied Meteorology*, 37: 1547-1560.

Bader, D.C., and McKee, T.B., 1985. Effects of shear, stability and valley characteristics on the destruction of temperature inversions. *Journal of Climate and Applied Meteorology*, 24: 822-832.

Beltrami, H. and Kellman, L., 2003. An examination of short- and long-term air-ground temperature coupling. *Global and Planetary Change*, 38: 291-303.

Bilello, M.A., 1966. Survey of arctic and subarctic temperature inversions. Hanover, New Hampshire: U.S. Army Cold Regions Research and Engineering Laboratory, *Technical Report 161*: 1-15.

Borgen, J., and Gustavsson, T., 1989. Modelling of local climate for prediction of road slipperiness. *Physical Geography*, 10: 147-164.

Brown, R.J.E., 1973. Influence of climatic and terrain factors on ground temperatures at three locations in the permafrost region of Canada. In *Proceedings, 2nd International Conference on Permafrost, Yakutsk, USSR*. North American Contribution: 27-34.

Brown, R.J.E. and Péwé, T., 1973. Distribution of permafrost in North America and its relationship to the environment: a review, 1963-1973. In *Proceedings, 2nd International Conference on Permafrost, Yakutsk, USSR*. North American Contribution: 71-100.

Bonnaventure, P., and Lewkowicz, A.G., 2008. Mountain permafrost probability mapping using the BTS method in two climatically dissimilar locations, northwest Canada. *Canadian Journal of Earth Sciences*, 45: 443-455.

Burn, C.R., 1998b. Field investigations of permafrost and climate change in northwestern North America. In Lewkowicz, A.G. and Allard, M. (eds.), *Proceedings, 7th International Conference on Permafrost, 23-26 June, 1998, Yellowknife, Northwest Territories*. Quebec City: Collection Nordicana 57, 107-120.

Burn, C.R., 2004. The thermal regime of cryosols. In Kimble, J.M. (ed.), *Cryosols: Permafrost-affected Soils*. Berlin: Springer-Verlag, Berlin, Chapter 3: 391-413.
a mountain basin: Peter Sinks, Utah. *Journal of Applied Meteorology*, 42: 752-768.

Clements, C.B., Whiteman, C.D., and Horrel, J.D., 2003. Cold-air pool structure and evolution in Burn, C.R., 1998a. The response (1958-1997) of permafrost and near-surface ground temperatures to forest fire, Takhini River valley, southern Yukon Territory. *Canadian Journal of Earth Sciences*, 35: 184-199.

Colette, A., Chow, F.K., and Street, R., 2003. A numerical study of inversion-layer breakup and the effects of topographic shading in idealized valley. *Journal of Applied Meteorology*, 42: 1255-1272.

Ednie, M., 2003. Evaluation of the basal temperature of snow (BTS) method to map permafrost in complex mountainous terrain, Wolf Creek, Y.T. Unpublished Thesis.

Environment Canada, 2008. Online at http://www.climate.weatheroffice.ec.gc.ca (Accessed February 9, 2008).

Environment Yukon, 2006. *Yukon Snow Survey.*

Etzelmüller B., Hoelzle, M., Heggem, E.S.F., Isaksen, K., Mittaz, C., Vonder Mühll, D., Ødegard, R.S., Haeberli, W., and Sollid, J.L, 2001. Mapping and modeling the occurrence and distribution of mountain permafrost. Norsk Geografisk Tidsskrift – Norwegian Journal of Geography, Vol 55: 186-194.

Fast, J.D., Zhong, S., and Whiteman, C.D., 1996. Boundary layer evolution within a canyonland basin. Part II: Numerical simulations of nocturnal flows and heat budgets. *Journal of Applied Meteorology*, 35: 2162-2178.

Francis, S., Smith, S., and Janowicz, R.,1997. Intégration des données et la zonation écologique du basin versant du ruisseau Wolf. *In* Pomeroy, J.W., Granger, R.J (eds.) *Wolf Creek Research Basin: Hydrology, Ecology, Environment.* Saskatoon: National Water Research Institute, 97-104.

Fu, P. and Rich, P.M. 1999. Design and implementation of the Solar Analyst: an Arcview extension for modeling solar radiation at landscape scales [online]. Available at http://www.esri.com/library/userconf/proc99/proceed/papers/pap867/p867.htm

Gold, L.W. and Lachenbruch, A.H., 1973. Thermal conditions in permafrost: a review of North American literature. In *Proceedings, 2nd International Conference on Permafrost, Yakutsk, USSR*. Washington: National Academy of Sciences, 3-23.

Goodrich, L.E., 1978. Some results of a numerical study of the ground thermal regime. In *3rd International Conference on Permafrost*, Edmonton, Canada: 30-34.

Goodrich, L.E., 1982. The influence of snow cover on the ground thermal regime. *Canadian Geotechnical Journal*, 19: 421-432.

Gustavsson, T., 1995. A study of air and road surface temperature variations during clear windy nights. *International Journal of Climatology*, 15: 919-932.

Gustavsson, T., Karlsson, M., Bogren, J., and Lindqvist, S., 1998. Development of temperature patterns during clear nights. *Journal of Applied Meteorology*, 37: 559-571.

Harris, S.A., 1981. Climatic relationships of permafrost zones in areas of low winter snow-cover. *Arctic*, 34:64-70

Harris, S.A., 1982. Cold air drainage in Fort Nelson, British Columbia. *Arctic*. 35(4): 537-541.

Harris, S.A., 1986. *The Permafrost Environment*. London : Croom Helm, 276pp.

Heginbotton, J.R., Dubreuil, M.A., Harker, P.T., 1995. Canada-Permafrost. In *National Atlas of Canada,* 5th Edition. Ottawa: National Atlas Information Service, Natural Resources Canada. Plate 2.1 MCR 4177, 1:7500000.

Hoelzle, M., Mittaz, C., Etzelmuller, B. and Haeberli, W., 2001. Surface energy fluxes and distribution models of permafrost in European mountain areas: an overview of current developments. *Permafrost and Periglacial Processes*, 12: 53-68.

Janowicz, J.R. 1999: Wolf Creek Research Basin - Overview. Wolf Creek Research Basin: Hydrology, Ecology, Environment. *In* Pomeroy, J.W., Granger, R.J (eds.) *Wolf Creek Research Basin: Hydrology, Ecology, Environment*. Saskatoon: National Water Research Institute, 125-134.

Jenness, J., 2005. Topographic Position Index extension for ArcView 3.x [online]. Arizona: Jenness Enterprises. Available at http://www.jennessent.com/arcview/tpi.htm

Jorgenson and Krieg, 1988. A model fro mapping permafrost distribution based on landscape component maps and climatic variables. In Senneset, K. (ed.), *Proceedings, 5th International Conference on Permafrost, 2-5 August 1988, Trondheim, Norway.* Trondheim: Tapir Publishers, Volume 1: 176-182.

Julissen, H., and Humlum, O., 2007. Towards a TTOP Ground Temperature Model for Mountainous Terrain in Central-Eastern Norway. *Permafrost and Periglacial Processes*, 18: 161-184.

Karunaratne, K.C., and Burn, C.R. 2004. Relations between air and surface temperature in discontinuous permafrost terrain near Mayo, Yukon Territory. *Canadian Journal of Earth Sciences,* 41: 1437-1451.

Klene, A.E., Nelson, F.E. and Shiklomanov, N.I., 2001. The n-factor in natural landscapes: variability of air and soil-surface temperatures, Kuparuk river basin, Alaska, USA. Arctic, *Antarctic and Alpine Research*, 33: 140-148.

Kondo, J., and Okusa, N., 1990. A simple numerical prediction model of nocturnal cooling in a basin with various topographic parameters. Journal of Applied Meteorology. 29: 604-619.

Kuwagata, T., and Kimura, F., 1995. Daytime boundary layer evolution in a deep valley. Part I: Observations in the Ina Valley. Journal of Applied Meteorology, 34: 1082-1091.

Lachenbruch, A.H., Cladouhos, T.T., and Saltus, R.W., 1988. Permafrost temperature and the changing climate. In Senneset, K. (ed.), *Proceedings, 5th International Conference on Permafrost, 2-5 August 1988, Trondheim, Norway*. Trondheim: Tapir Publishers, Volume 3: 9-17.

Laughlin, G.P., and Kalma, J.D., 1990. Frost risk mapping for landscape planning: a methodology. *Theoretical and Applied Climatology*, 42: 41-51.

Lewkowicz, A.G., 2008. Evaluation of miniature temperature loggers to monitor snowpack evolution at mountain permafrost sites, northwestern Canada. Permafrost and Periglacial Processess, 19: 323-331.

Lewkowicz, A.G., and Bonnaventure, P., 2008. Interchangeability of mountain permafrost probability models, northwest Canada. *Permafrost and Periglacial Processess*, 19: 49-62.

Lewkowicz, A.G. and Ednie, M., 2004. Probability mapping of mountain permafrost using the BTS method, Wolf Creek, Yukon Territory, Canada. *Permafrost and Periglacial Processes*, 15(1), 67-80.

Lewkowicz, A.G., and Smith, K.M., 2004. Temperature inversions and permafrost distribution in a mountain valley: preliminary results from Wolf Creek, Yukon Territory, Canada. Poster presentation, *American Geophysical Union Fall Meeting, San Francisco, December 2004.*

Lindkvist, L., and Lindqvist, S., 1997. Spatial and temporal variability of nocturnal summer frost in elevated complex terrain. *Agricultural and Forest Meteorology*, 87: 139-153.

Lovatt, A., and Lewkowicz, A.G., 2009. Characteristics of low-level temperatures inversions, Whitehorse, Yukon Territory: 1956-2003. *Journal of Applied Meteorology and Climatology,* In Press.

Lunardini, V., 1978. Theory of n-factors and correlation data. In *Proceedings, 3rd International Conference on Permafrost, Edmonton, Canada*: 40-46.

Manley, G., 1944. Topographical features and the climate of Britain: a review of some outstanding effects. *The Geographical Journal,* 103(6): 241-258.

McKee, T.B., and O'Neal, R.D., 1989. The role of valley geometry and energy budget in the formation of nocturnal valley winds. *Journal of Applied Meteorology*, 28: 445-456.

Müller, H., and Whiteman, C.D., 1988. Breakup of a nocturnal temperature inversion in the Dischma Valley during DISKUS. Journal of Applied Meteorology. 27: 188-194.

Oke, T.R., 1987. *Boundary Layer Climates*, 2nd Edition. New York: Methuen, 435pp.

Romanovsky, V.E., and Osterkamp, T.E., 1995. Interannual variations of the thermal regime of the active layer and near surface permafrost in Northern Alaska. *Permafrost and Periglacial Processes*, 6: 313-335.

Sakiyama, S.K., 1990. Drainage flow characteristics and inversion break-up in two Alberta mountain valleys. *Journal of Applied Meteorology*, 29: 1015-1030.

Smith, M.W., 1975. Microclimate influences on ground temperatures and permafrost distribution, Mackenzie Delta, Northwest Territories. *Canadian Journal of Earth Sciences*, 12: 1421-1438.

Smith, M.W., 1975. Microclimate influences on ground temperatures and permafrost distribution, Mackenzie Delta, Northwest Territories. *Canadian Journal of Earth Sciences*, 12: 1421-1438.

Smith, S.L. and Burgess, M., 2004. Sensitivity of permafrost to climate warming in Canada. *Geological Survey of Canada Bulletin,* 579.

Smith, M.W., Burn, C.R., Tarnocai, C. and Sproule, B., 1998. Air and soil temperature relations along an ecological transect through the permafrost zones of northwestern Canada. In

Smith, M.W. and Riseborough, D.W., 1983. Permafrost sensitivity to climate change. In *Proceeding, 4th International Conference on Permafrost.* Washington: National Academy Press, Volume 1: 1178-1183.

Smith, M.W. and Riseborough, D.W., 1996. Permafrost monitoring and detection of climate change. *Permafrost and Periglacial Processes*, 7: 301-309.

Smith, M.W. and Riseborough, D.W. 2002: Climate and limits of permafrost: A zonal analysis. *Permafrost and Periglacial Processes*, 13: 1-15.

Stocker-Mittaz, C., Hoelzle, M., and Haeberli, W., 2002. Modelling Alpine Permafrost Distribution Based on Energy-Balance Data: a First Step. *Permafrost and Periglacial Processes,* 13: 271–282.

Stull, R.B., 1973. Inversion rise model based on penetrative convection. *Journal of the Atmospheric Sciences*, 30: 1092-1099.

Tabony, R.C., 1985. Relations between minimum temperature and topography in Great Britain. *Journal of Climatology*, 5: 503-520.

Taylor, A.E., 1995. Field measurements of n-factors for natural forest areas, Mackenzie Valley, Northwest Territories. In *Current Research 1995-B*. Geological Survey of Canada, 89-98.

Taylor. A., Nixon, M., Eley, J., Burgess, M., and Egginton, P., 1998. Effect of atmospheric temperature inversions on ground surface temperatures and discontinuous permafrost, Norman Wells, Mackenzie Valley, Canada. In A.G. Lewkowicz & M. Allard (eds.), *Proceedings, Seventh International Conference on Permafrost, Yellowknife, N.W.T., June 23-27, 1998*. Quebec City: Nordicana, Centre d'études nordiques, 1043-1048.

Thompson, B.W., 1986. Small-scale katabatics and cold hollows. *Weather*, 41: 146-153.

Wahl, H.E., Fraser, D.B., Harvey, R.C., and Maxwell, J.B., 1987. *Climate of Yukon*. Atmospheric Environmental Service, Environment Canada, Climatological Studies 40.

Weiss, A., 2001. Topographic Position and Landforms Analysis. Poster presentation, *2001 ESRI User Conference, San Diego, California.*

Wheeler, J.O. 1961: *Whitehorse Map-area, Yukon Territory 105 D.* Geological Survey of Canada, Memoir 312.

Whiteman, C.D., 2000. *Mountain Meteorology*. New York: Oxford University Press, 355pp.

Woo, M., and Carey, S.K., 1997. Le pergélisol, le gel saisonnier et l'hydrologie des entes au basin de recherché du ruisseau Wolf (Yukon). *In* Pomeroy, J.W., Granger, R.J (eds.) *Wolf Creek Research Basin: Hydrology, Ecology, Environment*. Saskatoon: National Water Research Institute, 45-53.

Appendix A : UTM Coordinates (WGS84)

Wolf Creek			
site		x	y
WC-P9	08V	487967	6707128
WC-CR1	08V	488125	6707076
WC-CR2	08V	488173	6707049
WC-CR3	08V	488277	6706988
WC-CR4	08V	488349	6706886
WC-CR5	08V	488752	6706112
WC-CR6	08V	488727	6706662
WC-Talmark	08V	495600	6733707
WC-T1	08V	498063	6718720
WC-T2	08V	496884	6717738
WC-T3	08V	495789	6717167
WC-T4	08V	495372	6715760
WC-GSC	08V	489362	6705044
WC-Bowl	08V	486369	6709349
WC2006-DR	08V	489589	6704212
WC2006-1	08V	492407	6711343
WC2006-2	08V	484057	6706380
WC2006-3	08V	484570	6706316
WC2006-4	08V	484857	6706215
WC2006-5	08V	485136	6706254
WC2006-6	08V	485558	6706051
WC2006-7	08V	485467	6705779
WC2006-8	08V	485985	6711071
WC2006-9	08V	483786	6706039
WC2006-10	08V	484252	6705500
WC2006-11	08V	484541	6705454
WC2006-12	08V	484802	6705294

Johnson's Crossing			
site		x	y
JC2006-1	08V	605130	6717934
JC2006-2	08V	605004	6717929
JC2006-3	08V	605294	6717789
JC2006-4	08V	604396	6715860
JC2006-5	08V	604226	6716065
JC2006-6	08V	603124	6716540
JC2006-7	08V	603079	6716617
JC2006-8	08V	597983	6710210
JC2006-9	08V	603296	6715160
JC2006-10	08V	603241	6715327
JC2006-11	08V	603165	6715564
JC2006-12	08V	608099	6723489
JC2006-13	08V	601740	6714398

Sa Dena Hes			
site		x	y
SDH2006-1	09V	508396	6709739
SDH2006-2	09V	507951	6709900
SDH2006-3	09V	507331	6709200
SDH2006-4	09V	507194	6708746
SDH2006-5	09V	506513	6709195
SDH2006-6	09V	506687	6709488
SDH2006-7	09V	507041	6709595
SDH2006-8	09V	507191	6709781
SDH2006-9	09V	506516	6706281
SDH2006-	09V	503862	6701962
SDH2006-	09V	502181	6702863
SDH2006-	09V	499593	6698783
SDH2006-	09V	498290	6695356

Faro			
site		x	y
F2006-1	08V	587818	6902233
F2006-2	08V	594563	6905964
F2006-3	08V	594428	6905555
F2006-4	08V	594337	6905078
F2006-5	08V	584134	6900419
F2006-6	08V	589889	6906567
F2006-7	08V	587390	6909131
F2006-8	08V	587189	6908955
F2006-9	08V	587571	6905361
F2006-10	08V	587739	6905513
F2006-11	08V	587601	6905142
F2006-12	08V	587725	6904903
F2006-13	08V	587712	6904788

Keno			
site		x	y
K2006-1	08V	488064	7089343
K2006-2	08V	488478	7088786
K2006-3	08V	488506	7087936
K2006-4	08V	488912	7088738
K2006-5	08V	488642	7087444
K2006-6	08V	488610	7087537
K2006-7	08V	485945	7091655
K2006-8	08V	488670	7087329
K2006-9	08V	488977	7086980
K2006-10	08V	479769	7091372
K2006-11	08V	479002	7092072
K2006-12	08V	490593	7090648